To the Graduate Council:

I am submitting herewith a dissertation written by Oscar Dario Restrepo Tovar entitled "Ab-initio Calculations of the Charge-Density Response in Complex Materials". I have examined the final electronic copy of this dissertation for form and content and recommend that it be accepted in partial fulfillment of the requirements for the degree of Doctor of Philosophy, with a major in Physics.

Adolfo G. Eguiluz

_____

Major Professor

We have read this dissertation
and recommend its acceptance:

John J. Quinn

_____

Hanno H. Weitering

_____

Robert Hinde

_____

Accepted for the Council:

Anne Mayhew

_____

Vice Chancellor and
Dean of Graduate studies

(Original signatures are on file with official student records.)

Ab-initio Calculations of the Charge-Density Response in Complex Materials

A Dissertation

Presented for the

Doctor of Philosophy

Degree

The University of Tennessee, Knoxville

Oscar Dario Restrepo Tovar

August 2006

This dissertation is dedicated to my family: my parents, Jaime and Stella, my siblings, Jaime and Sandra, and my beloved wife, Perlita.

Acknowledgements

I am grateful with Professor Adolfo Eguiluz for his financial support through his NSF grant and his willingness to discuss and clarify physical concepts, as well as proper working techniques, in the meetings we held each week. I would like to give special thanks to Dr. Ben Larson at ORNL for the many questions and helpful physical insights he has given me over the years. I thank Wei Ku for providing the algorithms for the extraction of the Bloch States from the WIEN package at the initial stage of my research. I also acknowledge stimulating discussions with Idoia de Gurtubay. I appreciate K.-W. Lee and Jan Kunes collaboration through the DOE-CMSN PCSCS network, without their help the results presented in Chapter 5 would not have been possible. I would like to thank the members of my Ph. D. committee as well for their valuable critique of this Dissertation.

The computational training provided by the Joint Institute for Computational Science (JICS) helped me increase the speed of the density response program. Hopefully there will be more of these workshops in the future.

I am grateful with my parents for their continuing support throughout my life and for always trusting the decisions I have made. My brother and my sister have always given me strong encouragement to pursue my goals. My gratitude also goes to my aunts, uncles and cousins in Bogotá who have always been very supportive since I first started studying physics.

I thank all of my friends scattered around the world for their encouragement, especially Juan Pablo and Martin during these graduate years. Finally, I would like to thank my wife, Perla, for her unconditional love and support.

Abstract

Our main goal is to have a realistic description of the charge excitations in complex materials in the range of energies such as the coulomb energy U, which is in the eV range. Spectra of these charge excitations, for a large range of wave vector transfers, may provide signatures of the underlying electronic structures. The charge-density response function calculated within Time-dependent Density functional (TDDFT) is an ideal theoretical framework for the calculation of these excitations, since comparison with experimental data (in particular with non-resonant inelastic x-ray scattering experiments) can be done in absolute units (without the need of any adjustable parameters). The large phase space considered gives a rich testing ground of theory vs. experiment.

In Chapter 3 we study the collective excitations in MgB_2. We find a sharp feature in the charge-excitation spectra of single-crystal MgB_2 showing striking**,** periodic, energy dispersion with momentum transfer q along the c-axis. This excitation was observed for the first time by non-resonant inelastic x-ray scattering in collaborative work. Our Time-dependent density-functional theory calculations show that the observed spectra arises from a strong coupling between single-particle and collective degrees of freedom, mediated by large crystal local fields. As a result, the small-q collective mode residing in the single-particle excitation gap of the B π bands reappears periodically in higher Brillouin zones, a phenomenon which is traced to the layered structure of MgB_2.

In Chapter 4 we argue that the large density of states associated with the narrow bands of strongly-correlated materials may drive the formation of a collective electron-hole state, with an excitation energy on the order of the "Hubbard *U*." Whether the state is actually realized (as we predict for manganites) or not (for monoxides), depends on details of the hybridization between the correlated *d* orbitals and the oxygen-derived *p* orbitals. The crystal local fields play a crucial role in the appearance of this excitation.

We discuss in Chapter 5 the electron-hole excitations in the hydrated and non-hydrated Sodium Cobaltates compounds for sodium concentrations of 1/3. In both types of compounds we find a collective excitation at 9 eV induced by the Crystal Local Fields for

a large range of momentum transfers. It is shown how the inclusion of the water affects the screening at small energies allowing single-particle transitions to be present in the loss spectrum for small momentum transfers. For large values of momenta the loss function for the hydrated and non-hydrated systems are very similar due to the reduced polarizability of the water molecules.

Chapter 6 is devoted to the discussion of the loss function of NiO. For intermediate values of momentum transfer along the [111] direction we found that the main excitation at 7.5 eV observed in non-resonant inelastic scattering experiments is in good agreement with our theoretical results. On the contrary, our results in the optical limit when compared with ellipsometry measurements indicate the need to go beyond our theoretical framework.

Table of Contents

Table of Figures

Chapter 1 Overview

This Dissertation is based on the premise that a realistic treatment of the electronic structure of the complex materials which are central to current research in condensed matter physics is absolutely essential. This viewpoint is opposite to the use of simple models, such as the one-band Hubbard model, etc. A realistic treatment of the electronic excitations in these complex materials is key to the discovery of important interplay between correlated band structure and electron dynamics. Most ab-initio studies have focused on ground state properties with use of DFT. Here, we investigate the suitability of Time-Dependent DFT for the study of excitations in complex systems.

Our implementation of the dynamical charge density response function involves the use of the linearized augmented plane-wave (LAPW) method to calculate the ground state [3,4]. We focus on using the dynamical charge density response to investigate the underlying electronic structures of complex materials such as MgB_2 (Chapter 3), the CrO_2 (Chapter 4), manganites (Chapter 4) sodium cobaltates (Chapter 5) and the monoxides (Chapter 6). These systems are of great interest in the materials science community since they display physical properties that can be applied in industry, such as colossal magneto-resistance in the manganites, enhanced thermoelectric power in the sodium cobaltates, and superconductivity properties in MgB_2 and $Na_{1/3}CoO_2 \cdot yH_2O$. The complexity involves a proper analysis of the physics related to the localized electrons in these materials. The need for a significant upgrade in the number of atoms per unit cell that could be handled in the actual numerical implementation led to the development of a new (6000 lines) dynamical charge density response code that was written as an initial starting point for the work presented in this Dissertation. Other codes developed during the preparation of this Dissertation, that became very helpful for the analysis of the loss spectra, involve the evaluation of the partial DOS and JDOS and the orbital densities, examples of these calculations can be seen in Fig. 4.3 and Fig. 4.8.

The Density Functional Theory (DFT) [18] has been very successful in the study of ground state observables. The Local Density approximation (LDA) [19] works fine for materials involving delocalized orbitals. However, the DFT and the LDA, in particular, fail in describing the Mott gap. In order to gauge the efficiency of the LDA approximation, we compare our results with non-resonant inelastic x-ray scattering experiments (NIXS). NIXS measurements of the energy-loss spectra provide a unique tool for fundamental investigations of electronic correlations in condensed matter. However, until the advent of 3rd generation synchrotron sources [5], the strong photo-electric absorption associated with *d*-band materials and related compounds severely restricted the IXS investigation of these important systems. This new generation of x-ray sources allows measurements at higher momentum transfers thus providing a rich testing ground of experiment vs. theory. The comparison of our theoretical results with non-resonant inelastic x-ray experiments are done in absolute units (we do not use any fitting parameters), thus providing a strong and reliable, not only qualitative but also quantitative, description of our theoretical results. Since we not only use an approximate functional (LDA+U) but in the dynamics we use simple functionals (fxc=0, fxc(LDA), etc…) then it is great that non-resonant IXS is undergoing a rapid development; and we are grateful for having a collaborative team at ORNL (Dr. Ben Larson group).

Functionals such as the LDA+U [25], Self-Interaction Correction (SIC) [6], Exact Exchange (EXX) [7], etc., have been developed in recent years; they produce good gaps; there are ongoing efforts to calculate parameters such as the U from first principles [8]; the SIC has no parameter like U (but is still an approximate functional). The EXX has had success with narrow band insulators [9].

The LDA+U put physics by hand. But it lets us investigate correlated systems such as the Mott insulators. We investigate the performance of the LDA+U functional in a domain that has not been investigated much –that of electronic dynamics (excitations).

Chapter 2 gives a general introduction to Time-Dependent Density Functional Theory and provides the theoretical framework necessary to evaluate the dynamical density response.

In Chapter 3 we study the collective excitations in MgB_2. We find a sharp feature in the charge-excitation spectra of single-crystal MgB_2 showing striking, periodic, energy dispersion with momentum transfer q along the c-axis. Time-Dependent Density-Functional Theory calculations show that the observed spectra arises from a strong coupling between single-particle and collective degrees of freedom, mediated by large crystal local fields (CLFE). As a result, the small-q collective mode residing in the single-particle excitation gap of the B π bands reappears periodically in higher Brillouin zones, a phenomenon which is traced to the layered structure of MgB_2.

In Chapter 4 we argue that the large density of states associated with the narrow bands of strongly-correlated materials may drive the formation of a collective electron-hole state with an excitation energy on the order of the "Hubbard *U*." Whether the state is actually realized (as we predict for manganites) or not (for monoxides) depends on details of the hybridization between the correlated *d* orbitals and the oxygen-derived *p* orbitals. The crystal local fields play a crucial role in the appearance of this excitation.

We discuss in Chapter 5 the electron-hole excitations in the hydrated and non-hydrated Sodium Cobaltates compounds for Sodium concentrations of 1/3. In both types of compounds we find a collective excitation at 9 eV induced by the CLFE for a large range of momentum transfers. It is shown how the inclusion of the water affects the screening at small energies for small momentum transfers, allowing single-particle transitions to be present in the loss spectrum. For large values of momenta the loss function for the hydrated and non-hydrated systems are very similar due to the reduced polarizability of the water molecules.

In Chapter 6 we compare theoretical results of the response function for NiO with experimental data for intermediate and large momentum transfers. We find good agreement with experiment for intermediate q's (1-2 $Å^{-1}$) but our results for the dielectric constant in the optical limit, when compared with ellipsometry measurements, indicate the need to go beyond this LDA+U/RPA theory. We do not agree with studies such as the one presented in Ref. [35], which concluded that, on the basis of the reflectivity data of Ref. [42], one could adopt the value U=5 eV for optics. By contrast, we conclude that LDA+U/RPA theory is not a complete theory; the role of *U* in the dynamics must be

included before we can engage in general recommendations as to what value of U may work "universally". For large momentum transfers the experimental data shows strong d-d excitations inside the ~4 eV gap; our theoretical RPA results cannot capture correctly the energetic placement of these excitations (theoretically, they are found above the gap) indicating the need to go beyond RPA in the description of these strongly correlated excitation, for example by the inclusion of an improved exchange-correlation f_{xc} kernel.

In summary, in this Dissertation we present a new investigation of the dynamical screening in Transition Metal Oxides. We show remarkable new physics involving CLFE associated with the strong inhomogeneity of the electronic structure. We have made significant predictions to be checked via IXS. We uncover important interplay between correlated band structure and electron dynamics. We also demonstrate the importance of the interplay between theory and experiment and the need of first-principles approaches for a realistic description of the complex electronic structure of strongly correlated materials.

Chapter 2 Theoretical Framework

2.1 Time-Dependent Density Functional Theory (TDDFT)

TDDFT constitutes a formally exact generalization of DFT for the description of an interacting, many-electron system evolving in the presence of an external, time-dependent potential $v_{ext}(\vec{x},t)$. TDDFT is based on the Runge-Gross theorem [10] which is the time-dependent extension of the Hohenberg-Kohn theorem [18]. The Runge-Gross theorem states that the many-body densities $n(\vec{x},t)$ and $n'(\vec{x},t)$ evolving from a common initial state $\Psi_0(t)$ under the influence of two external potentials $v(\vec{x},t)$ and $v'(\vec{x},t)$ are always different provided that the potentials differ by more than a purely time-dependent function $v(\vec{x},t) \neq v'(\vec{x},t)+c(t)$. Thus there is a one-to-one mapping between densities and potentials. According to the Runge-Gross theorem any physical observable can in principle be calculated from the knowledge of the time-dependent many-body density.

Kohn and Sham introduced a fictitious system of non-interacting electrons having the same density as the physical system that allows for practical calculations of physical observables. The time-dependent KS equation is written as

$$i\frac{\partial \Psi_j(\vec{x},t)}{\partial t} = \left(-\frac{\nabla^2}{2} + v_{KS}[n](\vec{x},t)\right)\Psi_j(\vec{x},t). \tag{2.1}$$

The density of the interacting system is obtained from the KS orbitals as

$$n(\vec{x},t) = \sum_{j=1}^{N} \left|\Psi_j(\vec{x},t)\right|^2, \tag{2.2}$$

The Kohn-Sham potential is

$$v_{KS}[n](\vec{x},t) = v_{XC}[n](\vec{x},t) + v_{ext}(\vec{x},t) + v_H[n](\vec{x},t), \tag{2.3}$$

where $v_{ext}(\vec{x},t)$ is the external time-dependent field, $v_H[n](\vec{x},t)$ is the time-dependent Hartree potential generated by $n(\vec{x},t)$,

$$v_H(\vec{x},t) = \int d^3r' \frac{n(\vec{x}',t)}{|\vec{x}-\vec{x}'|}, \tag{2.4}$$

and $v_{xc}[n](\vec{x},t)$ is the exchange-correlation potential, which is unknown and in practice needs to be approximated. The "adiabatic" local density approximation (ALDA) [19] is the simplest approximation of the time-dependent xc potential

$$v_{xc}^{ALDA}[n](\vec{x},t) = \frac{d}{d\rho}\left(\rho\,\varepsilon_{xc}^{\text{hom}}(\rho)\right)\Big|_{\rho=n(\vec{x},t)}, \tag{2.5}$$

where ρ is the time dependent density and $\varepsilon_{xc}^{\text{hom}}$ is the xc energy per particle of the homogeneous electron gas. ALDA turned out to be a good approximation even for densities that change rapidly.

2.2 Time-Dependent Linear Density Response

In the linear-response regime, in TDDFT we introduce the dynamical density-response function for interacting electrons via the equation

$$\chi[n_0](\vec{x}t;\vec{x}'t') = \frac{\delta n[v_{ext}](\vec{x}t)}{\delta v_{ext}(\vec{x}'t')}\Big|_{v_{ext}[n_0]}, \tag{2.6}$$

where the functional derivative is evaluated at the ground-state potential —which is one-to-one with the ground-state density n_0, according to DFT ; note that from this observation it follows that the *dynamical* χ is a functional of n_0 (we will in general omit explicit reference to this functional dependence of χ). TDDFT allows us to introduce a similar definition for the density-response function $\chi_s[n_0]$ for uncorrelated (Kohn-Sham) electrons (the functional derivative is now taken with respect to the potential $v_s(\vec{x},t)$ in which the Kohn-Sham electrons evolve). The Kohn-Sham response function χ_s is expressed in terms of the static unperturbed Kohn-Sham orbitals $\Psi_k(\vec{x})$ as

$$\chi_s(\vec{x},\vec{x}',\omega)=\sum_{j,k}\left(f_k-f_j\right)\frac{\Psi_j(\vec{x})\Psi_k^*(\vec{x})\Psi_j^*(\vec{x}')\Psi_k(\vec{x}')}{\omega-\left(\varepsilon_j-\varepsilon_k\right)+i\eta} \tag{2.7}$$

Here, $\left(f_k, f_j\right)$ are the occupation numbers (0 or 1) of the KS orbitals. Summation in Eq. (2.7) ranges over both occupied and unoccupied orbitals.

Invoking the one-to-one mappings which are central to the TDDFT method, leads to the rigorous result (first proved by Petersilka, Gossmann and Gross [17]) that the density-response function obeys the *exact* integral equation (which we write down symbolically)

$$\chi=\chi_s+\chi_s\left(v+f_{xc}\right)\chi, \tag{2.8}$$

where the so-called many-body kernel f_{xc}, which accounts for all dynamical correlations between electrons and holes, is defined by the equation

$$f_{xc}\left[n_0\right](\vec{x}t;\vec{x}'t')=\left.\frac{\delta V_{xc}\left[n\right](\vec{x}t)}{\delta n(\vec{x}'t')}\right|_{n_0}. \tag{2.9}$$

The dynamical density-response function is linked *exactly*, in the Born approximation, to experimental cross sections for inelastic x-ray scattering (IXS). We are probing in detail electronic degrees of freedom which are summed over in, for example, the magnetic moments. In addition, we have access to the full richness of the quantum-mechanical phase space for electron-hole excitations, which in conventional optical measurements are probed in a much-more restricted way.

The theoretical framework is completed by recalling that the differential cross section for a process in which a hard x-ray undergoes a single scattering event, with transfer of energy $\hbar\omega$ and momentum $\hbar\vec{q}$ is given by

$$\frac{d^2\sigma}{d\Omega d\omega}=\left(\frac{d\sigma}{d\Omega}\right)_0 S(\vec{q};\omega) \tag{2.10}$$

$(d\sigma/d\Omega)_0 = r_0^2 \left(\vec{e}_i \cdot \vec{e}_f\right)^2 \omega_f / \omega_i$ being the Thomson cross section, where r_0 is the "classical electron radius" ($r_0 = e^2/mc^2$), and the remaining variables refer to the polarization vector and frequency of the incident ("*i*") and scattered ("*f*") photons.

In Eq. (2.10) we have introduced the dynamical structure factor $S(\vec{q};\omega)$, which, making use of the fluctuation-dissipation theorem, can be expressed as

$$S(\vec{q};\omega) = -2\hbar V \,\mathrm{Im}\,\chi_{\vec{G},\vec{G}}\left(\vec{q}-\vec{G}\right), \tag{2.11}$$

in terms of the (Fourier transform of) the density-response function χ. Equations (2.8), (2.10), and (2.11) embody a "first principles" approach for testing the interplay between electronic structure and IXS data. We emphasize that this comparison involves no ad hoc assumptions, such as conjectures about the nature of the final state or arbitrary scale factors.

Having made the previous point, it is important to expand a little on a related issue, which leads to a meaningful comparison with the IXS data —namely, this comparison is done in absolute units. In effect, we note that in Eq. (2.11) V is the volume of the macrocrystal on whose sides we apply periodic (Born-von Karman (BvK)) boundary conditions. Clearly, $S(\vec{q};\omega)$ is an extensive quantity. In practice, the thermodynamic limit is realized for sufficiently large BvK volumes; in that case, any residual (numerical) dependence of $S(\vec{q};\omega)$ on V is gone, and the only such dependence is via the overall factor of the BvK volume V; this can be checked via calculations for denser and denser meshes —which define a new V in each case. We can then (i.e., for sufficiently dense *k*-meshes) define a dynamical structure factor per unit volume, by pulling the factor V from the above result, i.e.,

$$s(\vec{q};\omega) = -2\hbar \,\mathrm{Im}\,\chi_{\vec{G},\vec{G}}\left(\vec{q}-\vec{G}\right), \tag{2.12}$$

thereby defining a scattering cross section per unit volume,

$$\frac{1}{V}\frac{d^2\sigma}{d\Omega d\omega} = \left(\frac{d\sigma}{d\Omega}\right)_0 s(\vec{q};\omega). \tag{2.13}$$

$s(\vec{q};\omega)$ evaluated from the solution of Eq. (2.8) can be compared in absolute units with IXS experimental data.

In our response code, all matrix elements are evaluated from the knowledge of the Bloch States extracted from the all-electron WIEN2k package [20]. These matrix elements involve l content from l=0 to l=4, our numerical results show that increasing l up to 10 in the expansion of the Kohn-Sham Bloch States does not lead to significant changes in the charge density response.

The basic physical idea behind the LSDA+U method is to insert Hubbard-like physics on top of the LSDA [25]. We emphasize that the main justification for the use of the LSDA+U functional is that we are introducing qualitatively-correct many-body physics — e.g., the *suppression of charge fluctuations due to atomic-like correlations*. At the same time, by construction, the occupied and empty states within the subspace of localized orbitals are shifted relative to each other, which drives the formation of the gap (this is the job performed by *U*).

The LSDA+U functional has been tested successfully many times in recent years, by comparing predicted ground-state observables such as magnetic moments vs. experiment. Such exercise represents an "ab initio" test of the LSDA+U functional. Frequently, the performance of the functional, and the quality of the underlying ground state, is assessed in terms of spectroscopic observables, such as photoemission line shapes. In this context, it should be noted that the eigensolutions of the LSDA+U functional are expected, on intuitive grounds, to be closer to physical quasiparticle states than is the case for Kohn-Sham states. However, the significance of the LSDA+U "orbitals" does not follow uniquely from a well-defined many-body approximation for the electron self-energy.

The use of the LSDA+U functional raises a conceptual issue which must be addressed, namely, the Bloch eigensolutions of the LSDA+U functional are not Kohn-Sham states. Thus, strictly, we are not in a position to evaluate a Kohn-Sham response function χ_S on the basis of the LSDA+U band structure and "orbitals." In brief, the approach adopted here embodies the evaluation of a physically-motivated density-response function obtained via a TDDFT-like scheme from the knowledge of the LSDA+U ground state, combined with RPA dynamics. We refer to this scheme as LSDA+U/RPA. The fact that the

LSDA+U functional provides a good approximation for the ground-state density (and magnetic moment), underlies our scheme —which admittedly relies on the assumption that the orbitals coming out of the LSDA+U ground state calculation are meaningful.)

Chapter 3 Low-Energy Charge Density Excitations in MgB_2

The recent discovery of Superconductivity at a high T_c (~39 K) in MgB_2 [11] has renewed interest in this material. MgB_2 consists of hexagonal planes of boron atoms separated by planes of Mg atoms.The simple hexagonal structure of this material allows the use of ab-initio methods to investigate its electronic properties. The unusually high Tc superconductivity is driven by electron-phonon interaction. It has been found that MgB_2 has two superconducting gaps [12] instead of only one like in most BCS superconductors. There is strong coupling between the E_{2g} phonon mode of the Boron atoms and the σ band electrons generating a large gap. The second gap is due to weak π electron-phonon coupling.

Previous studies by Wei Ku et al. [13] have predicted a sharp collective mode in the optical regime induced by the 5 eV gap between parallel bands in MgB_2 (see Fig. 3.1). We have found a sharp feature in the charge-excitation spectra of single-crystal MgB_2 showing striking, periodic, energy dispersion with momentum transfer q along the c-axis, our theoretical results show that the observed spectra arises from a strong coupling between single-particle and collective degrees of freedom, mediated by large crystal local fields [15].

Let us begin by recalling that the notation $\varepsilon_{\vec{G},\vec{G}'}$ for the "microscopic" dielectric "function" of a periodic crystal is simply a short hand, introduced according to

$$\varepsilon_{\vec{G},\vec{G}'}\left(\vec{k};\omega\right) \equiv \varepsilon\left(\vec{k}+\vec{G},\vec{k}+\vec{G}';\omega\right), \tag{3.1}$$

where $\varepsilon\left(\vec{k}+\vec{G},\vec{k}+\vec{G}';\omega\right)$ is the double Fourier transform of the real-space dielectric function $\varepsilon\left(\vec{x},\vec{x}';\omega\right)$. The structure of the wave-vector arguments on the right hand side

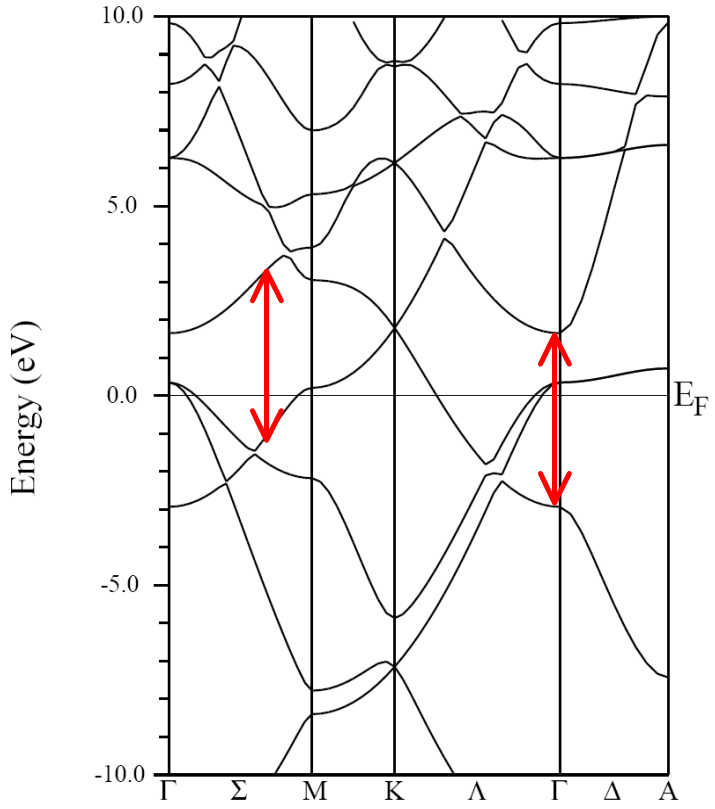

Fig. 3.1. Band structure of MgB_2. The arrows show the 5 eV gap.

of Eq. (3.1) follows from translational invariance on a Bravais lattice, from which it also follows that *the wave vector $\vec{k}$ lies inside the first Brillouin zone (BZ)*.

Now, given a wave vector $\vec{q}$ which belongs outside the first BZ, there exists one (and only one) vector of the reciprocal lattice, which we denote by $\vec{G}_q$, such that

$$\vec{q} - \vec{G}_q = \vec{k} \,. \tag{3.2}$$

That is, $\vec{G}_q$ is the unique $\vec{G}$-vector which brings $\vec{q}$ into the first BZ, $\vec{k}$ being the result of such operation. Our notation emphasizes throughout the fact that the wave vector $\vec{q}$ is a key physical variable in the problem, as it characterizes the photon-electron scattering event, $\hbar\vec{q}$ being the momentum transfer (see Eq. (3.4)). The vector $\vec{G}_q$ is uniquely defined, for a given $\vec{q}$. By contrast, the vector $\vec{k}$ will rarely be used explicitly, as it is a "dependent" variable, $\vec{q}$ being the "independent" variable.

Under the condition that Eq. (3.2) holds, we have the obvious condition that

$$\varepsilon_{\vec{G},\vec{G}'}\left(\vec{q} - \vec{G}_q; \omega\right) = \varepsilon_{\vec{G},\vec{G}'}\left(\vec{k}; \omega\right), \tag{3.3}$$

which implies a "periodicity" in the screening process: As $\vec{q}$ runs from, e.g., $\vec{G}_{BZ}/2$ to $\vec{G}_{BZ}$ in the second BZ, $\varepsilon_{\vec{G},\vec{G}'}\left(\vec{q} - \vec{G}_q; \omega\right)$ provides a replica of the dielectric matrix in the first BZ ($\varepsilon_{\vec{G},\vec{G}'}\left(\vec{k}; \omega\right)$) as $\vec{k}$ runs, in the "reverse sense," from $-\vec{G}_{BZ}/2$ to the Γ-point (as $\vec{q}$ "grows," $\vec{k}$ "decreases"). Similarly, as $\vec{q}$ goes from $\vec{G}_{BZ}$ to $3\vec{G}_{BZ}/2$ in the third BZ, the left hand side of Eq. (3.3) provides a replica of the right hand side as $\vec{k}$ runs (in the same sense as $\vec{q}$) from the Γ-point to $\vec{k} = \vec{G}_{BZ}/2$ (i.e., in this case both wave vectors "grow" together). And so on. Note that $\vec{G}_q$ remains fixed, as $\vec{q}$ runs through a given BZ.

Whether the "periodicity" built into Eq. (3.3) manifests itself experimentally is not a trivial issue, as the dielectric matrix is not an "observable" (except in optical experiments, and then only if crystal local fields were negligible). In fact, the electronic response to hard x-rays is given by the *dynamical structure factor* $S\left(\vec{q}; \omega\right)$, which is related to (the Fourier-transform of) the *density-response function* χ via the fluctuation-dissipation theorem

$$S(\vec{q};\omega) = -2\hbar V \,\mathrm{Im}\,\chi_{\vec{G}_q,\vec{G}_q}\left(\vec{q}-\vec{G}_q;\omega\right), \tag{3.4}$$

where, if $\vec{q}$ lies in the first BZ, $\vec{G}_q = \vec{0}$ (this extends our convention of Eq. (3.2) in an obvious way). Equation (3.4) can also be expressed in terms of ε (a step which is not needed, in the TDDFT framework, which is geared toward the direct evaluation of χ), by noting the relation (which holds in the exact theory), valid for arbitrary $\vec{G},\vec{G}'$:

$$\chi_{\vec{G},\vec{G}'}\left(\vec{q}-\vec{G}_q;\omega\right) = v^{-1}\left(\vec{q}-\vec{G}_q+\vec{G}\right)\left(\left[\varepsilon\left(\vec{q}-\vec{G}_q;\omega\right)\right]^{-1}_{\vec{G},\vec{G}'} - \delta_{\vec{G},\vec{G}'}\right) \tag{3.5}$$

i.e., the physical response is related to the *inverse* of the dielectric *matrix* $\varepsilon_{\vec{G},\vec{G}'}$. In Eq. (3.5), $v\left(\vec{q}-\vec{G}_q+\vec{G}\right) = 4\pi e^2/\left|\vec{q}-\vec{G}_q+\vec{G}\right|^2$; also, in Eq. (3.5) (and elsewhere) ε (written simply as such) is a symbolic notation for the full dielectric matrix; similarly, ε^{-1} denotes the inverse of that matrix in $\vec{G},\vec{G}'$ space.

We stress that the non-diagonal elements of this matrix are responsible for the *crystal local-field effects*, which account for the difference between the physical response $\left[\varepsilon\left(\vec{q}-\vec{G}_q;\omega\right)\right]^{-1}_{\vec{G}_q,\vec{G}_q}$ and its counterpart $1/\varepsilon_{\vec{G}_q,\vec{G}_q}\left(\vec{q}-\vec{G}_q;\omega\right)$ for a hypothetical material with uniform electron density, for which the dielectric matrix would be diagonal. *We emphasize that Eq.* (3.6)*, which is the basis of our discussion of the physics of the response of MgB_2, is written in a form that highlights the difference between these two functions.*

Equation (3.4) makes clear that the relevant element of the density response matrix is the $\vec{G}_q,\vec{G}_q$ element, and *the same changes when the photon wave-vector transfer $\vec{q}$ enters a new BZ*. How a given $\vec{G},\vec{G}'$ element of ε —and the "periodicity" suggested by Eq. (3.3)— "propagates" into the $\vec{G}_q,\vec{G}_q$ element of ε^{-1} is a key point in our discussion.

The above considerations are general. The case of MgB_2 is particularly simple, as is visualized in part with the help of Fig. 3.2 and Fig. 3.3, in which we show the dielectric matrix for $\vec{q} = \vec{k} = \left(0,0,0.29\text{Å}^{-1}\right)$, and $\vec{q} = \left(0,0,2.08\text{Å}^{-1}\right)$, respectively. We notice that the latter wave vector belongs in the third BZ; the corresponding $\vec{G}_q$ is $\vec{G}_q = (2\pi/c)(0,0,1)$, whose magnitude is $1.79\text{Å}^{-1} = (2.08-0.29)\,\text{Å}^{-1}$; that is, the wave vectors considered in Fig. 3.2 and Fig. 3.3 are connected according to Eq. (3.2). It is

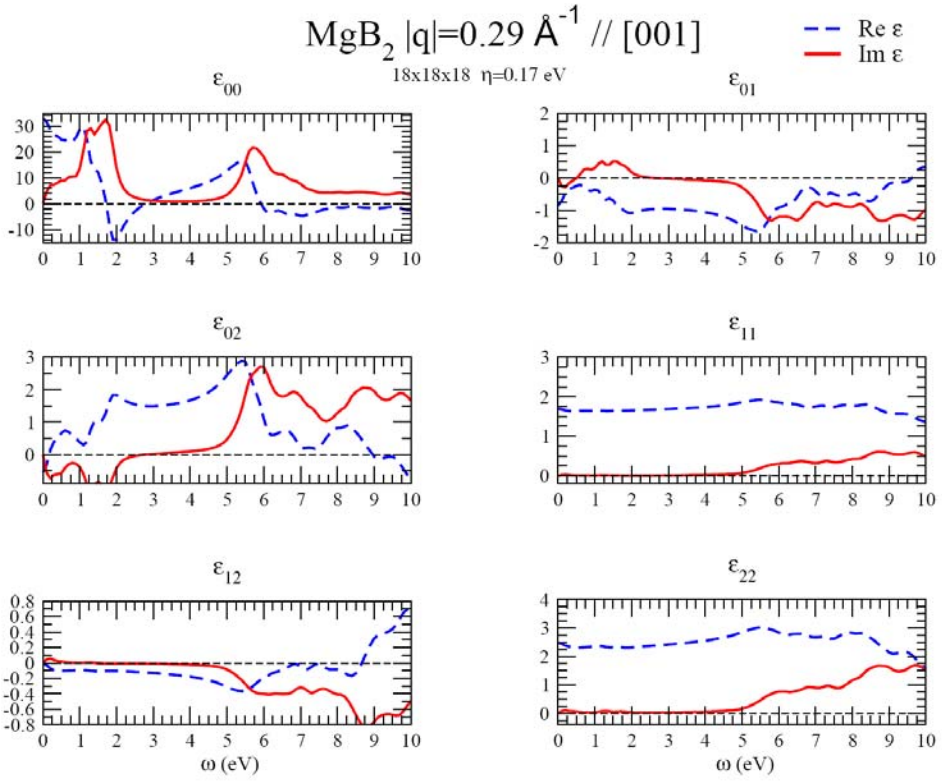

Fig. 3.2. Dielectric matrix of MgB_2 for a (relatively) small wave vector in the first BZ. We note that , since we actually plot a symmetrized dielectric matrix, the figure only shows the "right triangle" of the 3x3 matrix. The $\varepsilon_{00} = \varepsilon_{\vec{G}=0,\vec{G}=0}$ element features the "zero" crossing of the dielectric function induced by the excitation gap discussed by Ku et al. [13]

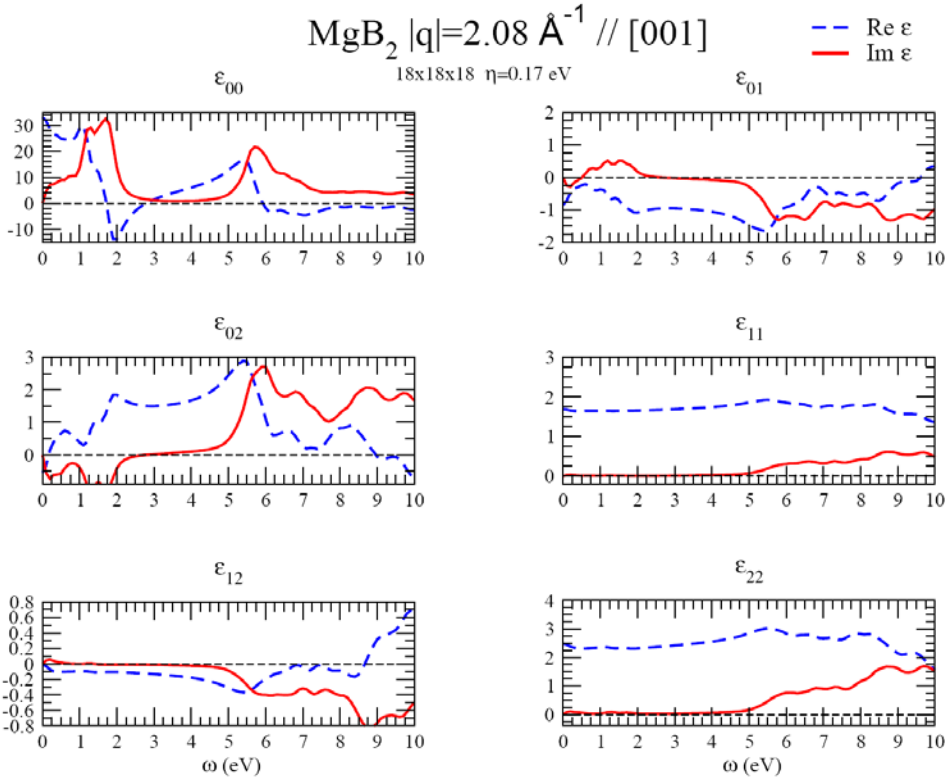

Fig. 3.3. Dielectric matrix of MgB_2 for a wave vector in the third BZ. Note: the $\vec{q}$-vectors in Fig. 3.2 and Fig. 3.3 are related by a $\vec{G}_q$-vector ($\vec{G}_q = (2\pi/c)(0,0,1)$); thus, according to Eq. (3.3), the matrix ε must be identical in both figures —which is the case, obviously.

apparent that both matrices are identical. In Fig. 3.3 we use the following conventions: $\varepsilon_{00} \equiv \varepsilon_{\vec{G}=0,\vec{G}=0}$; $\varepsilon_{11} \equiv \varepsilon_{\vec{G}_q,\vec{G}_q}$, with $\vec{G}_q = (2\pi/c)(0,0,1)$; $\varepsilon_{22} \equiv \varepsilon_{\tilde{G},\tilde{G}}$, with $\tilde{G} \equiv (2\pi/c)(0,0,-1)$; the same convention is used for the $\vec{G}-$vectors labeling the off-diagonal elements. *It is important to note that these conventions are also used in Eq.* (3.6) (see below for further discussion). In the case of Fig. 3.2, in which $\vec{q}$ is in the first BZ, the elements of ε are simply labeled by the same two $\vec{G}-$vectors, $\vec{G} = (2\pi/c)(0,0,1)$, and $\vec{G} = (2\pi/c)(0,0,-1)$, *in the same order* as used in Fig. 3.3 and Fig. 3.5 (unfortunately, the notation $\varepsilon_{\vec{G}_q,\vec{G}_q}$ cannot be used "universally," as it does not apply for the first BZ). With these conventions, the elements of ε can be compared one-by-one in Fig. 3.2 and Fig. 3.3 (and Fig. 3.5).

We emphasize that in Fig. 3.2 and Fig. 3.3 we only show a 3x3 subset of the full dielectric matrix ε, corresponding to the three shortest $\vec{G}-$vectors, given by $\vec{G} = \vec{0}$, $\vec{G} = (2\pi/c)(0,0,1)$, and $\vec{G} = (2\pi/c)(0,0,-1)$. As it turns out, this same matrix does the job in the case of the first three BZs. In the case of the *fourth* BZ, the vector $\vec{G} = (2\pi/c)(0,0,-1)$ is replaced by $\vec{G} = (2\pi/c)(0,0,2)$; *however, the dielectric matrix remains 3x3*. That a 3x3 matrix may be large enough to describe the $S(\vec{q};\omega)$ of MgB_2 for all q's entering the non-resonant IXS data of Cai *et al*. [15] quite accurately is something that comes out of actual calculation. *This finding is related to the layered structure of MgB_2, and to the fact that the length scale of the polarization process in real space is controlled by orbitals which are rather extended —i.e., there are no d orbitals.* This feature is what allows us to draw a simple ("semi-analytical") picture of the response for large wave vectors.

We move on to a discussion of the $S(\vec{q};\omega)$ of MgB_2. For definiteness, here we will refer explicitly to $\vec{q}$'s in the second BZ (our discussion actually holds in general, i.e., for higher BZ's). It is apparent in Fig. 3.4 that $S(\vec{q};\omega)$ does display a clear "periodicity:" The energy position of its main loss feature retraces its position in the first BZ. That the strength of the loss feature in the second BZ is larger than in the first zone can be understood from the fact that $\mathrm{Im}\,\chi$ scales as q^2 —and, thus, so does $S(\vec{q};\omega)$.

The "periodic" behavior of $S(\vec{q};\omega)$ featured in Fig. 3.4 can be nicely interpreted on the basis of the following exact expression for the inverse of an arbitrary NxN matrix [16] (see Appendix C), in which we have adapted the notation to our physical situation:

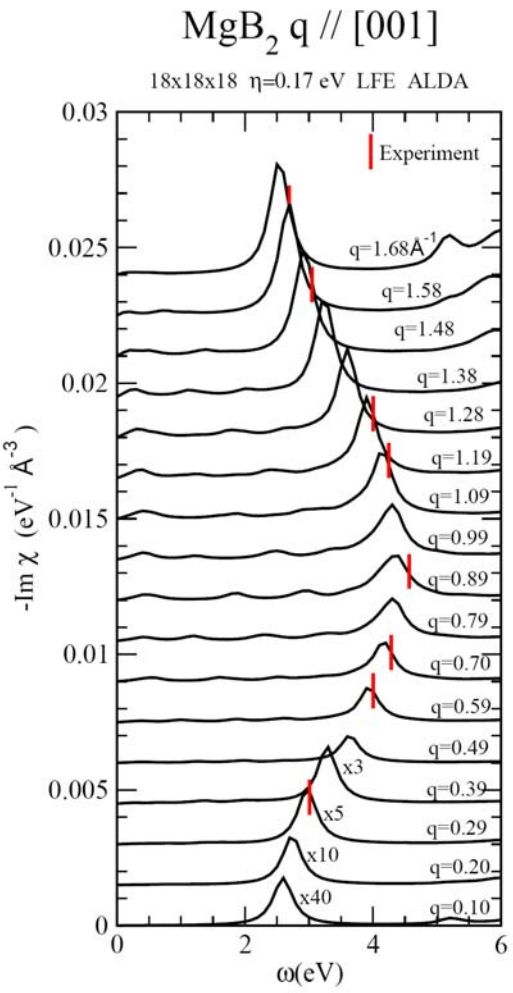

Fig. 3.4. Imaginary part of the density response function of MgB2 for wave vector transfers spanning the first two BZ's. The energetic position of the "low-energy" loss feature present in the dynamical structure factor (see Eq. (3.4)) measured by Cai et al. [15] is indicated by a vertical bar. The calculated response function corresponds to a solution of the TDDFT integral equation within the "adiabatic" LDA, or ALDA.

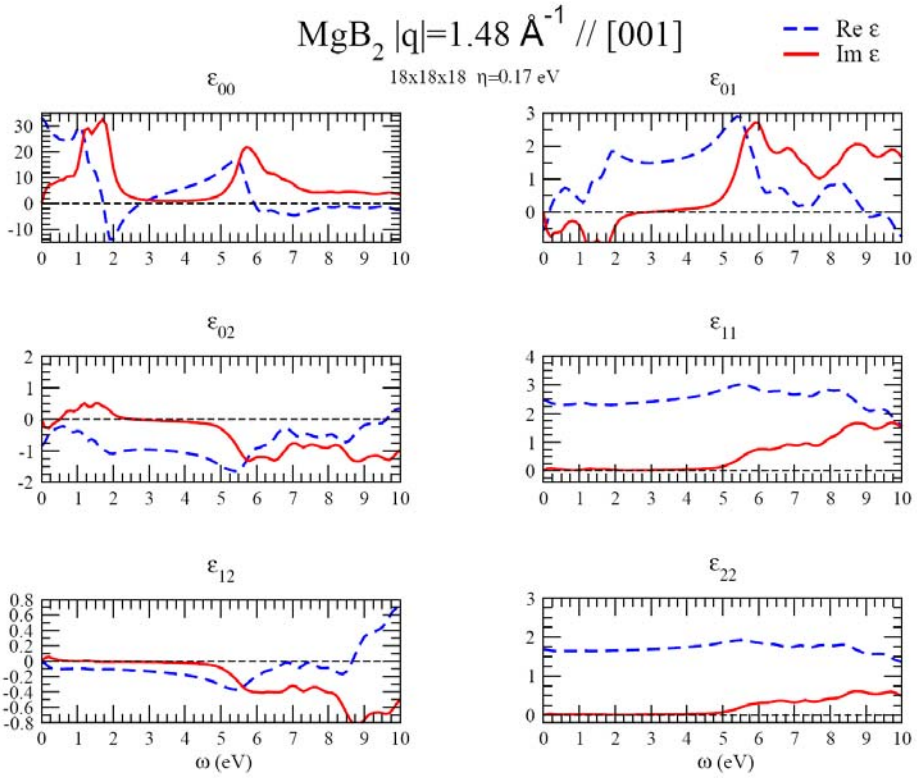

Fig. 3.5. Dielectric matrix of MgB2 for a q-vector about half way in the second BZ; the corresponding $\vec{G}_q$ is the same as in Fig. 2, namely, $\vec{G}_q = 2\pi/c(0,0,1)$. Here $\varepsilon_{11} = \varepsilon_{Gq,Gq}$. As it turns out, ε_{00} in Fig. 3.5 is quite close to its form at the edge of the second BZ, $\vec{q} = \vec{G}_{BZ} = 2\pi/c(0,0,1)$, for which $\vec{q} - \vec{G}_q = 0$; in that limit, ε_{00} equals its counterpart for $\vec{k} = \vec{0}$, as illustrated approximately by the ε of Fig. 3.2. It is crucial to note that in the present case the collective loss arises "indirectly" from $1/\varepsilon_{00}$, via the second term in Eq. (3.6). By contrast, in the case of Fig. 3.2 the collective mode arises directly from $1/\varepsilon_{00}$ (scalar response). Fig. 3.5, together with Eq. (3.6), thus contain a dramatic illustration of the impact of crystal local fields —which vanish if the non-diagonal elements of ε were zero; in that case, $F = 0$ in Eq. (3.6). NB: the statement about "collective loss" is exact for $\vec{q} \to \vec{G}_{BZ}$, as in this limit the response is overwhelmed by the physics built into ε_{00} (via the second term in Eq. (3.6)); similarly, in the first BZ (Fig. 3.2), this statement is most precise for small wave vectors, becoming "exact" for $\vec{q} \to \vec{0}$.

$$\left[\varepsilon\left(\vec{q}-\vec{G}_q;\omega\right)\right]^{-1}_{\vec{G}_q,\vec{G}_q}=\frac{1}{\varepsilon_{\vec{G}_q\vec{G}_q}\left(\vec{q}-\vec{G}_q;\omega\right)}+F_{\vec{G}_q}\left(\vec{q},\vec{q}-\vec{G}_q;\omega\right)\left[\varepsilon\left(\vec{q}-\vec{G}_q,\omega\right)\right]^{-1}_{\vec{G}=\vec{0},\vec{G}=\vec{0}} \quad (3.6)$$

where we have made the following definitions,

$$F_{\vec{G}_q}\left(\vec{q},\vec{q}-\vec{G}_q;\omega\right)=-\frac{W\left(\vec{q},\vec{q}-\vec{G}_q;\omega\right)}{\varepsilon_{\vec{G}_q\vec{G}_q}\left(\vec{q}-\vec{G}_q;\omega\right)}\ , \quad (3.7)$$

with

$$W\left(\vec{q},\vec{q}-\vec{G}_q;\omega\right)=\frac{Det\left[\varepsilon\left(\vec{q}-\vec{G}_q;\omega\right)\right]-\varepsilon_{\vec{G}_q,\vec{G}_q}\left(\vec{q}-\vec{G}_q;\omega\right)M_{\vec{G}_q,\vec{G}_q}\left(\vec{q}-\vec{G}_q;\omega\right)}{M_{\vec{G}=\vec{0},\vec{G}=\vec{0}}\left(\vec{q}-\vec{G}_q;\omega\right)}\ , \quad (3.8)$$

where $M_{\vec{G}=\vec{0},\vec{G}=\vec{0}}\left(\vec{q}-\vec{G}_q;\omega\right)$ and $M_{\vec{G}_q,\vec{G}_q}\left(\vec{q}-\vec{G}_q;\omega\right)$ are the minors for the $\vec{G}=\vec{0},\vec{G}'=\vec{0}$ and $\vec{G}=\vec{G}_q,\vec{G}'=\vec{G}_q$ elements of ε, respectively. Considering a 3x3 dielectric matrix we can write

$$\begin{aligned}M_{\vec{G}=\vec{0},\vec{G}=\vec{0}}\left(\vec{q}-\vec{G}_q;\omega\right)=&\varepsilon_{\vec{G}_q,\vec{G}_q}\left(\vec{q}-\vec{G}_q;\omega\right)\varepsilon_{\tilde{G},\tilde{G}}\left(\vec{q}-\vec{G}_q;\omega\right)\\&-\varepsilon_{\vec{G}_q,\tilde{G}}\left(\vec{q}-\vec{G}_q;\omega\right)\varepsilon_{\tilde{G}\vec{G}_q}\left(\vec{q}-\vec{G}_q;\omega\right)\end{aligned} \quad (3.9)$$

and

$$\begin{aligned}M_{\vec{G}_q,\vec{G}_q}\left(\vec{q}-\vec{G}_q;\omega\right)=&\varepsilon_{\vec{G}=\vec{0},\vec{G}=\vec{0}}\left(\vec{q}-\vec{G}_q;\omega\right)\varepsilon_{\tilde{G},\tilde{G}}\left(\vec{q}-\vec{G}_q;\omega\right)\\&-\varepsilon_{\vec{G}=0,\tilde{G}}\left(\vec{q}-\vec{G}_q;\omega\right)\varepsilon_{\tilde{G},\vec{G}=\vec{0}}\left(\vec{q}-\vec{G}_q;\omega\right)\end{aligned} \quad (3.10)$$

The motivation for the way in which we have grouped the algebra of 3x3 matrix inversion was already anticipated in the paragraph below Eq. (3.5). Indeed, the first term on the right hand side corresponds to the density response for a material with a uniform electron density (which, of course, does not exist, but is approximated rather well by simple metals); thus, by design, the second term sets the stage for a meaningful description of the role of the crystal local fields in the screening process.

We stress that the structure of Eq. (3.6) is a direct generalization of the result given by Sturm, Schülke, and Schmitz [14] for the case of a 2x2 dielectric matrix. Thus, it may be argued that the essence of the response of MgB_2 for large *q's* is similar to the physics discussed in the Sturm *et al.* paper. However, as it turns out, MgB_2 —because of its layered structure, and strongly-inhomogeneous electron density along the c-axis— provides a far more striking example of the impact of the crystal local fields than discussed by Sturm *et al.* for simple metals (technically, this is because in simple metals the "coupling function" *F* in Eq. (3.6) is quite small).

Let us expand on the physics of Eq. (3.6). First, and with reference to Fig. 3.5 and Fig. 3.6, In Fig. 3.5 the conventions are the same as those used in Fig. 3.3. The $\vec{G}$-vector $\vec{G}_q = (2\pi/c)(0,0,1)$ defined in Fig. 3.3 plays the same role for the present $\vec{q}$-vector, which is now in the second BZ; the vector $\vec{q} - \vec{G}_q$ lies in the "negative *k*-vector side" of the first BZ, while it was in the "positive" side of the first BZ in Fig. 3.3, for which $\vec{q}$ was in the third BZ. We note that the first term in Eq. (3.6), the inverse of $\varepsilon_{\vec{G}_q,\vec{G}_q}\left(\vec{q}-\vec{G}_q\right) = \varepsilon_{11}$, by itself, would correspond to *incoherent response —single electron-hole excitation—* in the would-be second-BZ for a uniform-density material. (The $S(\vec{q};\omega)$ for the wave vector transfer of Fig. 3.5 is in Fig. 3.4.) *It is crucial to our argument that, as illustrated by* Fig. 3.6*, in MgB_2 this term amounts to background in the $S(\vec{q};\omega)$ of* Fig. 3.4*, in the energy region of the main loss feature.*

By contrast, the second term in Eq. (6) includes the factor $\left[\varepsilon\left(\vec{q}-\vec{G}_q,\omega\right)\right]^{-1}_{\vec{G}=\vec{0},\vec{G}=\vec{0}}$, whose imaginary part is proportional to the $\vec{G}=\vec{0},\vec{G}'=\vec{0}$ element of the response function for the wave vector $\vec{q}-\vec{G}_q$, which lies in the first BZ. *This is the key factor*, as it reintroduces in the second BZ the collective mode induced by the "excitation gap" present in ε_{00} in Fig. 3.2, i.e., the excitation discussed by Ku *et al.* [13]. *This is clearly illustrated in* Fig. 3.6.

The factor $F_{\vec{G}_q}\left(\vec{q},\vec{q}-\vec{G}_q;\omega\right)$ couples the single-particle electron-hole degrees of freedom and the collective mode for large wave vectors, in the sense already discussed by Sturm e*t al.* [14] The role played by this factor (a complex function) is to "turn on" the physics of the collective mode in the second BZ. To put it still another way: In MgB_2 the physics of the second term in Eq. (6) (and hence, the physical response function) is

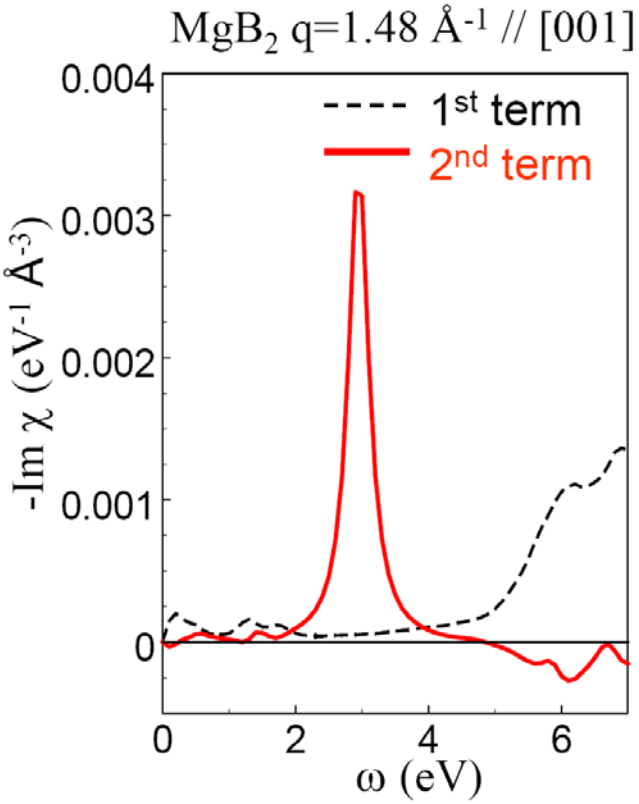

Fig. 3.6. We illustrate the two contributions to Eq. (3.6) in MgB2 for the second-BZ wave vector transfer of Fig. 3.5. For this wave vector, the first term in Eq. (3.6), which corresponds to a "scalar response" appropriate for a hypothetical homogeneous material, amounts to a small background, for energy transfers corresponding to the loss feature measured by Cai et al. The key physics is contained in the second term of Eq. (3.6), and the same corresponds to a crystal-field-induced reintroduction of the collective mode generated by the excitation gap in the band structure of MgB2 for small wave vectors in the first BZ.

controlled by the loss function $\mathrm{Im}\left[\varepsilon\left(\vec{q}-\vec{G}_q,\omega\right)\right]^{-1}_{\vec{G}=\vec{0},\vec{G}=\vec{0}}$, i.e., *the physics of the response in the second BZ is essentially the same as that of the first BZ.*

In MgB_2 the coupling function *F* does its job perfectly: *Its imaginary part has no structure in the neighborhood of the main loss feature*; thus, according to Eq. (3.6), the physics of $\mathrm{Im}\left[\varepsilon\left(\vec{q}-\vec{G}_q;\omega\right)\right]^{-1}_{\vec{G}_q,\vec{G}_q}$ —i.e., the physics of $S\left(\vec{q};\omega\right)$— in the vicinity of the main loss feature, is controlled by the loss function $\mathrm{Im}\left[\varepsilon\left(\vec{q}-\vec{G}_q,\omega\right)\right]^{-1}_{\vec{G}=\vec{0},\vec{G}=\vec{0}}$ entering the second term of Eq. (3.6). An equivalent statement is that $\mathrm{Re}\left[\varepsilon\left(\vec{q}-\vec{G}_q,\omega\right)\right]^{-1}_{\vec{G}=\vec{0},\vec{G}=\vec{0}}$ plays no role in the neighborhood of the main loss feature; *if it did, the physics of Eq.*(3.6) *would be obscure!*

Finally, it is straightforward to see that as $\vec{q}$ runs through the second BZ (i.e., as it goes from the edge of the first BZ to the edge of the second BZ) $\left[\varepsilon\left(\vec{q}-\vec{G}_q,\omega\right)\right]^{-1}_{\vec{G}=\vec{0},\vec{G}=\vec{0}}$ traverses the physics of the collective mode in the first BZ in the reverse direction. In Fig. 3.7 the first and second terms in Eq. (3.6) are calculated for a momentum transfer belonging to the fourth BZ (q=3.27 Å^{-1} along [001]). In this case $\left|\vec{q}-\vec{G}_q\right|=0.29\,\text{Å}^{-1}$, where $\vec{G}_q=2\pi/c\left(0,0,2\right)$. In the inset of Fig. 3.7 it is shown how the real part of $F_{\vec{G}_q}\left(\vec{q},\vec{q}-\vec{G}_q;\omega\right)$ does not affect the loss feature at 3 eV appearing in the $\left[\varepsilon\right]^{-1}_{00}$ term.

The electron-hole degrees of freedom in MgB_2 are quite remarkable, as the excitation of long-lived collective charge-density fluctuations is possible on a length scale comparable with the size of the orbitals doing the screening. This behavior is shown explicitly in Fig. 3.8 where we have plotted the orbital density (wave function squared) of an occupied state in MgB2: the Boron derived orbitals are rather extended along the z axis allowing strong coupling between charge-density fluctuations in this direction.

In summary, the second term in Eq. (3.6) is responsible for two related effects: It brings back the physics of the small wave-vector response —the collective mode induced by the excitation gap— to the second BZ, and it generates the distinctive periodicity of $S\left(\vec{q};\omega\right)$ observed in Fig. 3.4. It is also worth emphasizing that MgB_2 embodies a striking realization of crystal local fields effects (see Fig. 3.9). By contrast, for simple metals, for which the structure of Eq. (3.6) also holds, these effects are small, as the coupling function *F* is small —which is why the periodicity of Fig. 3.4 is not realized in, e.g., Al.

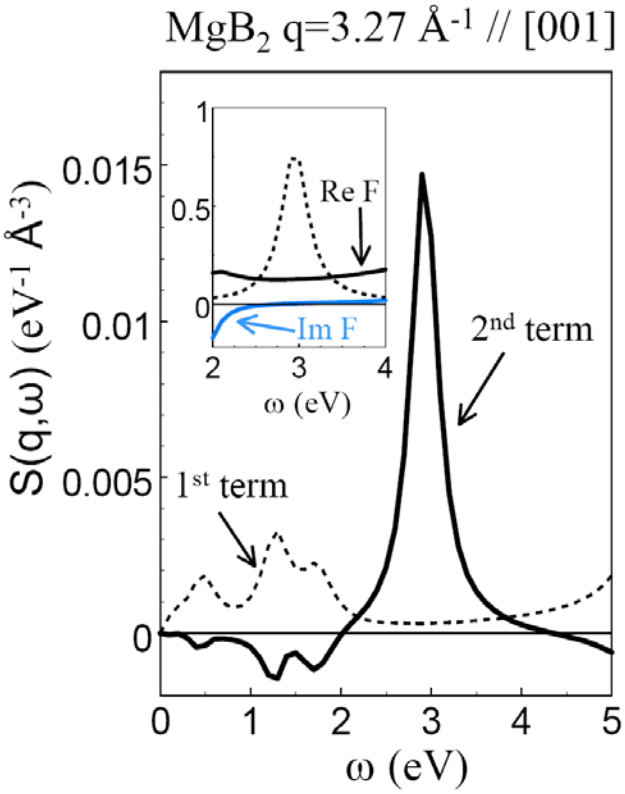

Fig. 3.7. Contributions calculated from the first and second terms in Eq. (3.6) to the S(q,ω) at q=3.27Å^{-1} along [001]. The insert shows the real and imaginary parts of the F factor and the $[\varepsilon]_{00}^{-1}$ for the corresponding $|\vec{q}-\vec{G}_q| = 0.29$ Å^{-1}, where $\vec{G}_q = 2\pi/c\,(0,0,2)$.

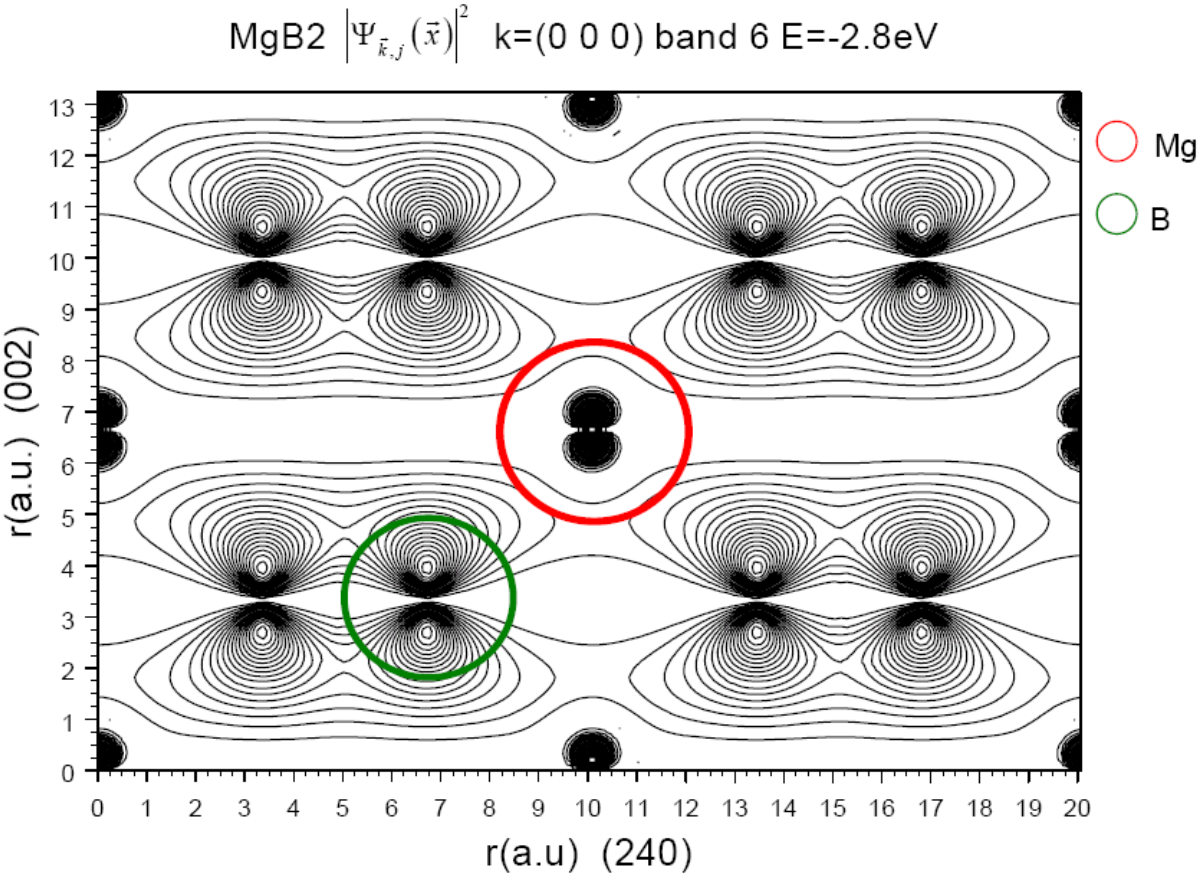

Fig. 3.8. Orbital density of an occupied state in MgB_2. The excitation of long-lived collective charge-density fluctuations is possible on a length scale comparable with the size of the orbitals doing the screening.

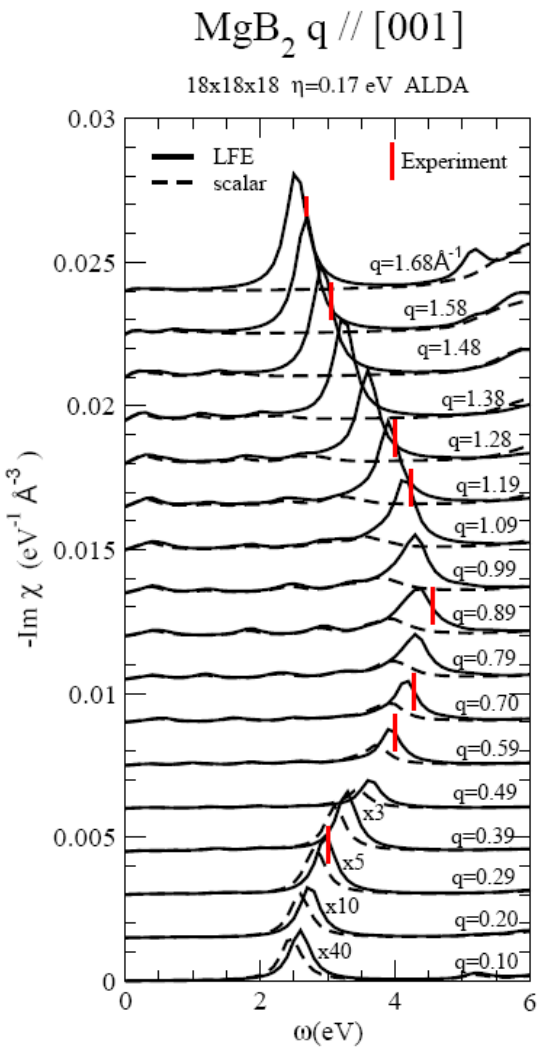

Fig. 3.9. Illustration of the large impact of the crystal local fields ("CLFE") on the basis of the full calculation of the response function.

Chapter 4 Collective Electron Hole State in Strongly Correlated Compounds

In this Chapter we reveal novel features of the charge excitations, which control the physics for energies on the order of the "Hubbard *U*." In particular, we predict that, for a class of materials typified by $CaMnO_3$ and $LaMnO_3$ (the end points of the $La_{1-x}Ca_xMnO_3$ family displaying colossal magnetoresistance [21] for $x \approx 1/3$) and CrO_2 (a half-metal of interest in spintronics [22]) the electron-hole response is dominated, for large wave vectors, by a collective state.

For the compounds for which we predict a sharp collective state, the charge excitations are controlled by *two* band complexes —involving strongly hybridized cation-derived *d* states and anion-derived *p* states— lying on both sides of a "Mott gap." For another class of materials, typified by the monoxides NiO and CoO, the charge excitations are shown to be qualitatively different —the collective mode is not realized. For the latter compounds the charge excitations include a *third* band complex; the additional "band" corresponds to unhybridized oxygen-derived states, lying towards the bottom of the spin-minority states, which conspire against (what we describe as) a natural tendency toward collective-mode formation.

4.1 Momentum Dependence in the Density Response of CrO_2

We have performed calculations of the response function of ferromagnetic CrO2 starting from a LSDA+U (U=3 eV) ground state for various wave vector transfers along the [001] direction. Our discussion will be focused on the most prominent feature in the loss spectrum, namely the q dependent excitation near 12.5 eV (Fig. 4.1), which is absent in the scalar calculation. This excitation is present for q's ranging from 0.92 to 3 A^{-1} // [001] and its maximum magnitude occurs for q=1.85 A^{-1}.

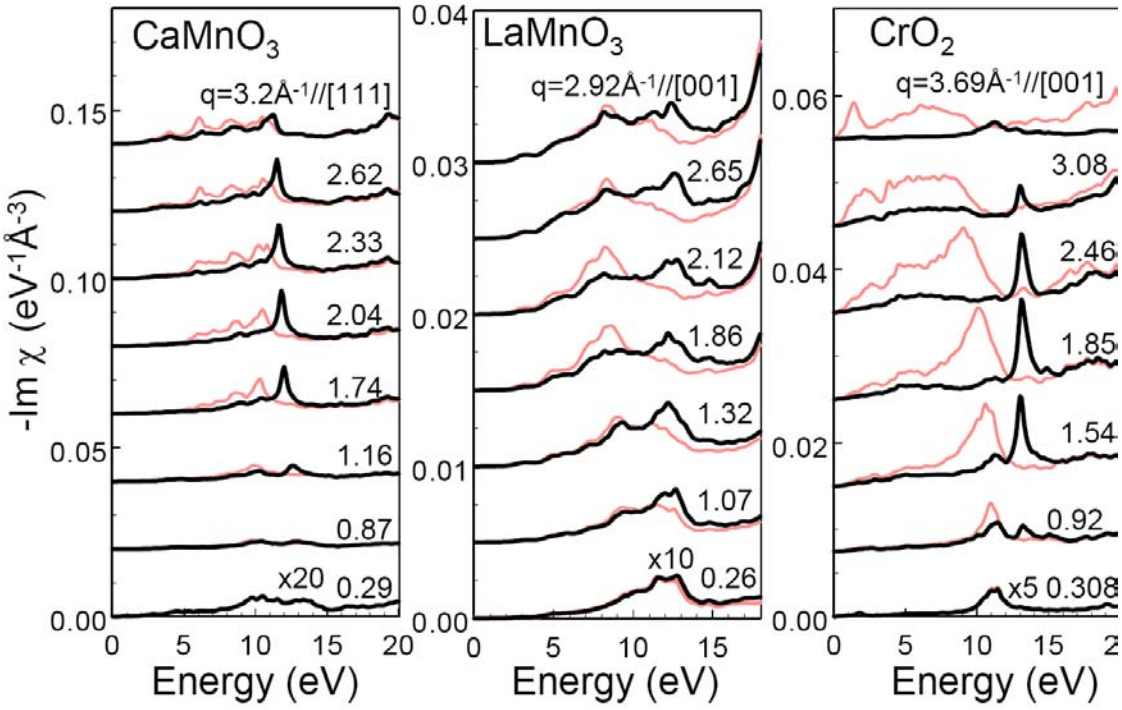

Fig. 4.1. Imaginary part of the dynamical density response function for CrO_2, $CaMnO_3$ and $LaMnO_3$, for a large range of wave vector transfers. The most striking feature of the calculated spectra is the sharp collective electron-hole state discussed in the text, and whose genesis is ultimately the sharp drop in the JDOS illustrated in Fig. 4.3 for the case of CrO_2, corresponding to the edge of the excitation channels provided by e_g-e_g processes (aided by *pp* processes which occur within a *two-band* excitation band structure). Note that the spectral weight of the collective mode is maximal for rather large wave vectors, which is an ideal situation for experimental observation via non-resonant inelastic scattering (NIXS).

Various tests allowed us to identify a subspace of dimension 4, containing the essential physics of the excitation at 12.5 eV. This subspace turns out to be defined by G-vectors pointing along the [-1 0 -1], [1 0 -1], [0 -1 -1] and [0 1 -1] directions, their magnitude being 2.58 A^{-1}, we refer to these G-vectors as G*. The relevant characteristic of these vectors is that they all have a negative z-component, pointing in the opposite direction to the transfer vector q. This feature will be important in our following discussion since, as shown in Table 1, for q's greater than 1.5 A^{-1} the magnitude of |q+G*| becomes smaller than the magnitude of q ("Umklapp process"), this implies that the physics for these large q's (excitation at 12.5 eV) is related to the physics for smaller q's (|q+G*|). At its simplest, the physics is contained in the diagonal elements of this 4x4 matrix; we refer to these elements as $\varepsilon_{\vec{G}^*,\vec{G}^*}(\vec{q},\omega)$ (We actually have to consider the entire G* shell of the dielectric matrix in order to obtain the full strength of the excitation, nevertheless, the physics that accounts for the 12.5 eV excitation is already present in $\varepsilon_{\vec{G}^*,\vec{G}^*}(\vec{q},\omega)$).

The imaginary part of $\varepsilon_{\vec{G}^*,\vec{G}^*}(\vec{q},\omega)$ is shown, for different values of q, in Fig. 4.2, the most significant aspect of these curves is the large drop-off at energies near 9 eV. It turns out that this drop-off or "wall" is the key ingredient in generating the excitation at 12.5 eV, indeed, by Krammers-Kroning considerations, it will generate a "wiggle" in the real part of $\varepsilon_{\vec{G}^*,\vec{G}^*}(\vec{q},\omega)$, defining a possible collective mode.

We have defined an epsilon effective $\varepsilon_{eff}\left(\vec{q}-\vec{G}_q;\omega\right)$ such that its inverse is proportional to the *dynamical structure factor*,

$$S(\vec{q};\omega)=\frac{-2\hbar V}{v\left(\vec{q}-\vec{G}_q+\vec{G}\right)}\mathrm{Im}\left[\frac{1}{\varepsilon_{eff}\left(\vec{q}-\vec{G}_q;\omega\right)}\right] \tag{4.1}$$

$\varepsilon_{eff}\left(\vec{q}-\vec{G}_q;\omega\right)$ is defined in the following way,

$$\varepsilon_{eff}\left(\vec{q}-\vec{G}_q;\omega\right)=\varepsilon_{\vec{G}_q,\vec{G}_q}\left(\vec{q}-\vec{G}_q;\omega\right) - \sum_{\vec{G}_1,\vec{G}_2\neq\vec{G}_q}\varepsilon_{\vec{G}_q,\vec{G}_1}\left(\vec{q}-\vec{G}_q;\omega\right)\left[\varepsilon^{-1}\right]_{\vec{G}_1,\vec{G}_2}\varepsilon_{\vec{G}_2,\vec{G}_q}\left(\vec{q}-\vec{G}_q;\omega\right). \tag{4.2}$$

Table 1. Values of q and $q+G^*$ of the loss function of CrO_2 for q // [001] in units of $2\pi/c$.

$\|q\|$ (A^{-1})	$\|q+G^*\|$ (A^{-1})
0.308	2.33
0.92	1.88
1.54	1.55
1.85	1.45
2.46	1.45
3.08	1.70
3.69	2.10

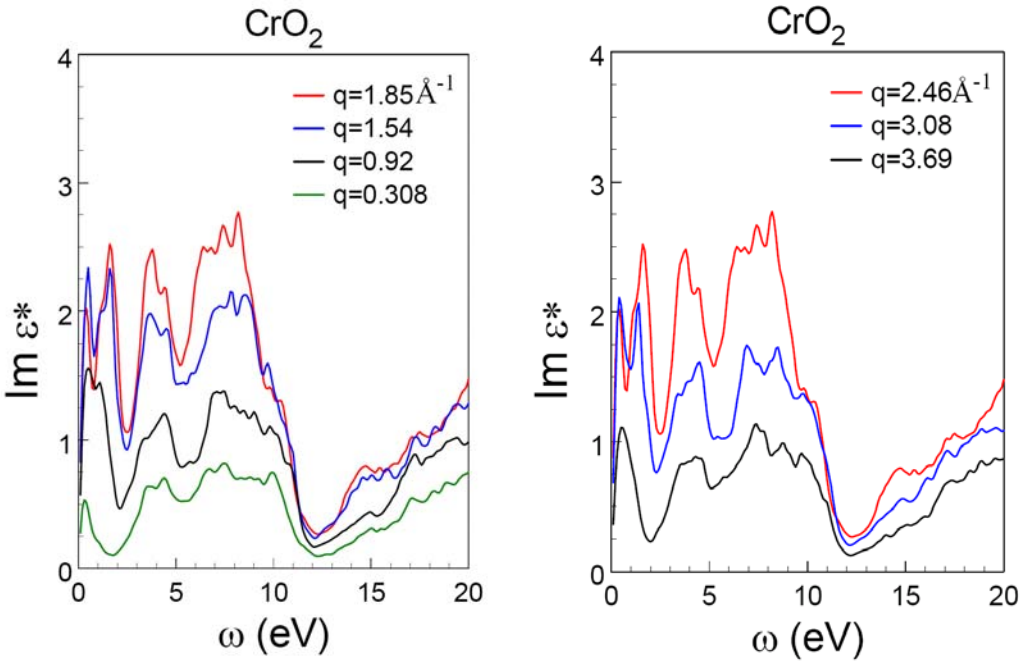

Fig. 4.2. Imaginary part of ε_{G^*,G^*} for various values of q for CrO_2.

Because of the structure of Eq. (4.2), it is clear that the inverse of the submatrix entering the right hand side, if the same is replaced by just $\varepsilon_{\vec{G}^*,\vec{G}^*}(\vec{q},\omega)$ will contain a Lorentz oscillator type of lineshape; actual calculation bears this out.

This is then the essence of the effect, which consists of the impact of the wall in $\varepsilon_{\vec{G}^*,\vec{G}^*}(\vec{q},\omega)$ in $\varepsilon_{eff}(\vec{q},\omega)$, via the inverse $1/\varepsilon_{\vec{G}^*,\vec{G}^*}(\vec{q},\omega)$.

Now it is clear that replacing the inverse of the submatrix in Eq. (4.2) by $1/\varepsilon_{\vec{G}^*,\vec{G}^*}(\vec{q},\omega)$, while it shows the main effect, is a bad approximation from a quantitative standpoint; physically, the screening effect due to the remaining elements of the 4x4 matrix in G*-space turn out to be important.

The origin of the "wall" in $\varepsilon_{\vec{G}^*,\vec{G}^*}(\vec{q},\omega)$ is traced back to the JDOS (Fig. 4.3), its energy location (~9 eV) is set by the drop-off in the JDOS as we run out of possible e_g channels. This energy scale is clearly visualized in the Cr-e_g partial DOS, associated with the "relative" location of the empty and occupied e_g states (Fig. 4.3) for both, minority and majority, spin channels. Although a sharp drop-off in the JDOS is a necessary condition for having a "wall" in $\varepsilon_{\vec{G}^*,\vec{G}^*}(\vec{q},\omega)$ it is not a sufficient condition, the strength of the imaginary part of $\varepsilon_{\vec{G}^*,\vec{G}^*}(\vec{q},\omega)$ is also controlled by the oscillator strength of the q-dependent matrix elements.

A sharper "wall" in $\varepsilon_{\vec{G}^*,\vec{G}^*}(\vec{q},\omega)$ clearly will produce a stronger peak in $1/\varepsilon_{\vec{G}^*,\vec{G}^*}(\vec{q},\omega)$ thus strengthening the magnitude (via $\varepsilon_{eff}(\vec{q},\omega)$) of the excitation at 12.5 eV in the loss function. In the case of CrO_2 the magnitude of the "wall" in $\varepsilon_{\vec{G}=0,\vec{G}=0}(\vec{q},\omega)$ diminishes as the value of q is increased, we can then ask why there is no indication of a strong excitation in the loss function spectrum for q ~0 ?, in fact it is the weakest spectrum in Fig. 4.1. The reason is simple, for q~0, the loss function can be calculated by inverting $\varepsilon_{\vec{G}=0,\vec{G}=0}(\vec{q},\omega)$ (we make the approximation $\varepsilon_{eff}(\vec{q},\omega) \approx \varepsilon_{\vec{G}=0,\vec{G}=0}(\vec{q},\omega)$ for small q's),

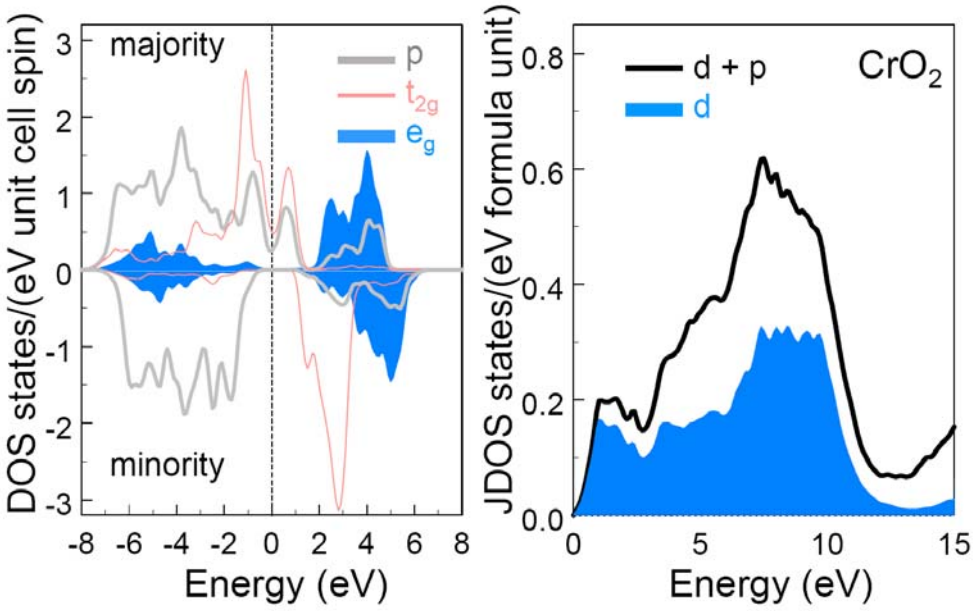

Fig. 4.3. Partial DOS and JDOS of CrO_2.

$$\mathrm{Im}\,\chi(\vec{q},\omega) = \mathrm{Im}\left[\frac{1}{v\varepsilon_{\vec{G}=0,\vec{G}=0}(\vec{q},\omega)}\right] \tag{4.3}$$

the factor $1/v$ (inverse of the coulomb term, it is proportional to q^2) is very small for q~0 thus the strong excitation produced by the "wall" in $1/\varepsilon_{\vec{G}=0,\vec{G}=0}(\vec{q},\omega)$ is greatly reduced by this factor (Fig. 4.1). In synthesis, for small q's, the magnitude of the excitation in the loss function is the product of a competition between the inverse of the Coulomb factor $1/v$ in Eq. (4.3) and the strength of the "wall" in $\varepsilon_{\vec{G}=0,\vec{G}=0}(\vec{q},\omega)$.

In Fig. 4.2 it is shown that the magnitude of the imaginary part of $\varepsilon_{\vec{G}^*,\vec{G}^*}(\vec{q},\omega)$ for q=1.85 A^{-1} is greater than for any other q's in which the excitation is present, the reason for this behavior is related to the fact that, for q=1.85 A^{-1}, $\varepsilon_{\vec{G}^*,\vec{G}^*}(\vec{q},\omega)$ corresponds to an ε with an argument $\left|\vec{q}+\vec{G}^*\right|$ closer to the origin than for any of the other q's (see Table 1), thus having a bigger "wall". The largest magnitude in the imaginary part of $\varepsilon_{\vec{G}^*,\vec{G}^*}(\vec{q},\omega)$ defines a sharper drop-off at energies near 9 eV, thus strengthening the magnitude of the excitation at 12.5 eV. It is worth noting that for large q's we can no longer talk about a competition between the factor of $1/v$ and the strength of the "wall" as the presence of the latter is relevant in $\varepsilon_{\vec{G}^*,\vec{G}^*}(\vec{q},\omega)$ and not in $\varepsilon_{\vec{G}=0,\vec{G}=0}(\vec{q},\omega)$; in fact for q=1.85 A^{-1} one can argue that the factor of $1/v$ is not competing with the strength of the "wall" but rather helping to have a strong excitation at 12.5 eV.

The CLFE and eg contributions to the collective mode in CrO2 are shown in Fig. 4.4.

4.2 Momentum Dependence in the Density Response of $CaMnO_3$

In order to confirm the generality of our method based on the analysis of $\varepsilon_{eff}(\vec{q},\omega)$ to account for the physics of the loss function in strongly inhomogeneous systems we have also performed calculations of the response function of anti-ferromagnetic $CaMnO_3$ for various wave vector transfers along the [001] and the [111] directions. We have used as our starting point the ground state obtained by using the LSDA+U method with U=4 eV.

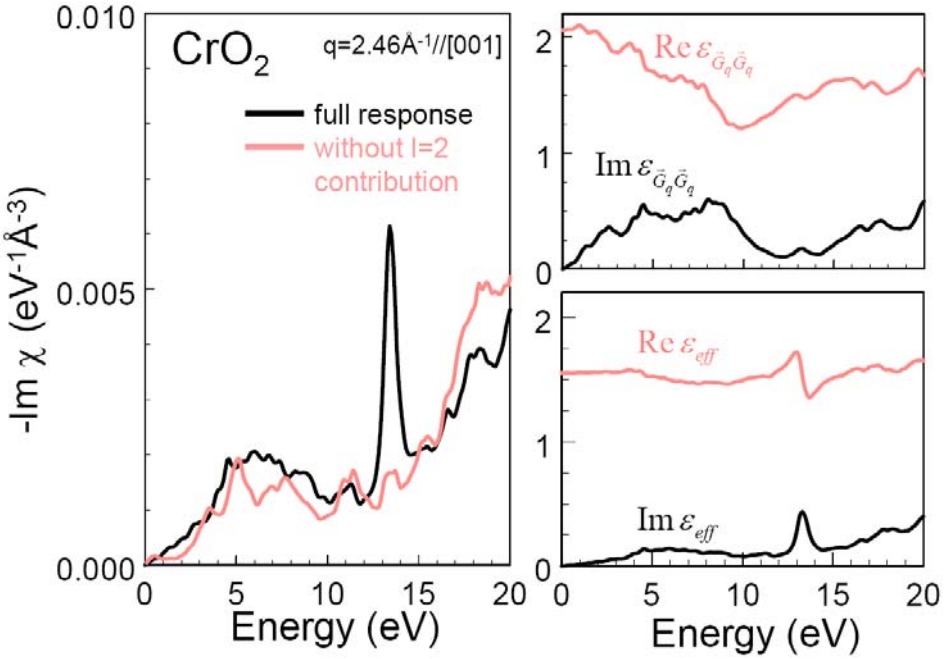

Fig. 4.4. CLFE and e_g contributions to the collective mode in CrO_2. The left panel illustrates how the collective electron-hole state is suppressed if the *d-d* transitions at the Cr sites are eliminated from Kohn-Sham response function. The right panel illustrates that the collective mode is due to the impact of the crystal local field effects due to strong charge inhomogeneity.

We have plotted in Fig. 4.1. Imaginary part of the dynamical density response function for CrO2, CaMnO3 and LaMnO3, for a large range of wave vector transfers. The most striking feature of the calculated spectra is the sharp collective electron-hole state discussed in the text, and whose genesis is ultimately the sharp drop in the JDOS illustrated in Fig. 4.3, there is a large impact of the crystal local fields in the loss function of $CaMnO_3$. Similar to the case of CrO_2, for q along the [111] direction, an excitation at 12 eV is generated by the matrix calculation. Interestingly, the loss spectra for q along the [001] although it also shows an excitation not present in the scalar calculation the same is much smaller than the one present for q's along the [111] direction (Fig. 4.5). It is then immediate to ask if our method based on the analysis of $\varepsilon_{eff}(\vec{q},\omega)$ will explain not only the appearance of these excitations in the loss function but also their directional dependence. We will show that indeed our approach accounts for both aspects of the observed physics.

By investigating $\varepsilon_{eff}(\vec{q},\omega)$ for q's along the [111] direction we found a subspace of G*-vectors that turns out to be the relevant one to account for the observed excitation. It consists of the shell of G-vectors defined by [-2 0 0] [0 -2 0] and [0 0 -2], again, as in CrO_2, these G*-vectors lead to an "Umklapp" process, for the range of q's where the excitation is present, in which the magnitude of $|\vec{q}+\vec{G}*|$ is smaller than the magnitude of q (see

Table **2**). The essential physics is contained in the diagonal elements of the G* shell ($\varepsilon_{\vec{G}*,\vec{G}*}(\vec{q},\omega)$). In Fig. 4.6 these elements are shown for 3 q's, the relevant feature in this plot is that all the elements have a sharp "wall" in the range of 10 eV, the same type of feature found in CrO_2! As shown in Fig. 4.7 the partial JDOS for the Mn-eg states exhibits a drop-off near 10 eV induced by the depletion of eg channels. This energy scale is clearly set by the "global" location of the eg states (see Fig. 4.7). It is important to note at this point that by contrast, in the case of monoxides, such as NiO and CoO, the JDOS does not have a well defined "wall" like in the rutiles and manganites. Indeed, as can be seen in the partial DOS for NiO shown in Fig. 4.7, the O-p derived states and the e_g-states do not hybridized, i.e., one can talk of a three band system where the O-p states occupy a third band just below the Ni-d band. As a result, the JDOS in NiO does not have

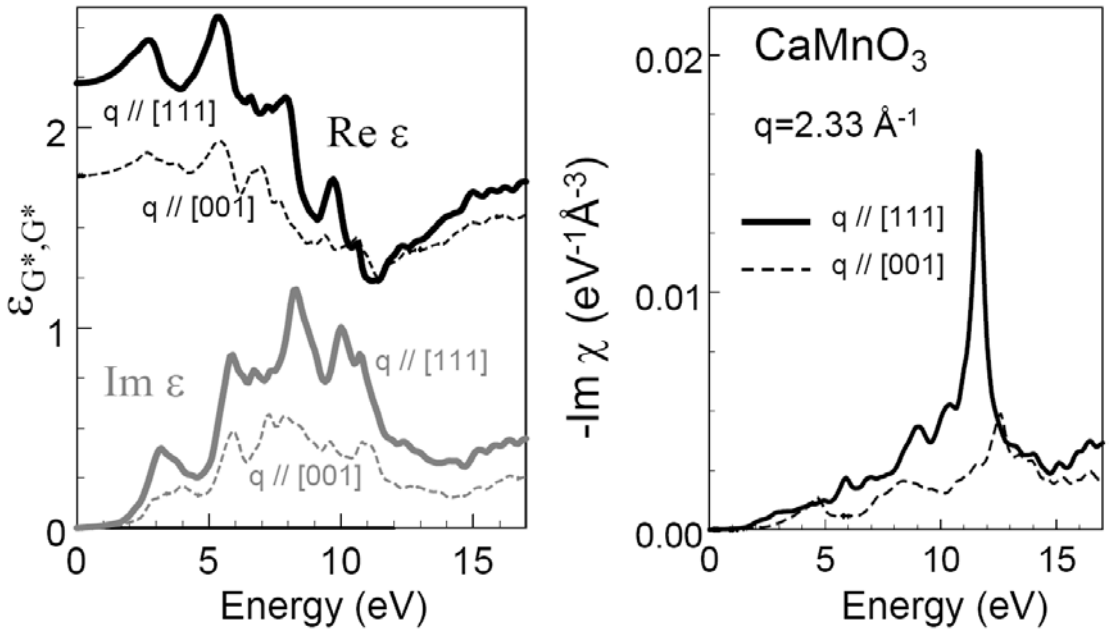

Fig. 4.5. The strongest drop-off in ε_{G^*,G^*} for q's // [111], due to a larger overlap of the electron and hole wave functions (matrix elements), accounts for the larger magnitude of the excitation at 12 eV compared with q's // [001].

Table 2. Values of q and $q+G*$ of the loss function of $CaMnO_3$ for q // [111] in units of $2\pi/a$.

$\|q\|$ (A^{-1})	$\|q+G^*\|$ (A^{-1})
0.29	1.53
0.87	1.37
1.16	1.38
1.74	1.58
2.04	1.74
2.33	1.93
2.62	2.15
3.2	2.68

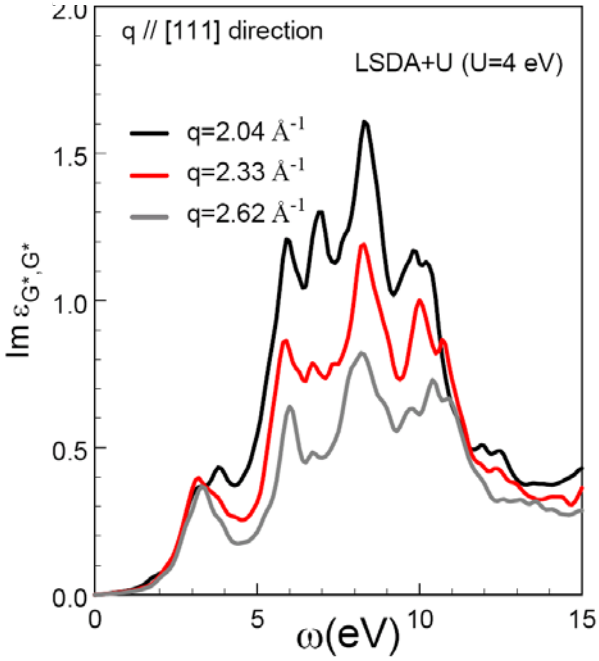

Fig. 4.6. Imaginary part of $\varepsilon_{G*,G*}$ for various values of q for $CaMnO_3$.

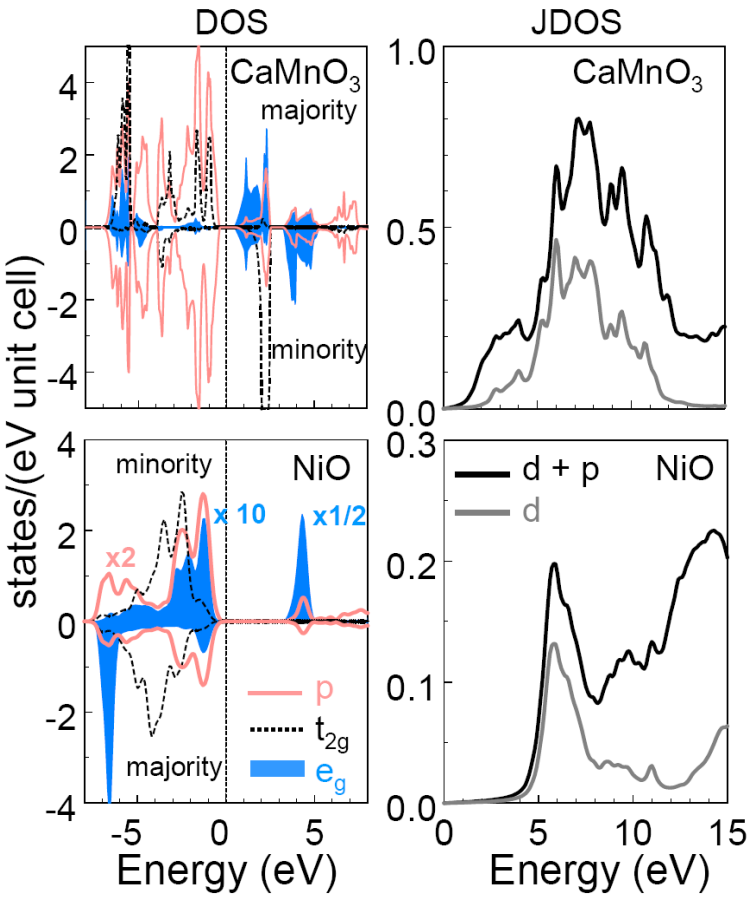

Fig. 4.7. Density of states (DOS) and joint density of states (JDOS) for CaMnO3 and NiO. The case of CaMnO3 (left panels) typifies materials for which the excitation channels involving *pp* processes at the O sites *cooperate* with channels involving *dd* processes at the cation sites. As a result, the excitation band structure corresponds to the *two-band* picture put forth at the outset —which leads to collective-mode formation. By contrast, the case of NiO (right panels) typifies materials for which the former channels *compete* with the latter, corresponding to a three band excitation picture which does not lead to collective mode formation. Note that whether a material belongs to either class is determined by the *pd* hybridization (or absence of it) toward the bottom of the band of e_g states.

a sharp drop-off since the partial JDOS for the O-p states interferes with the "natural" drop-off that will originate if we take into consideration only the occupied and empty d bands (see Fig. 4.7).

Performing calculations in $CaMnO_3$ with only a diagonal G* shell in $\varepsilon_{eff}(\vec{q},\omega)$ clearly induces an excitation but the screening effects of the complete G* shell are needed to account for the appropriate energy location (to recover the strength of the excitation it is actually necessary to consider more terms in $\varepsilon_{eff}(\vec{q},\omega)$ combining G*-vectors with G-vectors from nearby shells).

Now, let us turn our attention to the loss spectra for q's along the [001] direction; in Fig. 4.5 it is shown that the loss function has a small excitation around 12.5 eV. This excitation is much smaller than the one present for q's along the [111] direction. What is the reason for this anisotropy? Again, making use of our definition of $\varepsilon_{eff}(\vec{q},\omega)$ we have found that the G*-vectors responsible for this small excitation are [-2 -2 -2], [2 -2 -2], [-2 2 -2] and [2 2 -2], although these vectors have a negative z-component, which would lead to an "Umklapp" process in the z-direction they do not necessarily lead to a smaller magnitude for $|\vec{q}+\vec{G}*|$ compared to q. As we have discussed previously, the smaller the value of $|\vec{q}+\vec{G}*|$ the sharper the "wall" will be. A comparison of the imaginary part of $\varepsilon_{\vec{G}*,\vec{G}*}(\vec{q},\omega)$ for q's along the [001] direction vs. q's along the [111] direction (Fig. 4.5) shows how the "wall" is much stronger in the latter case, leading to a better defined excitation in the loss spectra. In Fig. 4.8 we show a typical Electron-hole pair that enters the calculation of the matrix elements that contribute to the formation of the "wall" for energies ~10 eV. One can see that near the Mn sites the orbital state has an "e_g-like" symmetry.

Significantly, in view of available wave-vector resolved inelastic x-ray scattering (IXS) data for $LaMnO_3$ [28], the picture of the electron-hole excitations which comes out of our calculations differs drastically from assignments made from the knowledge of just the (correlated-) band structure. Indeed, our results illustrate the fact that dynamical screening effects must be accounted for, before peak-assignment can be made. The dynamical screening in the compounds of interest is found to be controlled by crystal local-field effects (CLFE) due to strong charge inhomogeneity. As a consequence, the

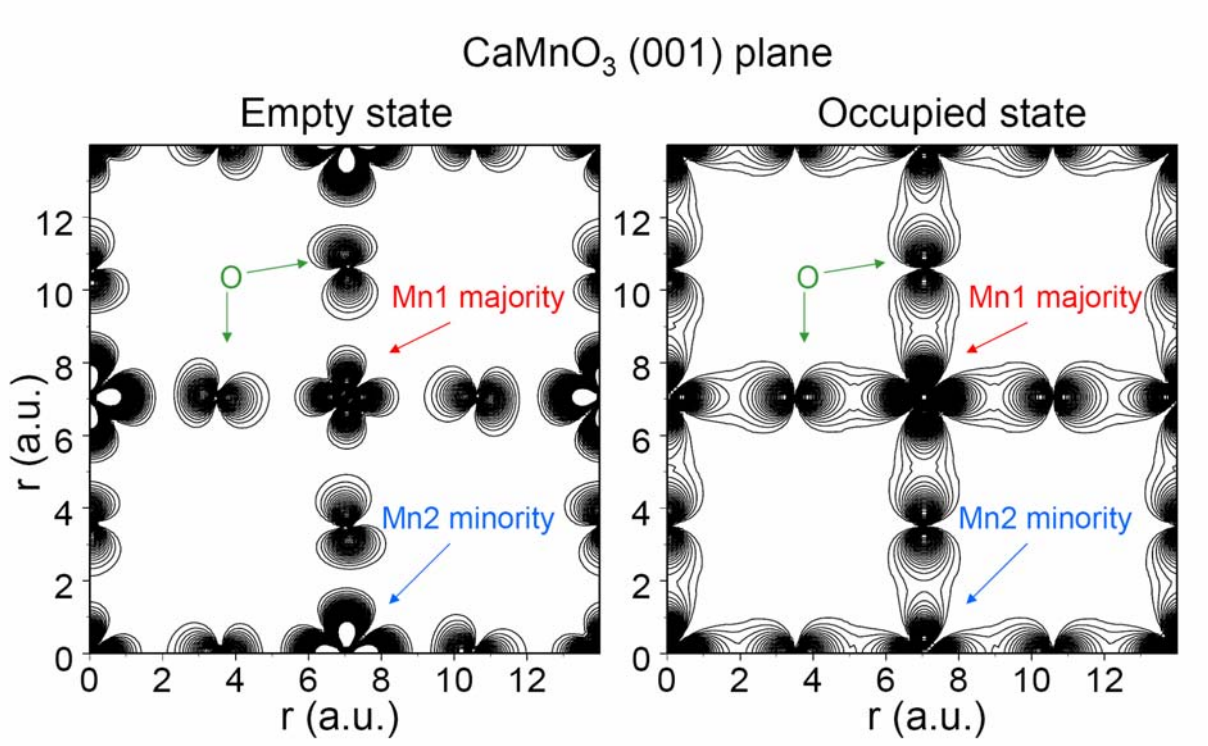

Fig. 4.8. Electron-hole states of the matrix elements that contribute to the "wall" in the imaginary part of ε at energies ~9 eV.

electron dynamics differs from expectations based on the simple dielectric function usually invoked even in complex materials. Incidentally, the size of the CLFE renders the collective excitation discussed in this chapter so prominent that it should be observed via *non-resonant* IXS [29]. The CLFE and e_g contributions to the collective mode in $CaMnO_3$ are shown in Fig. 4.9.

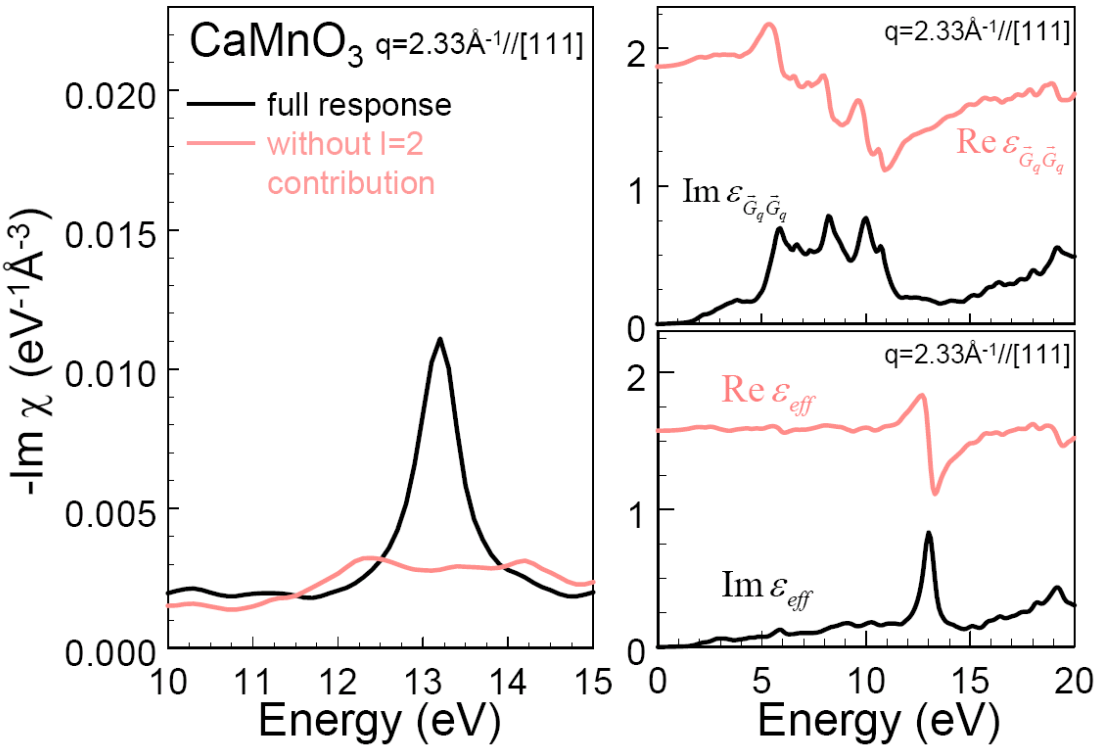

Fig. 4.9. CLFE and eg contributions to the collective mode in CaMnO3. The left panel illustrates how the collective electron-hole state is suppressed if the *d-d* transitions at the Mn sites are eliminated from Kohn-Sham response function. The right panel illustrates that the collective mode is due to the impact of the crystal local field effects due to strong charge inhomogeneity.

Chapter 5 Charge Density Response in $Na_{1/3}CoO_2 \cdot yH_2O$

The recent discovery of superconductivity on the system $Na_xCoO_2 \cdot yH_2O$ for x~1/3 when intercalated with water [30] (T_c=4.5 K) has led to intense research aiming to understand its superconductive properties. The parent compound exhibits unusually high thermoelectric properties and is the subject of various studies to understand the origin of the high thermoelectric effect. Na_xCoO_2 has a very rich phase diagram, it is a Curie-Weiss metal for $0.5 < x < 1$, a charge transfer insulator at $x = 0.5$ and a normal paramagnetic metal for $x < 0.5$. An accurate description of the electronic structure associated with the Co 3*d* and O 2*p* bands in this complex material becomes a key issue. The correlation problem and its impact on the nature of the ground state has been addressed recently [23] via correlated-band theory (LDA+U method). It has been shown that charge disproportionation and gap opening occur for values of the "Hubbard U" larger than 3 eV, although experimentally at x~1/3 the parent compound is actually a metal.

The crystal structure of the parent compound consists of quasi two-dimensional CoO_2 sheets, with intercalated Na ions; the Co ions form a triangular lattice. Na donates its electron to the CoO_2 planes, the doping level of the plane is then controlled by the Na concentration. In the presence of layers of water molecules, at x=1/3, becomes a (possible unconventional) superconductor. The Sodium Cobaltate with water, with 44 atoms in the unit cell represents a significant upgrade of previous calculations; we had to upgrade our (parallel) Fortran90 code that calculates χ_S to handle correctly the memory requirements for this system.

We study the electron-hole pair excitations for the hydrated and non hydrated compounds at x=1/3 since they provide signatures of the electronic structure. In the optical limit the water molecules are shown to change the screening properties (thus, the effective electron-electron interaction) in the loss function for small energies. For large

values of momentum transfer the hydrated and non-hydrated compounds show very similar spectra, mainly this is due to the fact that the effect of the presence of the water molecules on the screening properties becomes small. We compare our results with EELS data [26,27].

We start by comparing the band structures of the hydrated and non-hydrated systems. If we consider a crystal structure, in the hydrated case, that does contain inversion symmetry; the band structures at small energies are very similar in these two cases (see Fig. 5.1); the water molecules do not seem to affect the energy levels near the Fermi Level. By considering a hydrated crystal structure without inversion symmetry (the positions of the water molecules are taken from J. D. Jorgensen et al. [24]) the comparison with the non-hydrated case is not as clean as in the previous case. In Fig. 5.2, the Density of States of the hydrated and non-hydrated systems (with and without inversion symmetry) is very similar indicating that indeed the presence of the water molecules has a very small effect in the electronic structure near the Fermi Level. The water molecules contribute to the interstitial DOS for energies larger than 4 eV.

In Fig. 5.3 it is shown how the CLFE induced excitation near 8 eV in the loss spectra has a non-monotonic q-dependence in both the hydrated and non-hydrated compounds. The collective excitation in these compounds occurring at 8 eV involves d-d transitions and it starts to become increasingly small after 4 $Å^{-1}$. The O-p derived transitions in these compounds enhance this excitation since a strong hybridization exists between the O near the cobalt planes and the Co (Fig. 5.2).

In the optical limit (Fig. 5.4) there is a strong and well defined collective mode induced by the CLFE in the non-hydrated material at 10 eV involving d-d transitions. This result is striking since is the first time we encounter such large CLFE for small values of q! As we have seen in Chapter 4, this type of results occurred in Manganites and rutile structures only for large values of momentum transfers.

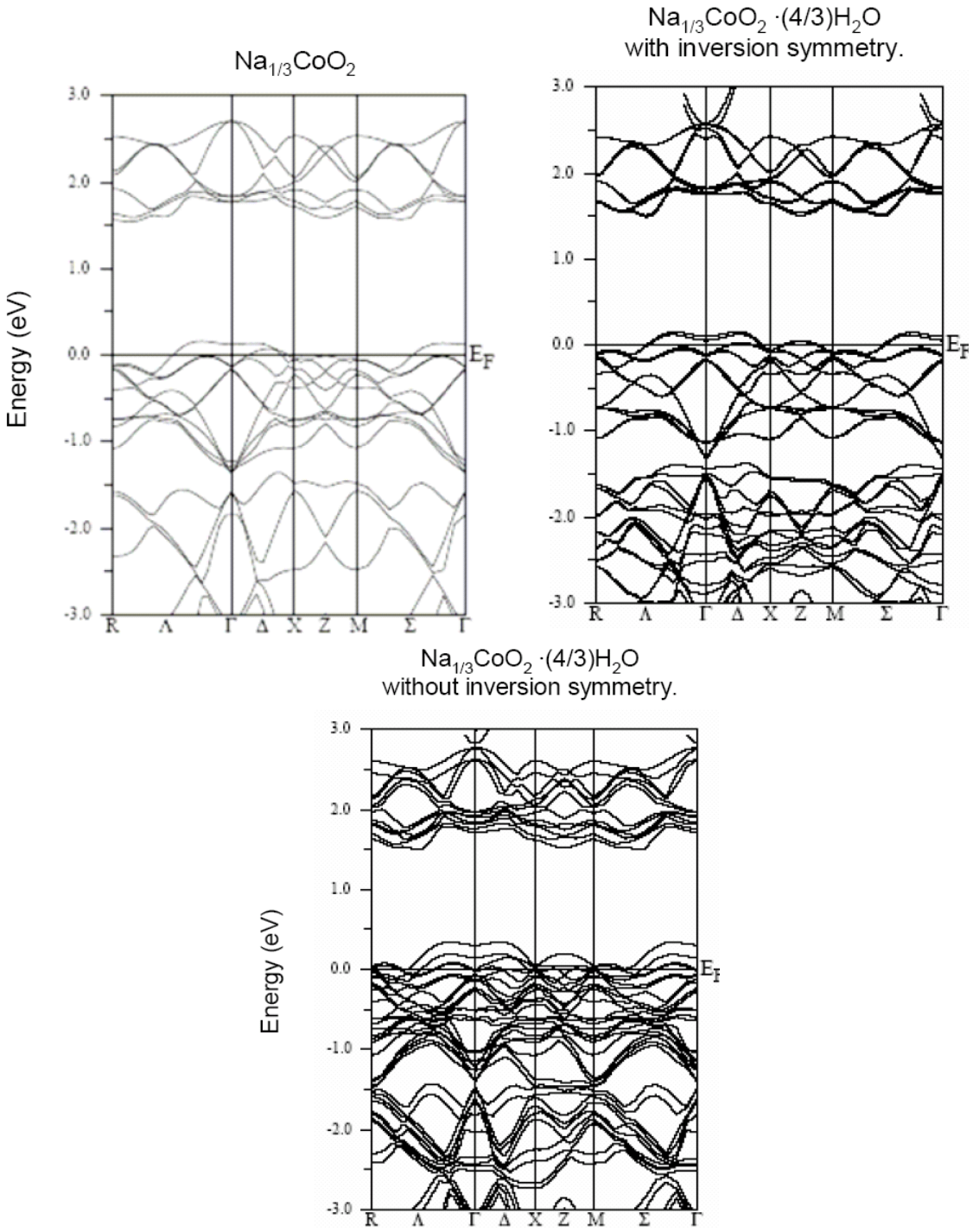

Fig. 5.1. The band dispersion of the hydrated system with inversion symmetry is very similar to the non-hydrated system.

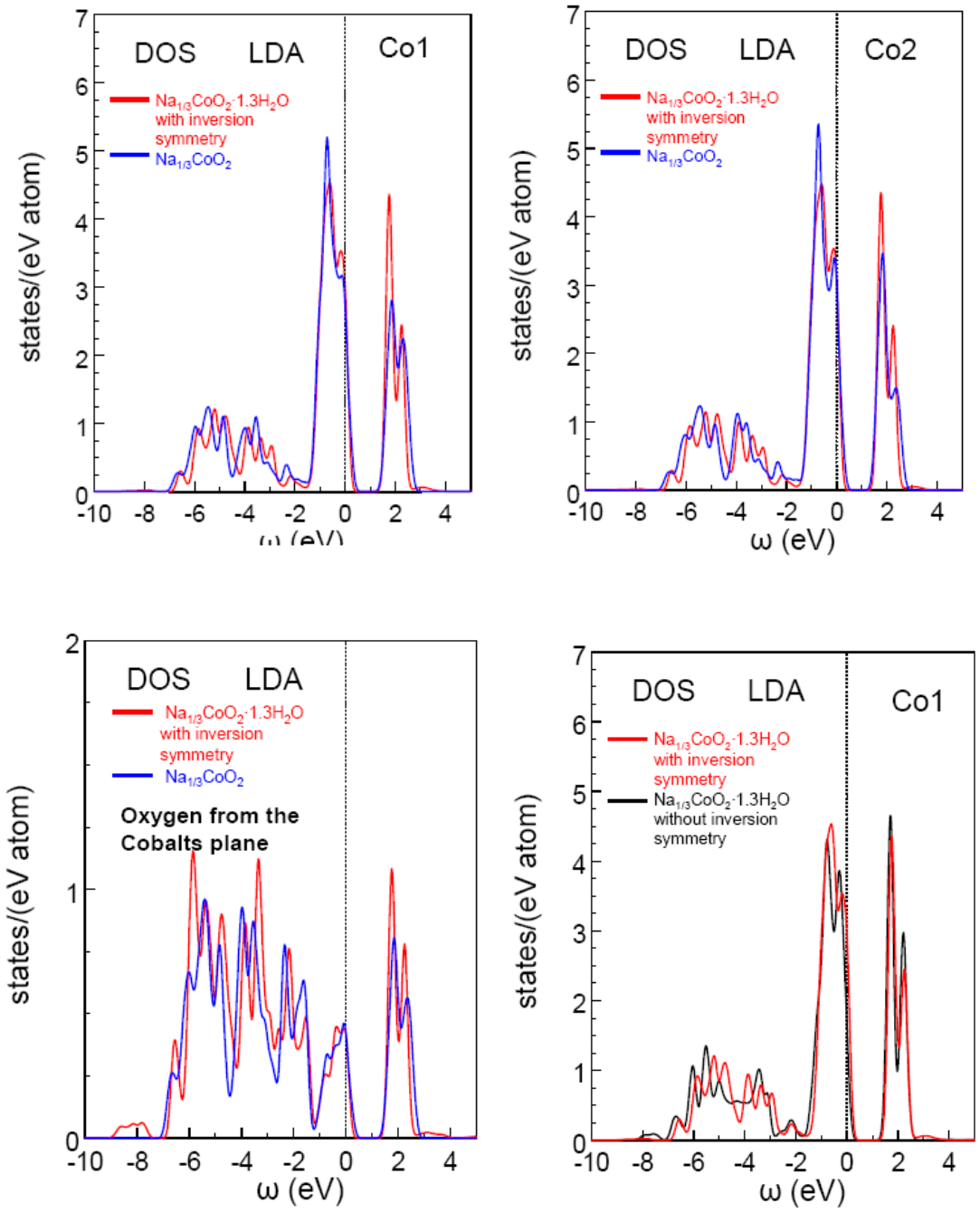

Fig. 5.2. The DOS from the Co and O layers is very similar for both hydrated (with or without inversion symmetry) and non-hydrated systems.

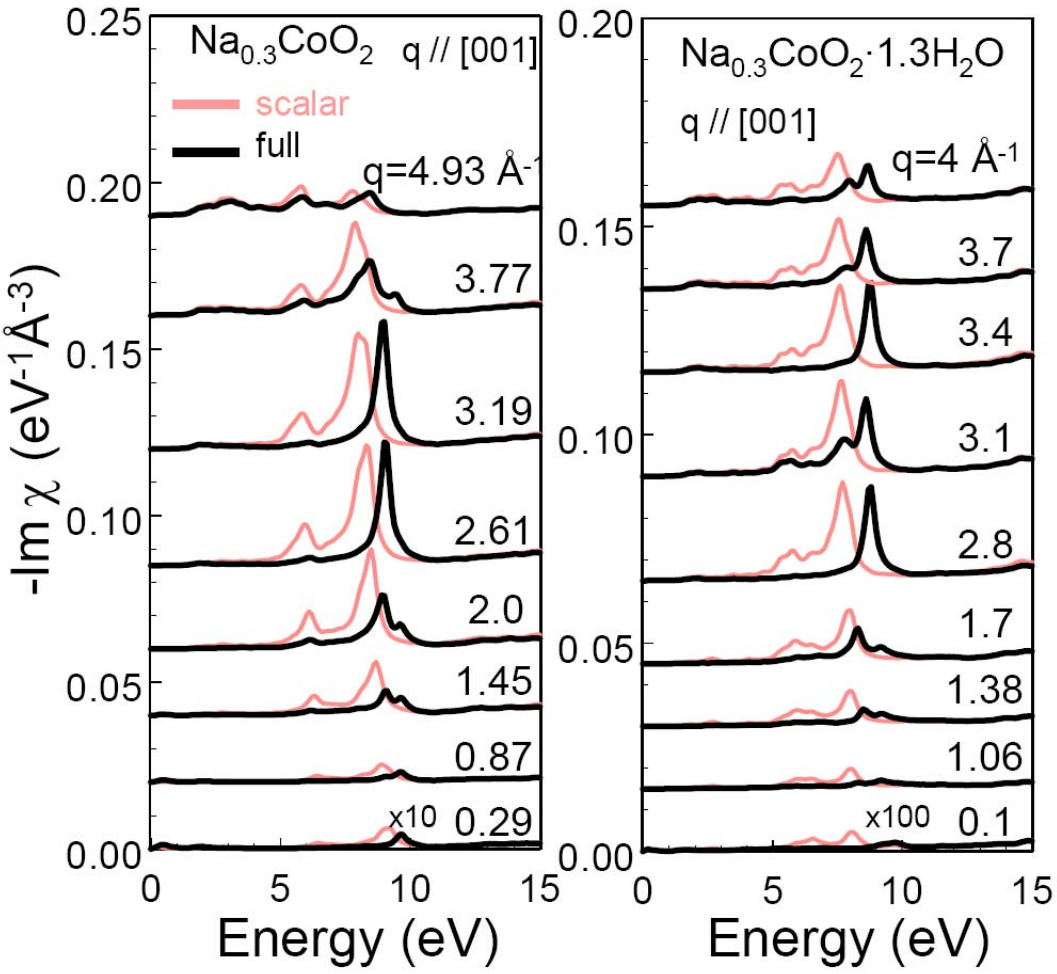

Fig. 5.3. Large Crystal Local Field Effects (CLFE) in the density response function for all values of momentum transfer q in both compounds (the calculations for the hydrated material are done with a structure that has inversion symmetry).

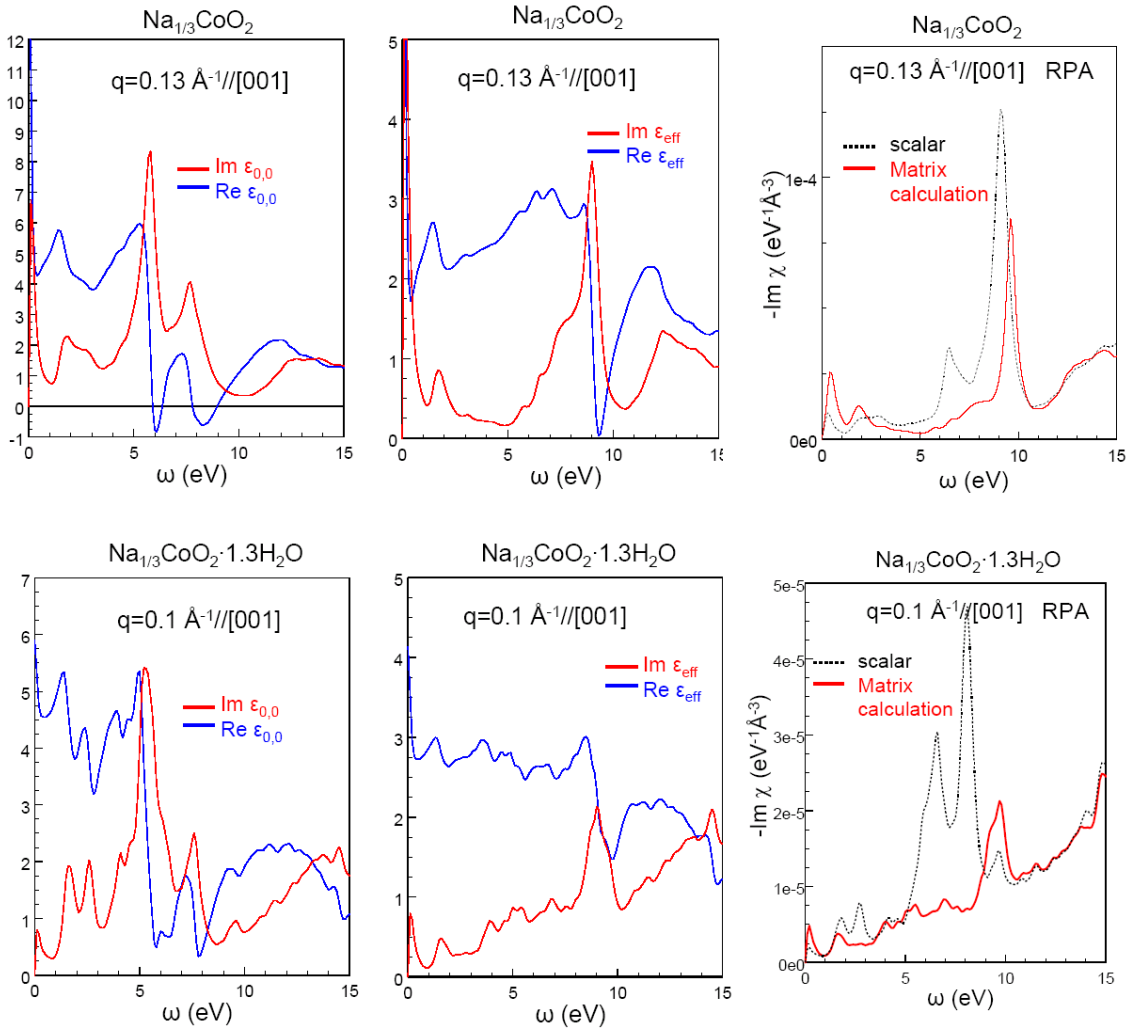

Fig. 5.4. Evidence of large Crystal Local Field Effects (CLFE) in the optical limit for both compounds (the plots for the hydrated material correspond to the case where the system has inversion symmetry). This shows the impact of the strong crystal potential along the [001] direction on the non-diagonal elements of the dielectric matrix. The presence of water makes the electronic screening weaker as seen by comparing the Re ε_{eff} for each system.

These findings are consistent with the existence of a strong crystal potential along the [001] direction in the Sodium Cobaltates; one can argue that this strong potential is responsible for the strong CLFE observed for small q's since it allows strong charge coupling along the z direction. At small q's the changes in the screening effects due to the polarization of the water in the hydrated system leads to a much weaker d-d collective excitation induced by the CLFE at ~10 eV (in comparison to the strong excitation at 10 eV in $Na_{0.3}CoO_2$) (see Fig. 5.4). Also the excitations between 5 and 7 eV, in the hydrated system, arise from single-particle transitions; this excitations are absent in the non-hydrated system. The predicted electron hole-pair excitation involving t_{2g} electrons at low energies in $Na_{0.3}CoO_2$ is not present in the hydrated system without inversion symmetry (Fig. 5.5), indicating that further theoretical tests have to performed to understand the differences at small energies between the compounds with and without inversion symmetry and to be able to perform a reliable comparison with the unhydrated system.. We compare our results with the experiments performed by H. X. Yang et al. who have calculated ε based on experimental data [26] and also using the WIEN2k code [27]. In constrast with their results we show that the CLFE are crucial for obtaining the correct theoretical spectrum in the optical limit.

For large q's there is still strong impact of the CLFE (Fig. 5.6) in both the hydrate and non-hydrated compounds. This result was somehow expected since we have already seen Chapter 4 that for complex materials such as the rutiles and the manganites the CLFE play a significant role in obtaining the correct spectra at large q's. A comparison of the density response of the hydrated system with and without inversion symmetry leads to very similar results; although the result with inversion symmetry seems to still have some reminiscence of the excitation involving t_{2g} states at small energies (~0.5 eV) for the non-hydrated compound.

In Fig. 5.7 it is shown how the loss function for the hydrated and non-hydrated compounds are very similar at large q's, this resemblance is traced to the fact that the water molecules only affect the screening for small values of q.

In summary, we have calculated the electron-hole excitations in the hydrated and non-hydrated Sodium Cobaltates compounds for Sodium concentrations of 1/3. In both types

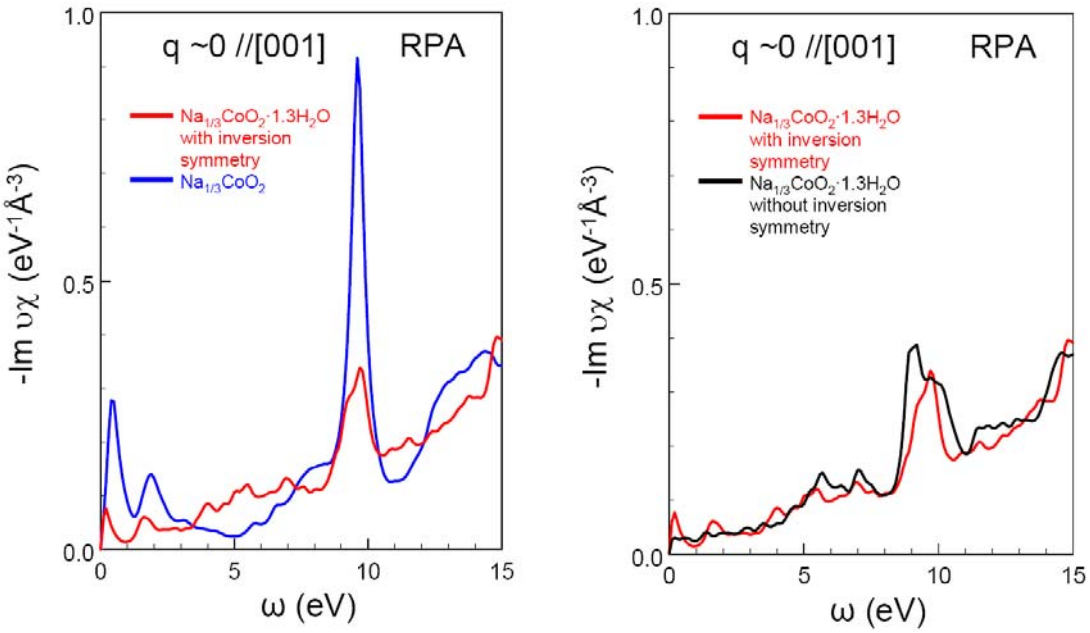

Fig. 5.5. In the optical limit there is a strong and well defined collective mode induced by the CLFE in the non-hydrated material at 10 eV involving d-d transitions. The O-p derived transitions in this compound enhance this excitation. The predicted electron hole-pair excitation involving t_{2g} electrons at low energies in $Na_{0.3}CoO_2$ is not present in the hydrated system without inversion symmetry.

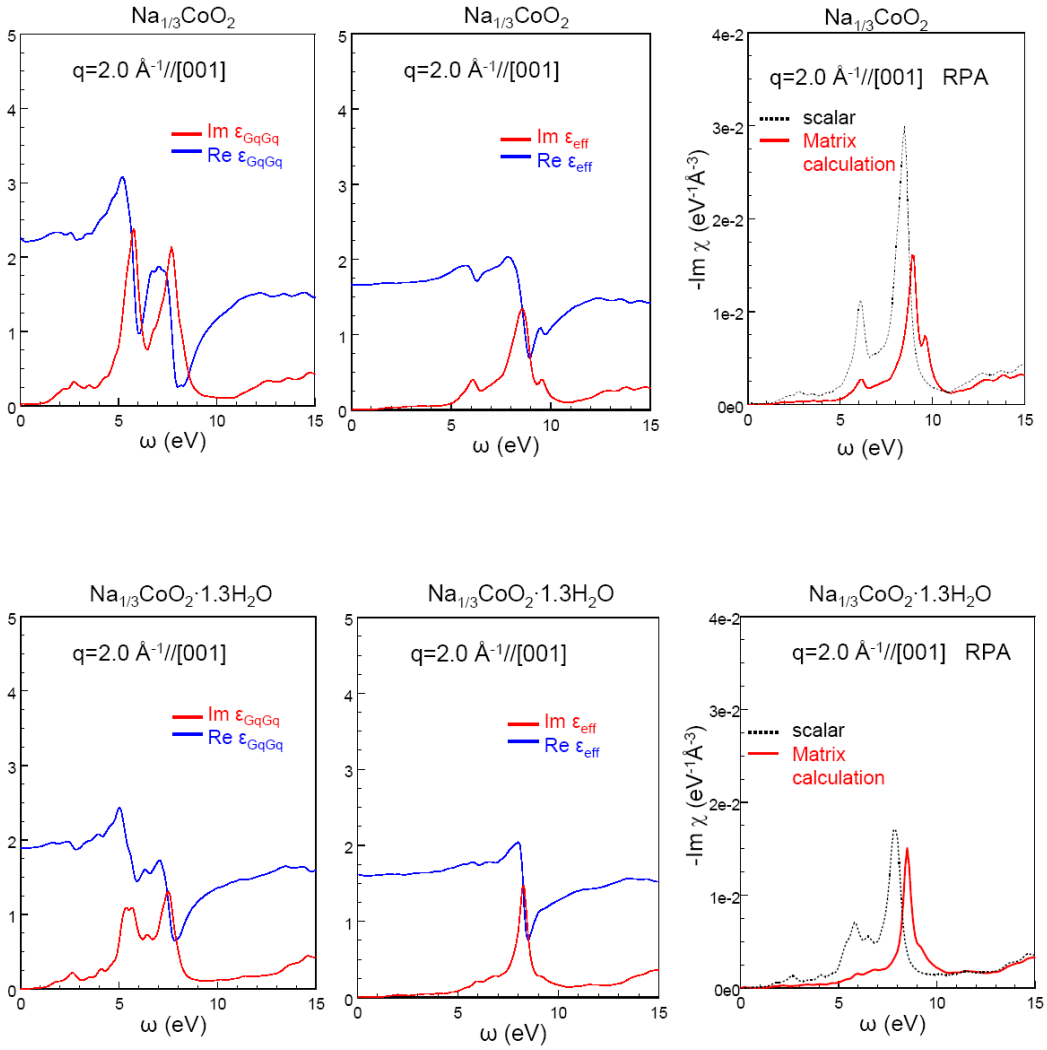

Fig. 5.6. For large q's there is still strong impact of the CLFE. The polarization of the water molecules is greatly reduced making the density response function of both systems not very different. For this large value of q the loss function is dominated by the d-d collective excitation at 8-9eV.

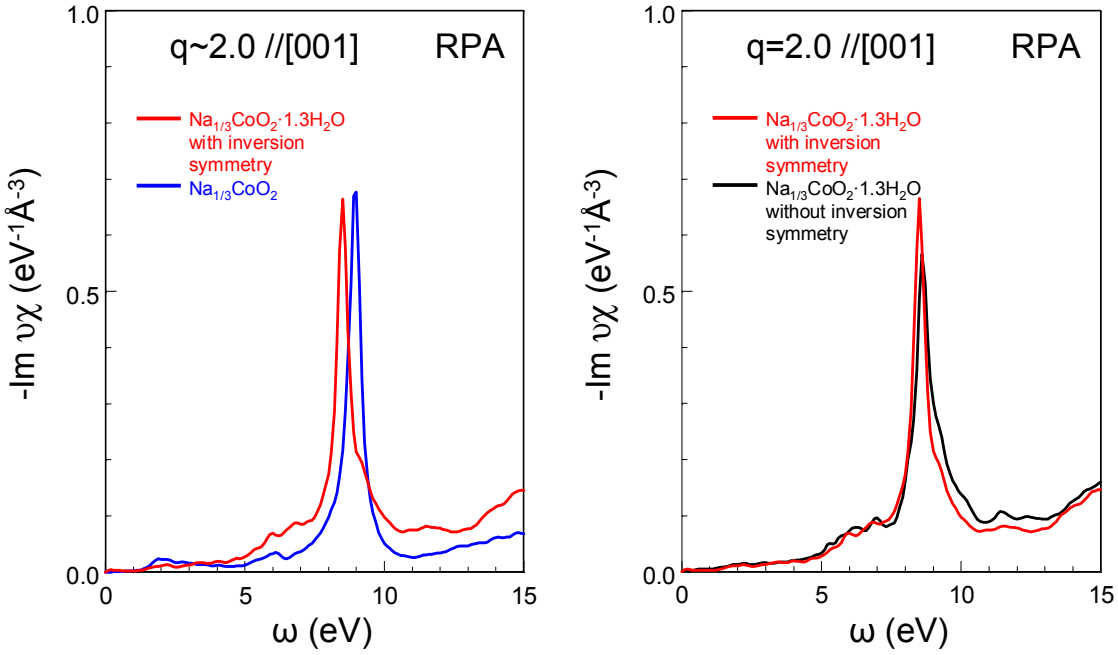

Fig. 5.7. For large q's the density response function for both compounds looks very similar due to the reduced polarizability of the water molecules.

of compounds we find a d-d collective excitation at 9 eV induced by the CLFE for a large range of momentum transfers. It is shown how the inclusion of the water affects the screening at small energies for small momentum transfers, allowing single-particle transitions to be present in the loss spectrum. For large values of momenta the loss function for the hydrated and non-hydrated systems are very similar due to the reduced polarizability of the water molecules.

Chapter 6 Electron-Hole Excitations in NiO[1]

The failure of LSDA to account for the strong correlations in materials like NiO, that has an experimental gap of 4 eV [32] but it is predicted to be a semi-conductor with a gap of 0.3 eV by DFT-LSDA calculations, has led to strong theoretical interest in the development of new methods that handle correlations in this system in a proper way [31]. In this chapter we evaluate the performance of the LSDA+U functional via calculations of the electron-hole excitations in NiO, which are compared with non-resonant inelastic X-ray scattering (IXS) and ellipsometry measurements. We also show results for CoO for large momentum transfer compared with experimental data at the end of the chapter.

We start with reference to Fig. 6.1, which contains a key message, at the outset. The figure shows the measured $s(\vec{q};\omega)$ for a representative wave vector transfer, together with two calculations of the same quantity (Eq. (2.12)), obtained starting from LSDA and LSDA+U ground states, respectively, from which χ_s was evaluated, and the response χ was subsequently obtained by solving the integral Eq. (2.8) within RPA [33]; in the case of the LSDA+U ground state, this is what we are going to refer to as the LSDA+U/RPA method. The LSDA+U–based calculation here corresponds to the choice $U = 8\,\mathrm{eV}$, which is the value suggested by constrained-DFT calculations (implemented in LSDA) [34].

Fig. 6.1 highlights in a striking way the qualitative failure of the LSDA description of the electronic structure of NiO. Indeed, the LSDA–based spectrum not only displays the well-known problem of the size of the optical gap, but the whole line shape of $s(\vec{q};\omega)$ is completely off, containing spurious peaks. By contrast, the LSDA+U–based $s(\vec{q};\omega)$ works remarkably well (other than the exaggerated value of the calculated electron-hole

[1] Most of this chapter is taken from an article we have published recently [43].

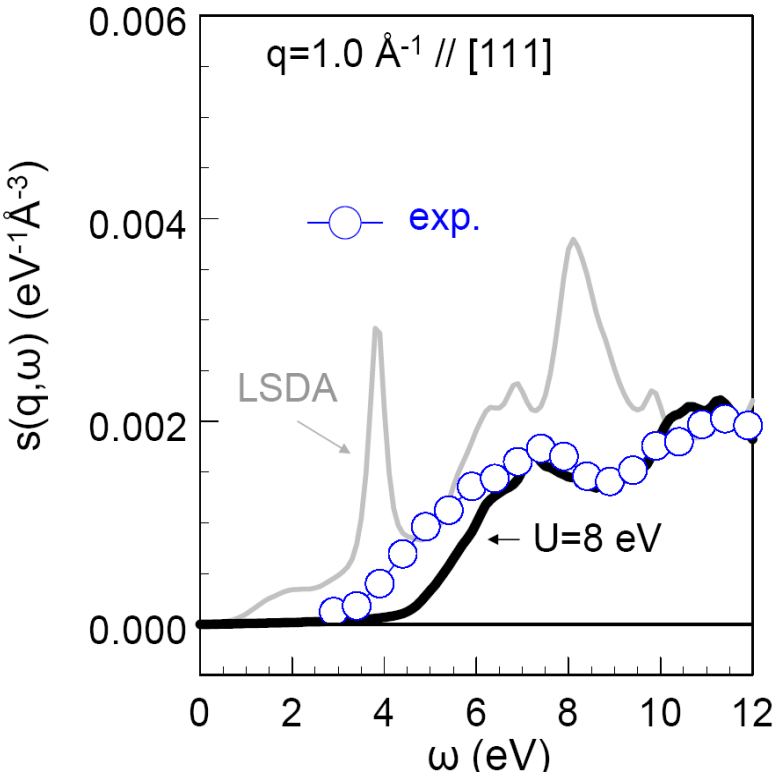

Fig. 6.1. Comparison of the measured $s(\vec{q};\omega)$ for NiO for $|\vec{q}| = 1.0\text{Å}^{-1}$ along [111] with results on the basis of LSDA and LSDA+U ground states.

gap), which argues in favor of the quality of the underlying LSDA+U electronic structure. This message will be emphasized further in the remainder of this presentation.

Fig. 6.2 shows the experimental $s(\vec{q};\omega)$ covering a range of wave vector transfers along the [111] direction. It is apparent that the dominant feature above the ~ 4 eV optical gap is a loss lying at ~ 7.5 eV. Interestingly, the spectral weight of this loss depends rather markedly on wave vector transfer; in fact (not shown in Fig. 6.2), the loss is not observed for small q's, and is diminished for q's larger than about $2\,\text{Å}^{-1}$.

The central issue contained in Fig. 6.3 is that the $s(\vec{q};\omega)$ calculated within LSDA+U/RPA for $U = 8\,\text{eV}$ reproduces the IXS data faithfully, for all three wave vectors. We will argue that this agreement is rooted on the physics of the 7.5 eV excitation, i.e., the agreement is not "accidental." This will allow us to conclude that the experimental data of Fig. 6.2 measures (indirectly) the LSDA+U electronic structure of Fig. 6.4 which corresponds to $U = 8\,\text{eV}$. (Consistent with this, it is self-suggestive that the LSDA+U/RPA spectrum obtained in Fig. 3 for $U = 5\,\text{eV}$, a value which we consider in this paper for illustrative/pedagogical purposes, clearly mis-represents the physics contained in the data of Fig. 6.2)

In Fig. 6.4 we display what turns out to be the key subset of the electronic structure of NiO which is at stake in the present argument. The same refers to minority e_g states, for which the left panel shows the density of states (DOS), and the right panel shows the joint density of states (JDOS). That the minority states are favored in this argument in place of the majority states is traced to the fact that the former provide a more abundant supply of empty states. Incidentally, note that this statement illustrates the fact that our investigation probes the empty states on the same footing with the occupied states, thus providing a "one shot" investigation of the whole correlated–band structure in the vicinity of the optical gap.

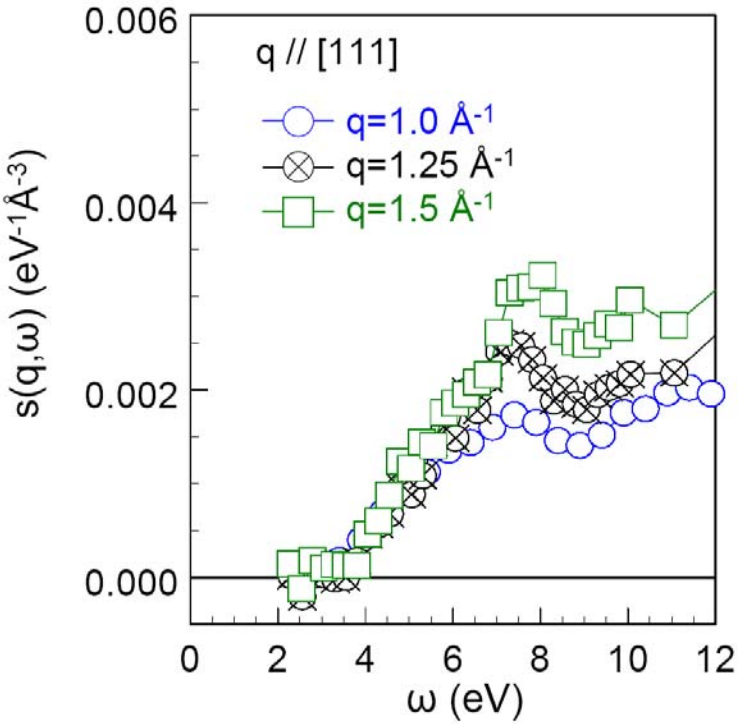

Fig. 6.2. IXS data for $s(\vec{q};\omega)$ for three wave vectors directed along the [111] direction.

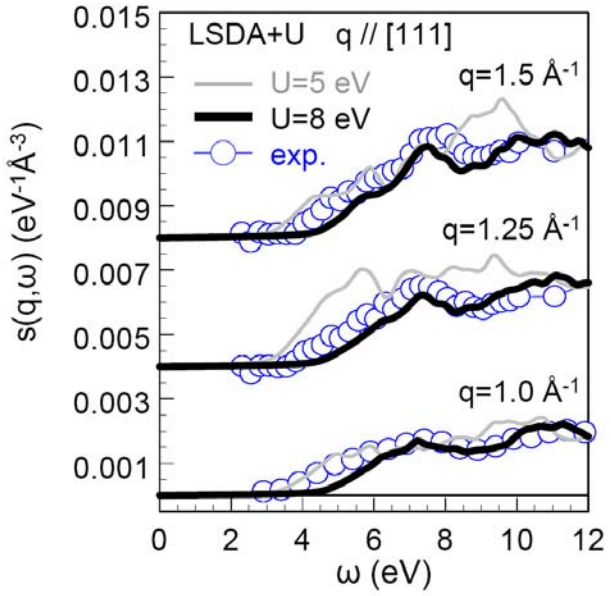

Fig. 6.3. Comparison between calculated $s(\vec{q};\omega)$ and the IXS data of Fig. 6.2.

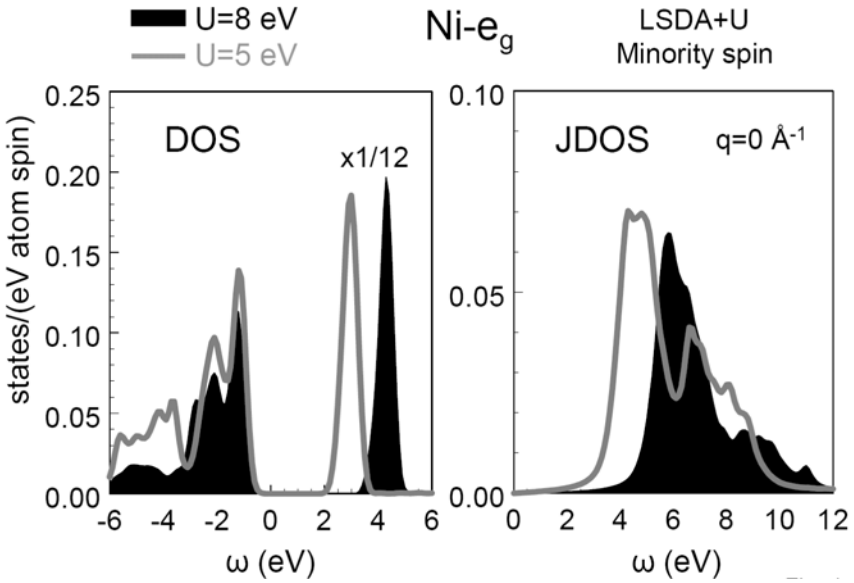

Fig. 6.4. LSDA+U calculated DOS (left panel) and JDOS (right panel) for the minority Ni-derived e_g states.

Fig. 6.5 shows the dielectric function of NiO for one of the q's relevant in Fig. 6.2 (actually, the figure displays the $\vec{G}=0,\vec{G}'=0$ element of the dielectric matrix; the same contains the main physics, in the present case). The feature which dominates the physics contained in Fig. 6.5 for q along [111] is the sizeable hump (structured peak) in $\mathrm{Im}\,\varepsilon$. *It is important to notice that the same correlates well with the corresponding e_g–e_g feature in the JDOS (Fig. 4) which obtains for* $U=8\,\mathrm{eV}$. (Note that this is consistent with the statement made in the previous paragraph about the subset of the electronic structure shown in Fig. 6.4 providing the crucial electron-hole channels.) Now an $\mathrm{Im}\,\varepsilon$ with this lineshape determines, by the structure of the Kramers-Kronig relation, a $\mathrm{Re}\,\varepsilon$ whose energy dependence is dominated by the pronounced "wiggle" observed in Fig. 6.5 —and this wiggle *occurs in the energy interval relevant in* Fig. 6.2.

A dielectric function with a lineshape such as that of Fig. 6.5 is known to be a good candidate for bringing about a well-defined peak in the inverse dielectric function [37] — without the need for the existence of an actual zero in $\mathrm{Re}\,\varepsilon$. Since the inverse dielectric function is proportional to $\mathrm{Im}\,\chi$, such peak (if it is realized) translates into a loss peak in $s(\vec{q};\omega)$, according to Eq. (9). And this is precisely what comes out of the full LSDA+U/RPA calculations (via Eq. (5)), as seen in Fig. 3, in excellent agreement with the IXS data of Fig. 6.2. *Thus, the contribution from the e_g–e_g electron-hole "channels" of* Fig. 6.4 *to the response function induces the formation of a collective mode, whose energy happens to be ~ 7.5eV!*

Significantly, as is observed in Fig. 6.6, the dielectric function which obtains for $U=5\,\mathrm{eV}$ has the e_g–e_g peak in the "wrong energy," i.e., it lies too low *(we are still referring to q's directed along [111]; we will discuss propagation along [001] below)*. This leads to a collective mode in $s(\vec{q};\omega)$ lying at ~ 6eV, which is clearly in disagreement with experiment (Fig. 6.3). Moreover, the additional fine structure in the $\mathrm{Im}\,\varepsilon$ of Fig. 6.6 is spurious, as is also concluded from Fig. 6.3. This fine structure is traced directly to the enhanced structure in the DOS for the occupied e_g states of Fig. 6.4 (this enhancement is relative to the electronic structure for $U=8\,\mathrm{eV}$).

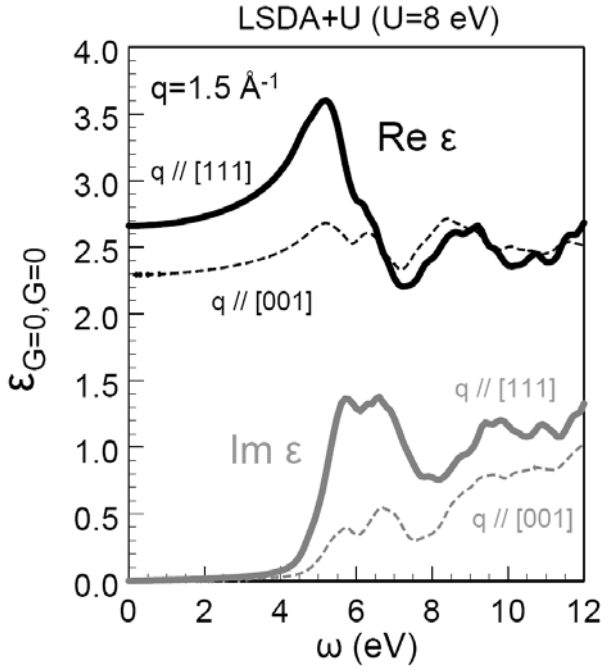

Fig. 6.5. Dielectric function of NiO calculated on the basis of the LSDA+U band structure for U=8 eV

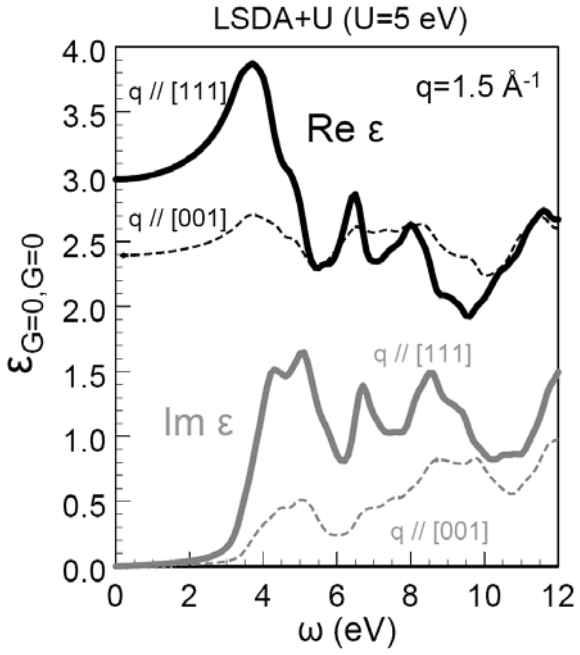

Fig. 6.6. Dielectric function of NiO calculated on the basis of the LSDA+U band structure for U=5 eV.

Thus, the IXS data of Fig. 6.2 *acts as a sensitive arbiter of the quality of the electronic structure of* Fig. 6.4. And the verdict is that the IXS data supports the LSDA+U electronic structure which obtains for $U = 8\,\mathrm{eV}$.

This message is further illustrated in Fig. 6.7 and Fig. 6.8. In the former, we show the $s(\vec{q};\omega)$ calculated for several values of U in the neighborhood of the value suggested by constrained LSDA calculations, $U = 8\,\mathrm{eV}$. It is apparent that the energy location of the "collective" feature is quite sensitive to the underlying choice of U and the ensuing electronic structure —*which as our analysis shows, manifests itself "cleanly" via the* $s(\vec{q};\omega)$ *it generates.* This conclusion is further emphasized by the results of Fig. 6.8.

It should be borne in mind that the above conclusions were reached within our RPA description of the electron dynamics. We submit that the same is expected to be reliable, given the (apparent) absence of strong many-body (beyond-RPA) features in the IXS data of Fig. 6.2 (these effects would include, e.g., strong modification of the lineshape near the gap, which could be imputed to the many-body kernel f_{xc}).

Now the success of the LSDA+U functional reported thus far notwithstanding, additional results, contained in Fig. 6.9 and Fig. 6.10 suggest that the LSDA+U/RPA response method does not represent a complete theory.

Let us consider Fig. 6.9 first. In it we show IXS data for $s(\vec{q};\omega)$ corresponding to three wave vector transfers directed along the [001] direction, together with the results of LSDA+U/RPA calculations. It is apparent that the spectra calculated for $U = 8\,\mathrm{eV}$ do not do as well as they did in Fig. 6.3. We interpret this situation as follows. The reason that $U = 8\,\mathrm{eV}$ turned out to work in Fig. 6.3 is that *in that case the loss spectra are controlled by the collective mode at 7.5 eV, whose physics is in turn controlled by the "global" energy location of the* e_g–e_g *electron-hole channels displayed in* Fig. 6.4. As discussed above, the LSDA+U functional for $U = 8\,\mathrm{eV}$ happens to place these excitation channels in the correct energy location, *as monitored by the IXS data* (more conventionally, this would be argued on the basis of photoemission and inverse-photoemission

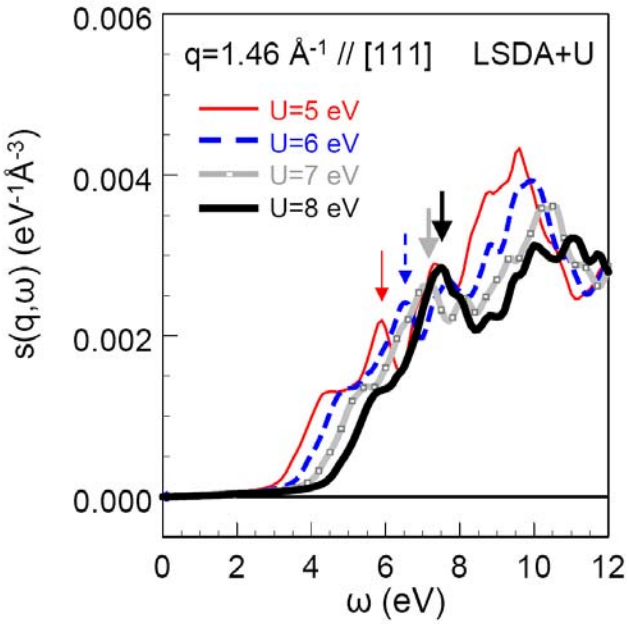

Fig. 6.7. Illustration of the dependence of the calculated energy position of the main above-gap loss feature for $q = 1.46 \text{Å}^{-1}$ along [111] on the value of U chosen in the underlying LSDA+U ground state.

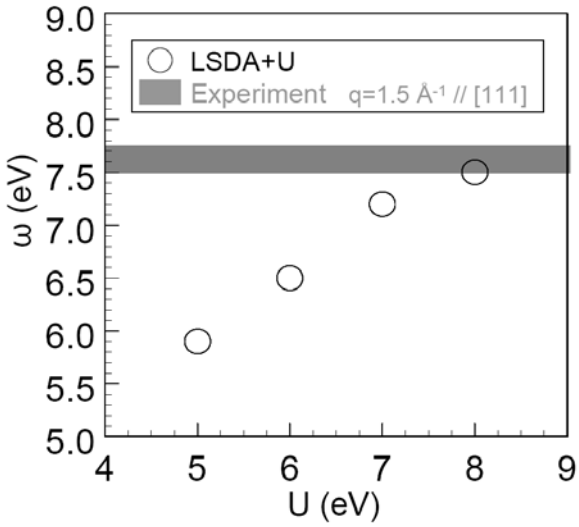

Fig. 6.8. Same as Fig. 6.7; here we record the calculated peak position vs. U together with the energetic position of the IXS peak (~7.5 eV).

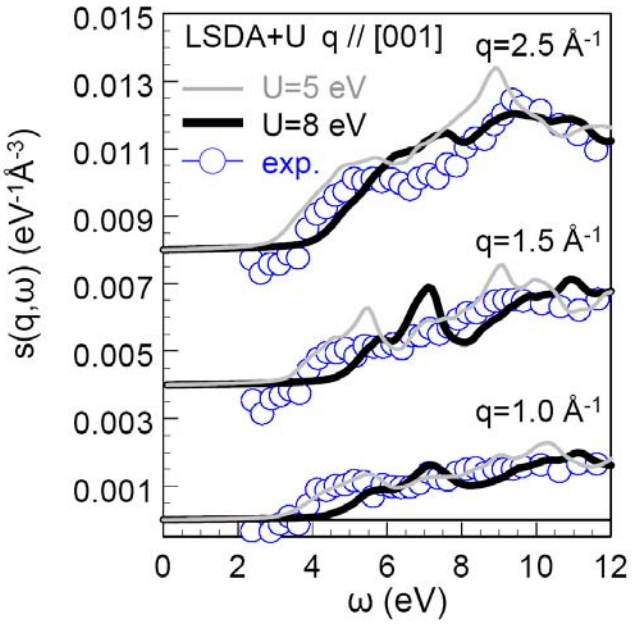

Fig. 6.9. Comparison between calculated and measured $s(\vec{q};\omega)$ for wave vector transfers directed along [001].

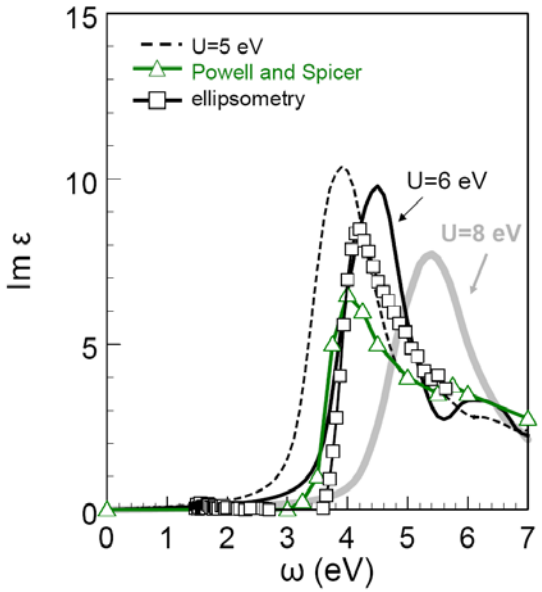

Fig. 6.10. Comparison between the calculated (in RPA) dielectric function of NiO, in the optical limit, with our ellipsometry data.

measurements). By contrast, the loss spectra for *q*'s along [001] are controlled by fine structure in the correlated band structure, and the same is hard to reproduce on the basis of a one parameter functional.

One may still ask why it is that LSDA+U/RPA theory for $U = 8\,\text{eV}$ yields a collective mode for *q*'s along [001], while the same is not present in the IXS data in Fig. 6.9 (this discrepancy is most evident in the spectrum for $q = 1.5\,\text{Å}^{-1}$). We believe that the answer is as follows. As Fig. 6.5 makes clear, the *matrix elements* which control how the JDOS (which "measures" exclusively the availability of electron-hole channels) "propagates" into $\text{Im}\,\varepsilon$, *clearly enhance the actual* e_g–e_g *excitation process, for q's along [111], vs. q's along [001]. This trend is clearly in agreement with experiment —it is consistent with the nature of the IXS data in* Fig. 6.3 *and* Fig. 6.9. *In fact, this enhancement is behind the success story of RPA dynamics we have for q's along [111].* (Ultimately, this behavior of the matrix elements is determined by overlaps between the lobes for e_g electron and hole orbitals.) Unfortunately, the matrix elements do not suppress completely the "remnant," weak e_g–e_g modulations in $\text{Im}\,\varepsilon$ for *q*'s along [001]; the upshot is that in the RPA these weak transitions still manage to yield the loss peak present in the calculated $s(\vec{q};\omega)$ of Fig. 6.9. We stress that actual calculation shows that the strength of the calculated loss in Fig. 6.9 is significantly enhanced by the crystal local fields (matrix nature of χ_s); thus, the full analysis is not trivial.

Now, since the underlying electronic structure for $U = 8\,\text{eV}$ has already been validated by our previous discussion, we submit that beyond-RPA effects, which in our TDDFT-like picture will be introduced by f_{xc}, must be important in the case of Fig. 6.9 (presumably, for $U = 8\,\text{eV}$); in other words, such many-body effects should "erase" the impact on the $s(\vec{q};\omega)$ of Fig. 6.9 of the weak structure in $\text{Im}\,\varepsilon$ for *q* along [001] (Fig. 6.6) .

Consider, finally, Fig. 6.10, which refers to the optical limit. First of all, we note that the dielectric functions obtained from our ellipsometry measurements deviate rather markedly from the dielectric functions of Powell and Spicer [41] which were obtained by Kramers-Kronig analysis of normal-incidence reflectivity measurements. Discrepancies between (more accurate) ellipsometry–derived measurements and reflectivity–derived

dielectric-function measurements are not unusual. These discrepancies result from the fact that in ellipsometry $\mathrm{Re}\,\varepsilon$ and $\mathrm{Im}\,\varepsilon$ are obtained directly from the measurement of parameters, while normal-incidence reflectivity dielectric function measurements involve Kramers-Kronig integration with extrapolations to zero energy and to infinite energy to obtain convergence. Going back to the performance of theory, what stands out in Fig. 6.10 is how poorly the spectrum calculated for the "ab initio" value of the on-site interaction, $U = 8\,\mathrm{eV}$, does.

In fact, and for the sake of the present discussion, we note that the LSDA+U/RPA optical spectrum would appear to be "optimal" for $U = 6\,\mathrm{eV}$. But, as spelled out at the outset, here we are not advocating using the results of Fig. 6.10 —and the previously-discussed IXS data as well— to "pin down" a "physical" value of *U*. On the contrary, the ellipsometry data, in conjunction with the IXS data, highlight the limitations of a response framework, the LSDA+U/RPA, in which the strong atomic–like correlations are controlled by a single parameter (the Hubbard *U*).

At this point, it may be useful to note that this situation is similar to the well-known example of the photoemission spectrum of Ni. In that problem, the simple Hubbard model is able to account for the existence of the 6 eV satellite peak —a hallmark of strong hole-hole correlations— and for the reduction in the exchange splitting (relative to single-particle theory). However, if the value of the Hubbard U is chosen in such a way that the theory reproduces the satellite structure, the description of the splitting worsens —and vice versa.

Moreover, accepting our premise that it is meaningful (at least qualitatively) to reason à la TDDFT, it is entirely possible that a numerical exercise such as the one illustrated in Fig. 8 is not very consequential. Indeed, it is likely that such comparison is hiding the effects of bona fide dynamical correlations, due, e.g., to the electron-hole attraction. A full assessment of the performance of the LSDA+U functional is thus expected to require the inclusion of such physics, which would introduce the U into a non-trivial f_{xc}. This is why we do not subscribe to the strategy of papers such as Ref. [35], which concluded that, on the basis of the reflectivity data of Ref. [42], one could adopt the value U=5 eV for optics. By contrast, and to reiterate, from Fig. 6.10 (and earlier, from Fig. 6.9, which

covers a larger phase space) we submit that LSDA+U/RPA theory is not a complete theory; the role of U in the dynamics must be included before we can engage in general recommendations as to what value of U may work "universally" (i.e., for the whole phase space) for a given material —and, as noted above, a single parameter theory may not be enough, for the entire electron-hole phase space .

This conclusion is not contradictory with our conclusion drawn earlier, on the basis of the IXS data of Fig. 6.2, namely, that the IXS data supported the $U = 8\,\mathrm{eV}$ electronic structure depicted in Fig. 6.4. As argued at length on the basis of Fig. 6.4-Fig. 6.8, the signature of the electronic structure of Fig. 6.4 built into Fig. 6.2 arises via the collective excitation featured in the IXS data. That physics is not present in, e.g., the optical data.

We turn now our attention to a very important result for large momentum transfers q>3 Å^{-1}. Experimentally, in these range of q's strong q-dependent d-d excitations inside the 4 eV gap dominate the loss spectra in NiO [44]. These excitations appear for q's along the [111] direction, on the contrary, for q's along the [100] direction these peaks vanish, as shown in Fig. 6.11. In our theoretical calculations, the energy placement of these excitations does not agree with experiment, the excitations are above the gap. The strong anisotropy observed experimentally is also in agreement with our theoretical loss function, although the energy location is different. Ultimately, the origin of this anisotropy is due to the difference in the overlap between the electron-hole pairs that enter the matrix elements, $\left\langle \Psi_{final} \left| e^{-i(\vec{q}\cdot\vec{x})} \right| \Psi_{initial} \right\rangle$, for each q direction: for q // [111] the overlap is maximal (Fig. 6.12) and for q // [100] is minimal (Fig. 6.13). We have also performed similar type of calculations for CoO. In this case, as also found in experiment, we found two types of d-d anisotropic excitations: One of them is strongest in the [111] direction and the other is in the [100] direction (see Fig. 6.11). In this material, the energy location of these excitations is also in disagreement with the theory, which again places these strong excitations above the gap due to the lack of binding. These findings reinforce the need for a more complete theory in which to treat strongly correlated materials, by improving the treatment of exchange-correlation effects in these complex materials.

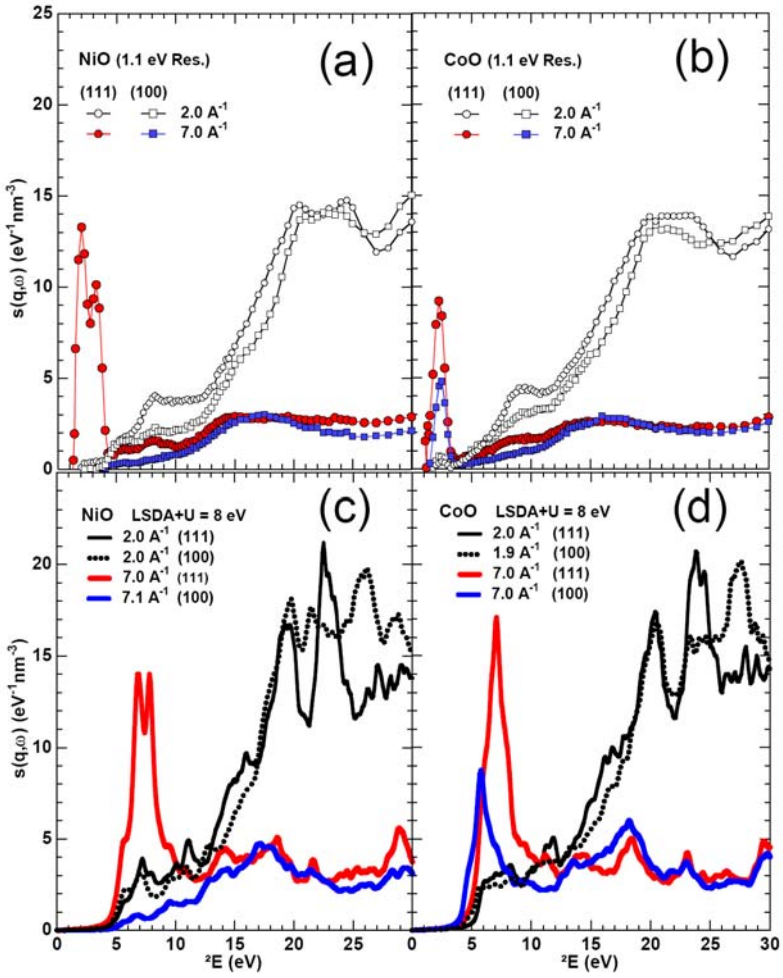

Fig. 6.11. Low-resolution (1.1 eV) NIXS measurements and LDA+U/RPA calculations of the dynamical structure factor for NiO and CoO. (a) Measurements along the [001] and [111] directions at low-q and high-q for NiO; (b) Similar measurements on CoO; (c) Calculations for NiO along the [001] and [111] directions at low-q and high-q; (d) Similar calculations for CoO.

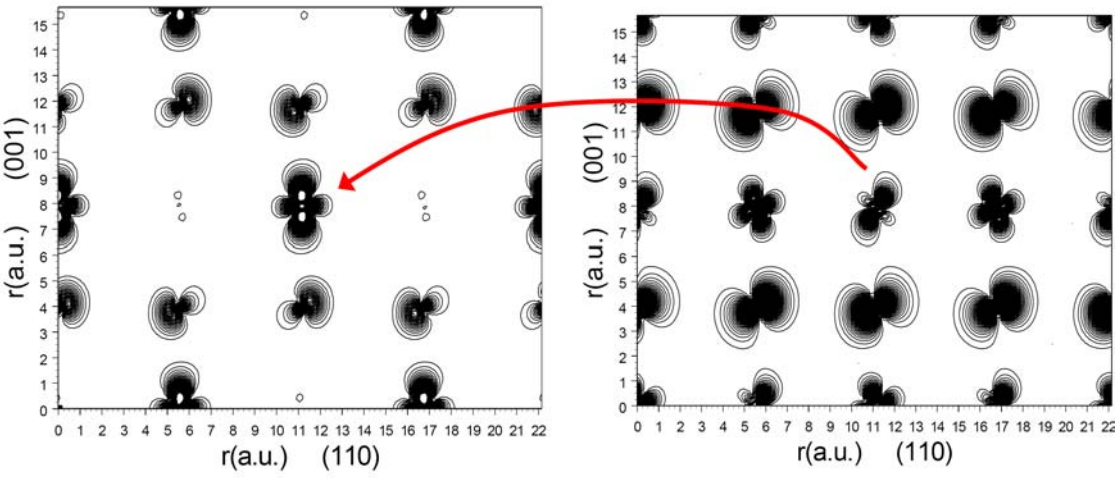

Fig. 6.12.Initial (right panel) and final (left panel) orbital density states for the transitions near the band threshold for NiO for q~4 Å-1// [111]. The red arrow indicates the transition occurring near the Ni atoms. The matrix element for this transition is written as $\left\langle \Psi_{final} \left| e^{-i(\vec{q}\cdot\vec{x})} \right| \Psi_{initial} \right\rangle$.

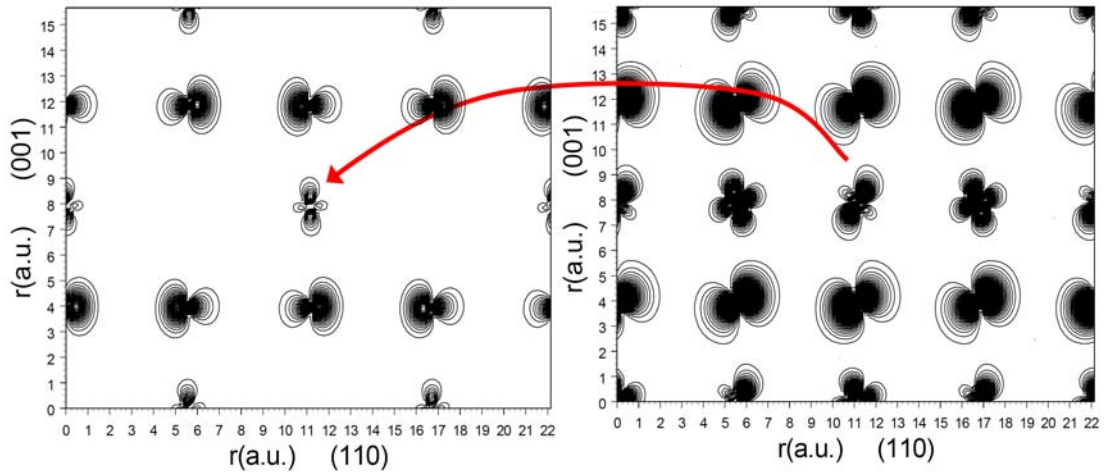

Fig. 6.13. Initial (right panel) and final (left panel) orbital density states for the transitions near the band threshold for NiO for q~4 Å-1// [100]. The red arrow indicates the transition occurring near the Ni atoms. The matrix element is written as $\left\langle \Psi_{final} \left| e^{-i(\vec{q}\cdot\vec{x})} \right| \Psi_{initial} \right\rangle$.

In summary, the $s(\vec{q};\omega)$ predicted on the basis of the LSDA+U/RPA method, for the constrained–LSDA value of U ($U = 8\,\mathrm{eV}$) is in excellent agreement with the IXS data of Fig. 6.2. Moreover, because of the collective nature of the measured loss, and the fact that the same provides a direct mapping of the electronic structure depicted in Fig. 6.4 for $U = 8\,\mathrm{eV}$, we conclude that the IXS data of Fig. 6.2 discriminates in favor of the corresponding electronic structure. We also stress that this result illustrates the merit of IXS, in combination with correlated–band–structure theory, for the investigation of the electronic structure of strongly-correlated materials. A complete theory would need to go beyond LSDA+U/RPA in several directions; most importantly, we have argued that beyond-RPA effects are likely to play a significant role in Fig. 6.9-Fig. 6.10. We have published some of these findings recently [43].

Bibliography

1. O. Gunnarsson, P. Gies, W. Hanke, and O. K. Andersen, Phys. Rev. B **40**, 12140-12146 (1989).

2. A. A. Quong and A. G. Eguiluz, Phys. Rev. Lett. 70, 3955 (1993).

3. A. G. Eguiluz, Wei Ku and J. M. Sullivan, J. Phys. Chem. Solids **61**, 383 (2000).

4. I. G. Gurtubay, J. M. Pitarke, Wei Ku, A. G. Eguiluz, B. C. Larson, J. Tischler, P. Zschack, and K. D. Finkelstein, Phys. Rev. B **72**, 125117 (2005).

5. P.A. Montano and A.T. Macrander, J. Phys. Chem. Solids **61**, 415 (1999).

6. J. P. Perdew and A. Zunger, Phys. Rev. B **23**, 5048 (1981).

7. T. Kotani, Phys. Rev. Lett. 74, 2989 (1995).

8. M. Cococcioni and S. de Gironcoli, Phys. Rev. B **71**, 035105 (2005).

9. Y.-H. Kim and A. Gorling, Phys. Rev. Lett. **89**, 096402 (2002).

10. E. Runge and E. K. U. Gross, Phys. Rev. Lett. **52**, 997 (1984).

11. J. Nagamatsu et al., Phys. Rev. Lett. **86**, 1877 (2001).

12. S. Souma et al., Nature **423**, 65 (2003).

13. W. Ku, W. E. Pickett, R. T. Scalettar, and A. G. Eguiluz, Phys. Rev. Lett. **88**, 057001 (2002).

14. K. Sturm, W. Schülke, and J. R. Schmitz, Phys. Rev. Lett. **68**, 228 (1992).

15. Y. Q. Cai, P. C. Chow, O. D. Restrepo, Y. Takano, K. Togano, H. Kito, H. Ishii, C. C. Chen, K. S. Liang, C. T. Chen, S. Tsuda, S. Shin, C. C. Kao, W. Ku, and A. G. Eguiluz (cond-mat/0605320, submitted to Phys. Rev. Lett.).

16. O. D. Restrepo and A. G. Eguiluz (to be published).

17. M. Petersilka, U. J. Gossmann, and E. K. U. Gross, Phys. Rev. Lett. **76**, 1212 (1996).

18. P. Hohenberg and W. Kohn, Phys. Rev. **136**, B864 (1964).

19. W. Kohn and L. J. Sham, **140**, A1133 (1965).

20. P. Blaha, K. Schwarz, G. K. H. Madsen, D. Kvasnicka and J. Luitz, WIEN2k, *An Augmented Plane Wave + Local Orbitals Program for Calculating Crystal Properties* (Karlheinz Schwarz, Techn. Universität Wien, Austria), 2001. ISBN 3-9501031-1-2.

21. E. Dagotto, T. Hotta, and A. Moreo, Phys. Rep. **344**, 1 (2001); M. B. Salamon and M. Jaime, Rev. Mod. Phys. **73**, 583 (2001)

22. W. E. Pickett and J. S. Moodera, Phys. Today **54**, 39 (2001).

23. J. Kunes, K.-W. Lee and W. E. Pickett "New Challenges in Superconductivity: Experimental Advances and Emerging Theories", (Kluwer Academic, Boston, 2004), 235-242.

24. J. D. Jorgensen, M. Avdeev, D. G. Hinks, J. C. Burley, and S. Short Phys. Rev. B 68, 214517 (2003).

25. V. I. Anisimov, J. Zaanen, and O. K. Andersen, Phys. Rev. B **44**, 943 (1991); V. I. Anisimov, *et al.*, Phys. Rev. B **48**, 16929 (1993); M. T. Czyżyk, and G. A. Sawatzky, *ibid.* **49**, 14211 (1994); A. I. Liechtenstein, V. I. Anisimov, and J. Zaanen, *ibid.* **52**, R5467 (1995).

26. H.X. Yang, J. Q. Li, R. J. Xiao, Y. G. Shi, and H. R. Zhang, Phys. Rev. B **72**, 075106 (2005).

27. R. J. Xiao, H. X. Yang, and J. Q. Li, Phys. Rev. B **73**, 092517 (2006).

28. T. Inami *et al*., Phys. Rev. B **67**, 045108 (2003).

29. W. Schülke, J. Phys. Condens. Matter **13**, 7557 (2001).

30. K. Takada, H. Sakurai, E. Takayama-Muromachi, F. Izumi, R. A. Dilanian, and T. Sasaki, Nature (London) **422**, 53 (2003).

31. O. Bengone, M. Alouani, P. Blochl, and J. Hugel, Phys. Rev. B **62**, 16392 (2000).

32. G. A. Sawatzky and J. W. Allen, Phys. Rev. Lett. 53, 2339 (1984).

33. E. Runge and E. K. U. Gross, Density-Functional Theory for Time-Dependent Systems, Phys. Rev. Lett. 52, 997 (1984).

34. For reviews of TDDFT see, E. K. U. Gross, J. F. Dobson, and M. Petersilka, in *Density Functional Theory II*, edited by R. F. Nalewajski (Springer, Berlin, 1996), p. 81; K. Burke and E. K. U. Gross, in *Density Functionals: Theory and Applications*, edited by D. Joubert (Springer, Berlin, 1998), p. 116.

35. O. Bengone, M. Alouani, P. Blöchl, and J. Hugel, Phys. Rev. B **62**, 16392 (2000).

36. S. L. Dudarev, G. A. Bottom, S. Y. Savrasov, C. J. Humphreys, and A. P. Sutton, Phys. Rev. B **57**, 1505 (1998).

37. For a recent review of IXS, see W. Schülke, J. Phys.: Condens. Matter 13, 7557 (2001).

38. M. Petersilka, U. J. Gossmann, and E. K. U. Gross, Phys. Rev. Lett. **76**, 1212 (1996).

39. T. Grabo, T. Kreibich, S. Kurth, and E. K. U. Gross, Orbital functionals in density-functional theory: the optimized effective potential method, in *Strong Correlations in Electronic Structure: Beyond the Local Density Approximation*, edited by V. Anisimov (Gordon and Breach, 1999); M. Petersilka, U. J. Gossmann, and E. K. U. Gross, Time-dependent optimized effective potential in the linear response regime, in *Electronic Density Functional Theory: Recent Progress and New Directions*, edited by J. F. Dobson, G. Vignale, and M. P. Das (Plenum, New York, 1997), p. 177.

40. The numerical convergence has been checked by performing calculations with 8x8x8, 12x12x12 and 14x14x14 *k*-meshes without observing appreciable changes in the spectra. Most of the results described herein have been obtained using a 12x12x12 *k*-mesh, with 189 *k*-points in the irreducible wedge of the Brillouin zone. For completeness, other numerical parameters entering our computations are as follow: The broadening parameter in the energy-denominator entering the Kohn-Sham response χ_s was taken to be 0.2 eV. The number of bands kept in the calculation of χ_s is typically 76 (counting the semicore states), which corresponds to keeping empty bands up to 70 eV above the gap; with this cut-off, our spectra are well converged for all energies less than 20 eV.

41. G. E. Jellison, Jr. and F. A. Modine, "Two-Modulator Generalized Ellipsometry: Experiment and Calibration," Appl. Opt. **36**, 8184-8189 (1997); G. E. Jellison, Jr. and F. A. Modine, "Two-Modulator Generalized Ellipsometry: Theory," Appl. Opt. **36**, 8190-8198 (1997).

42. R. J. Powell and W. E. Spicer, Phys. Rev. B **2**, 2182 (1970).

43. A. G. Eguiluz, O. D. Restrepo, B. C. Larson, J. Z. Tischler, P. Zschack, and G. E. Jellison, J. Phys. Chem. Solids **66,** 2281 (2005).

44. B. C. Larson, J. Z. Tischler, Wei Ku, Chi-Cheng Lee, O. D. Restrepo, A. G. Eguiluz, P. Zschack, and K. D. Finkelstein (to be published).

Appendices

Appendix A The Kohn-Sham Equation and the LAPW Method

The purpose of this appendix is to give a general introduction to the all-electron LAPW method. The LAPW basis permits a very accurate description of the electronic behavior near and far away from the nucleus. The strong electronic oscillations near the atomic nucleus are treated by using "atomic" wave functions, and the more "free" electrons far away from the nucleus are described by plane waves. In this appendix we start by showing how the LAPW basis is incorporated in the Kohn-Sham equation. We then give a short introduction on how the "atomic" wave functions are calculated and a general definition of the LAPW basis is given. In Section A.4 detailed formulas for the LAPW basis are written. These detailed formulas will be relevant in the actual calculation of the density response function as we show in Appendix B.

A.1 Kohn-Sham Equation

The Kohn-Sham equation is written as

$$\left(-\frac{\hbar^2}{2m}\nabla^2 + v_s[\rho](\vec{x})\right)\Psi_{\vec{k},j}(\vec{x}) = \varepsilon_{\vec{k},j}\Psi_{\vec{k},j}(\vec{x}), \tag{A1}$$

where $\vec{k}$ belongs to the first Brillouin Zone (1BZ), j is a band index and v_s is the Kohn-Sham potential that is a functional of the density, and corresponds to the external potential $V_{ext}(\vec{x})$, the bare Coulomb potential due to the nuclei, the Hartree potential $V_H(\vec{x})$ and the exchange-correlation potential $V_{XC}(\vec{x})$.

The density is calculated in the following way

$$\rho(\vec{x}) = \sum_{\vec{k}}^{BZ}\sum_{j}^{occ}\left|\Psi_{\vec{k},j}(\vec{x})\right|^2. \tag{A2}$$

In order to solve these equations we use the Rayleigh-Ritz variational principle. We expand the Bloch States in an appropriate basis; such as the LAPW basis:

$$\Psi_{k,j}(\vec{x}) = \sum_{\vec{G}} C_{\vec{k},j}\left(\vec{k}+\vec{G}\right)\Phi_{\vec{k}+\vec{G}}(\vec{x}), \tag{A3}$$

where $\vec{G}$ is a reciprocal lattice vector and $C_{\vec{k},j}\left(\vec{k}+\vec{G}\right)$ are the expansion coefficients for the Bloch States that minimize the total crystal energy. The resulting equation that needs to be solved is

$$\sum_{\vec{G}'}\left(H_{\vec{k}+\vec{G},\vec{k}+\vec{G}'} - \varepsilon_{\vec{k},j} S_{\vec{k}+\vec{G},\vec{k}+\vec{G}'}\right) C_{\vec{k},j}\left(\vec{k}+\vec{G}'\right) = 0, \tag{A4}$$

with

$$H_{\vec{k}+\vec{G},\vec{k}+\vec{G}'} \equiv \left\langle \Phi_{\vec{k}+\vec{G}} \left| -\frac{\hbar^2}{2m}\nabla^2 + v_s[\rho](\vec{x}) \right| \Phi_{\vec{k}+\vec{G}'} \right\rangle_{\Omega} \tag{A5}$$

$$S_{\vec{k}+\vec{G},\vec{k}+\vec{G}'} \equiv \left\langle \Phi_{\vec{k}+\vec{G}} \left| \Phi_{\vec{k}+\vec{G}'} \right\rangle_{\Omega}, \right. \tag{A6}$$

where Ω is the volume of the unit cell.

A.2 The LAPW Basis

In the LAPW method the unit cell is divided into an interstitial region and non-overlapping atomic (also called muffin-tin) spheres centered on each atom (Fig. A.1), for this reason two different basis sets are used to expand the wave functions. An expansion in plane waves is used for the interstitial region. For the atomic sphere region radial, atomic-like, basis functions u_l (solutions to the Schrodinger equation), as well as their energy derivatives $\dot{u}_l$, at a fixed energy E_l, are used; this choice of basis allows an accurate description of the strong variations in the density near the atoms. By choosing a fixed energy parameter Eq. (A4) becomes a generalized eigenvalue problem, allowing to obtain in a single diagonalization all the eigenvalues and eigenfunctions. The energy derivative of u_l is introduced; this is called 'linearization' of the problem

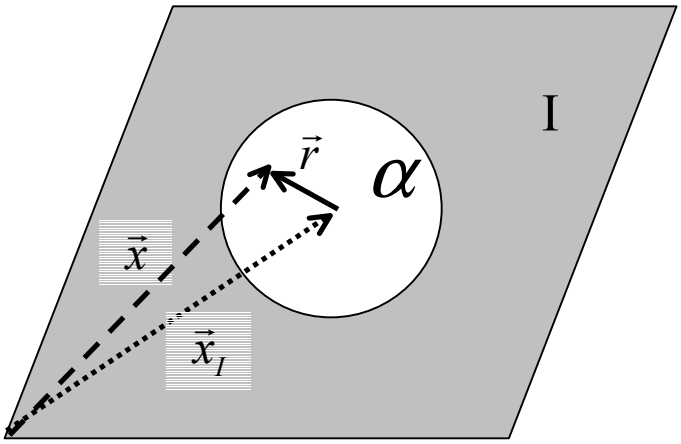

Fig. A.1. Unit cell divided into an interstitial (I) and atomic sphere region (α).

as it allows calculating u_l for an arbitrary value of the energy E (near E_l) through a Taylor expansion,

$$u_l^\alpha(r,E) = u_l^\alpha(r,E_l) + (E_l - E)\dot{u}_l^\alpha(r,E_l) + O(E_l - E)^2, \tag{A7}$$

where the functions u_l and $\dot{u}_l$ are evaluated at fixed energy parameters. The drawback of this procedure is that it does not allow accurate calculations of the wave functions when their corresponding energies are far from E_l (we cannot omit the term $O(E_l - E)^2$ in Eq. (A7), to solve this problem we need to include local orbitals, this procedure is explained in section (B.3).

In the following we are going to consider three vectors in the primitive unit cell. First an $\vec{r}$ vector which originates at the center of each atom acting as a local coordinate inside each atomic sphere; we then consider a general $\vec{x}$ vector which starts from the origin of our primitive unit cell and covers all space; finally a $\vec{x}_I$ vector which indicates the position of the Ith atom with reference to the origin of the primitive unit cell. These three vectors are related by the equation $\vec{r} = \vec{x} - \vec{x}_I$.

The basis functions in the LAPW basis are defined as

$$\Phi_{\vec{k}+\vec{G}}(\vec{x}) = \frac{1}{\sqrt{\Omega}} e^{i(\vec{k}+\vec{G})\cdot\vec{x}}, \ \vec{x} \in \text{I} \tag{A8}$$

and

$$\Phi_{\vec{k}+\vec{G}}(\vec{S}_\alpha + \vec{r}) = \sum_{lm}\Big[A_{lm}^\alpha(\vec{k}+\vec{G})u_l^\alpha(\vec{r},E_l) + B_{lm}^\alpha(\vec{k}+\vec{G})\dot{u}_l^\alpha(\vec{r},E_l)\Big] \times Y_{lm}(\Omega_{\vec{r}}), \ \vec{x} \in \alpha \tag{A9}$$

where the vector $\vec{S}_\alpha$ is the location of the α atom in the unit cell and $Y_{lm}(\Omega_{\vec{r}})$ are spherical harmonics. The $u_l^\alpha(\vec{r},E_l)$ are solutions to the Schrodinger equation and the $\dot{u}_l^\alpha(\vec{r},E_l)$ are their energy derivatives. The coefficients $A_{lm}^\alpha(\vec{k}+\vec{G})$ and $B_{lm}^\alpha(\vec{k}+\vec{G})$ are determined by matching the two basis functions in value and slope at the sphere boundary for each atom.

The $u_l^\alpha(\vec{r}, E_l)$ satisfy the radial equation

$$(h_l - E_l) r u_l^\alpha(r, E_l) = 0, \tag{A10}$$

with

$$h_l = -\frac{d^2}{dr^2} + \frac{l(l+1)}{r^2} + V^\alpha(\vec{r}), \tag{A11}$$

where $V^\alpha(\vec{r})$ is the spherical part of the potential in the atomic sphere α.

Derivation of Eq. (A10) with respect to the energy results in an equation for $\dot{u}_l^\alpha(\vec{r}, E_l)$

$$h_l \dot{u}_l^\alpha(\vec{r}, E_l) - E_l \dot{u}_l^\alpha(\vec{r}, E_l) = u_l^\alpha(\vec{r}, E_l). \tag{A12}$$

The normalization condition imposed inside the atomic sphere is

$$\int_0^{R_\alpha} r^2 \left(u_l^\alpha(\vec{r}, E_l)\right)^2 dr = 1. \tag{A13}$$

By differentiating Eq. (A13) with respect to E_l we see that $u_l^\alpha(\vec{r}, E_l)$ and $\dot{u}_l^\alpha(\vec{r}, E_l)$ are orthogonal

$$\int_0^{R_\alpha} r^2 u_l^\alpha(\vec{r}, E_l) \dot{u}_l^\alpha(\vec{r}, E_l) dr = 0. \tag{A14}$$

The normalization for $\dot{u}_l^\alpha(\vec{r}, E_l)$ is given by

$$\int_0^{R_\alpha} r^2 \dot{u}_l^\alpha(\vec{r}, E_l) \dot{u}_l^\alpha(\vec{r}, E_l) dr = N_l, \tag{A15}$$

where, in general, N_l will be a number different from one.

Based on this orthogonality relations we could find a solution to Eq. (A12) and then orthogonalize with respect to $u_l^\alpha(\vec{r}, E_l)$ to find $\dot{u}_l^\alpha(\vec{r}, E_l)$.

In the LAPW method the density and Kohn-Sham potential are also expanded in a very similar manner as the wave functions, lattice harmonics are used as basis functions in the atomic sphere and plane waves in the interstitial.

$$\rho(\vec{x}) = \sum_{\vec{G}} \rho_{\vec{G}} e^{i\vec{G}\cdot\vec{x}} \quad \vec{x} \in \text{I} \quad , \tag{A16}$$

and

$$\rho(S_\alpha + \vec{r}) = \sum_{LM} \rho_{LM}^{\alpha}(\vec{r}) K_{LM}(\Omega_{\vec{r}}) \quad \vec{x} \in \alpha. \tag{A17}$$

where the lattice harmonics are given by

$$K_{LM}(\Omega_{\vec{r}}) = \sum_{M'=-L}^{L} C_{LM}^{M'} Y_{LM'}(\Omega_{\vec{r}}), \tag{A18}$$

where the $C_{LM}^{M'}$ are chosen according to the site symmetry of the atom in order to produce $K_{LM}(\Omega_{\vec{r}})$ which are real. A detailed explanation on how to calculate the density is given in the "Charge density" appendix.

A.3 LAPW with Local Orbitals

The local orbital extension to the LAPW basis is directed a better description of the so-called Semicore states, low-lying valence states which cannot be treated as part of the core states, i.e., they can have some charge leaking out of the atomic spheres. As the computation of Eq. (A4) gives good results only for energy values near the linearization energy E_l we need to add another basis to threat these Semicore states. This procedure is done only in the atomic sphere region. The local orbital expansion when $\vec{x} \in \alpha$ is given by

$$\Phi_{LO}(\vec{S}_\alpha + \vec{r}) = \sum_{lm} \left[\tilde{A}_{lm}^{\alpha} u_l^{\alpha}(\vec{r}, E_l) + \tilde{B}_{lm}^{\alpha} \dot{u}_l^{\alpha}(\vec{r}, E_l) + \tilde{C}_{lm}^{\alpha} u_l^{\alpha}(\vec{r}, E_{lo}) \right] Y_{lm}(\Omega_{\vec{r}}), \tag{A19}$$

where $\tilde{A}_{lm}^{\alpha}$ and $\tilde{B}_{lm}^{\alpha}$ are determined by requiring that the local orbitals have zero value and slope at the atomic sphere boundary, the $\tilde{C}_{lm}^{\alpha}$ are found by imposing the normalization condition, Eq. (A14). Local orbitals are not required to match the basis functions in the interstitial as a result they do not have a $\vec{k}+\vec{G}$ dependence. The inclusion of local orbitals results in just a small increase of the size of the basis and it allows the proper treatment of localized Semicore states.

A.4 Wave Function Representation in the LAPW Method

Using Eq. (A8) we can write the Bloch State for the Interstitial region as

$$\Psi_{\vec{k}js}\left(\vec{x}\right)=\frac{1}{\sqrt{N\Omega_0}}\sum_{\vec{G}}C_{j,s}\left(\vec{k}+\vec{G}\right)e^{i\left(\vec{k}+\vec{G}\right)\cdot\vec{x}}\chi_s\,. \tag{A20}$$

The Bloch States inside the atomic spheres have a lengthier expression

$$\begin{aligned}\Psi_{\vec{k}js}^{I}\left(\vec{x}\right)=&\frac{4\pi\left(R_{MT}^{I}\right)^2}{\sqrt{N\Omega_0}}\sum_{l}\sum_{m}i^{l}Y_{lm}\left(\Omega_{\vec{r}}\right)\\&\times\left\{\sum_{\vec{G}}\left[C_{j,s}\left(\vec{k}+\vec{G}\right)Y_{lm}^{*}\left(\Omega_{\vec{k}+\vec{G}}\right)e^{i\left(\vec{k}+\vec{G}\right)\cdot\vec{X}_I}\left(a_{l,s,0}^{I,\vec{k},\vec{G}}u_{l,s}^{I}\left(\vec{r}\right)+a_{l,s,1}^{I,\vec{k},\vec{G}}\dot{u}_{l,s}^{I}\left(\vec{r}\right)\right)\right]\right.\\&+\sum_{\{\vec{H}(n)\}}\left[C_{j,s}^{local}\left(\vec{k}+\vec{H}\right)Y_{lm}^{*}\left(\Omega_{\vec{k}+\vec{H}}\right)e^{i\left(\vec{k}+\vec{H}\right)\cdot\vec{X}_I}\cdot\delta_{n,l}\right.\\&\left.\left.\times\left(a_{l,s,0}^{I,local}u_{l,s}^{I}\left(\vec{r}\right)+a_{l,s,1}^{I,local}\dot{u}_{l,s}^{I}\left(\vec{r}\right)+a_{l,s,2}^{I,local}u_{l,s}^{I,local}\left(\vec{r}\right)\right)\right]\right\}.\end{aligned} \tag{A21}$$

The following definitions have been made: N stands for the total number of unit cells in the macrocrystal, Ω_0 is the primitive unit cell volume. χ_s is a two component spinor; $s=+,-;\ \chi_+=\begin{pmatrix}1\\0\end{pmatrix}\ \chi_-=\begin{pmatrix}0\\1\end{pmatrix}$.

R_{MT}^{I} is the Muffin tin radius of the I$^{\text{th}}$ atom. $C_{j,s}\left(\vec{k}+\vec{G}\right)$ and $C_{j,s}^{local}\left(\vec{k}+\vec{H}\right)$ are expansion coefficients, the band index j, and the spin index s. $Y_{lm}^{*}\left(\Omega_{\vec{k}+\vec{G}}\right)$ are the conjugated spherical harmonics evaluated in the direction of the unit vector defined by

$\vec{k}+\vec{G}$. $a_{l,s,0}^{I,\vec{k},\vec{G}}, a_{l,s,1}^{I,\vec{k},\vec{G}}, a_{l,s,0}^{I,local}, a_{l,s,1}^{I,local}, a_{l,s,2}^{I,local}$ are the coefficients for the radial solution, its derivative and the local contribution.

$\{H(n)\}$ is a subgroup of reciprocal vectors $\vec{G}$. They are determined by the value of l given by the local orbitals. The number of $\vec{H}$ vectors for a specific l is given by $(2l+1)N$, where N is the number of atoms of the same kind in the primitive unit cell.

The radial functions are given by:

$$u_{l,s}^{I}(\vec{r}) = \frac{1}{r}\begin{pmatrix} P_{l,s}^{I}(r)\chi_s \\ i\alpha Q_{l,s}^{I}(r)(-\vec{\sigma}\cdot\hat{r})\chi_s \end{pmatrix}, \tag{A22}$$

$$\dot{u}_{l,s}^{I}(\vec{r}) = \frac{1}{r}\begin{pmatrix} \dot{P}_{l,s}^{I}(r)\chi_s \\ i\alpha \dot{Q}_{l,s}^{I}(r)(-\vec{\sigma}\cdot\hat{r})\chi_s \end{pmatrix}, \tag{A23}$$

$$u_{l,s}^{I,local}(\vec{r}) = \frac{1}{r}\begin{pmatrix} P_{l,s}^{I,local}(r)\chi_s \\ i\alpha Q_{l,s}^{I,local}(r)(-\vec{\sigma}\cdot\hat{r})\chi_s \end{pmatrix}. \tag{A24}$$

$P_{l,s}^{I}(r)$ is the mayor component of the radial solution. $Q_{l,s}^{I}(r)$ is the minor component of the radial solution. α is the Fine structure constant. $Y_{lm}(\Omega_{\vec{r}})$ are the spherical harmonics evaluated in the direction of the unit vector $\hat{r}$. $\vec{\sigma}$ is the Pauli matrix vector. $\dot{u}_{l,s}^{I}(\vec{r})$ is the energy derivative of $u_{l,s}^{I}(\vec{r})$. $u_{l,s}^{I,local}(\vec{r})$ corresponds to the local orbitals contribution.

To simplify the notation we can rewrite Eq. (A21) in the following way:

$$\Psi_{\vec{k}js}^{I}(\vec{x}) = \frac{4\pi\left(R_{MT}^{I}\right)^2}{\sqrt{N\Omega_0}}\sum_{l}\sum_{m} i^l \times\left\{\sum_{\vec{G},\beta=0}^{\beta=1} C_{j,s}\left(\vec{k}+\vec{G}\right)Y_{lm}^{*}\left(\Omega_{\vec{k}+\vec{G}}\right)e^{i\left(\vec{k}+\vec{G}\right)\cdot\vec{X}_I} a_{l,s,\beta}^{I}\left(\vec{k}+\vec{G}\right)u_{l,s,\beta}^{I}\left(\vec{r}\right)\right. \tag{A25}$$

where $\beta = 0,1,2$ corresponds to $u^I_{l,s,0}(\vec{r}) = u^I_{l,s}(\vec{r})$, $u^I_{l,s,1}(\vec{r}) = \dot{u}^I_{l,s}(\vec{r})$, and $u^I_{l,s,2}(\vec{r}) = u^{I,local}_{l,s}(\vec{r})$.

We can define the following function:

$$A^{Ij\vec{k}}_{l,m,s,\beta} = \begin{cases} \left\{ i^l \sum_{\vec{G}} C_{j,s}\left(\vec{k}+\vec{G}\right) Y^*_{lm}\left(\Omega_{\vec{k}+\vec{G}}\right) e^{i\left(\vec{k}+\vec{G}\right)\cdot\vec{X}_I} a^I_{l,s,\beta}\left(\vec{k}+\vec{G}\right) \right. \\ \left. + i^l \sum_{\left\{\vec{H}(n)\right\}} C^{local}_{j,s}\left(\vec{k}+\vec{H}\right) Y^*_{lm}\left(\Omega_{\vec{k}+\vec{H}}\right) e^{i\left(\vec{k}+\vec{H}\right)\cdot\vec{X}_I} a^{I,local}_{l,s,\beta} \delta_{n,l} \right\} ; \ \beta=0,1 \\ \left\{ i^l \sum_{\left\{\vec{H}(n)\right\}} C^{local}_{j,s}\left(\vec{k}+\vec{H}\right) Y^*_{lm}\left(\Omega_{\vec{k}+\vec{H}}\right) e^{i\left(\vec{k}+\vec{H}\right)\cdot\vec{X}_I} a^{I,local}_{l,s,\beta} \delta_{n,l} \right\} ; \ \beta=2 \end{cases} \quad \text{(A26)}$$

We can then write the wave function inside the atomic spheres in the following way:

$$\Psi^I_{\vec{k}js}(\vec{x}) = \frac{4\pi\left(R^I_{MT}\right)^2}{\sqrt{N\Omega_0}} \sum_l \sum_m \sum_{\beta=0}^{\beta=2} A^{Ij\vec{k}}_{l,m,s,\beta} u^I_{l,s,\beta}(\vec{r}) Y_{lm}\left(\Omega_{\vec{r}}\right). \quad \text{(A27)}$$

A.5 Orthogonality

Let us take the expression for the orthonormality of two Bloch states over the entire macrocrystal and do the transformation $\vec{x} \to \vec{x}' + \vec{R}$, where $\vec{R}$ is a lattice vector,

$$\begin{aligned} \int_{\Omega} d^3x \Psi^*_{\vec{k}js}(\vec{x}) \Psi_{\vec{k}'j's}(\vec{x}) &= \int_{\Omega} d^3x e^{-i\vec{k}\cdot\vec{R}} \Psi^*_{\vec{k}js}(\vec{x}) e^{-i\vec{k}'\cdot\vec{R}} \Psi_{\vec{k}'j's}(\vec{x}) \\ &= e^{-i\left(\vec{k}-\vec{k}'\right)\cdot\vec{R}} \int_{\Omega} d^3x \Psi^*_{\vec{k}js}(\vec{x}) \Psi_{\vec{k}'j's}(\vec{x}). \end{aligned} \quad \text{(A28)}$$

For this equation to be true it is necessary that $\vec{k} = \vec{k}'$.

We can then write this equation in the following way

$$\int_{\Omega} d^3x \Psi^*_{\vec{k}js}(\vec{x}) \Psi_{\vec{k}j's}(\vec{x}) = \sum_{\vec{R}} \int_{\Omega_0} d^3x \Psi^*_{\vec{k}js}(\vec{x}+\vec{R}) \Psi_{\vec{k}j's}(\vec{x}+\vec{R}). \quad \text{(A29)}$$

where Ω_0 is the volume of the primitive unit cell.

By performing the change of variables $\vec{x}' = \vec{x} + \vec{R}$, and applying Bloch's theorem we obtain the following result

$$\int_{\Omega} d^3x \Psi^*_{\vec{k}js}(\vec{x}) \Psi_{\vec{k}j's}(\vec{x}) = \sum_{\vec{R}} \int_{\Omega_0} d^3x' \Psi^*_{\vec{k}js}(\vec{x}') \Psi_{\vec{k}j's}(\vec{x}') e^{i(\vec{k}-\vec{k}')\cdot\vec{R}}. \quad \text{(A30)}$$

$$\begin{aligned} \int_{\Omega} d^3x \Psi^*_{\vec{k}js}(\vec{x}) \Psi_{\vec{k}j's}(\vec{x}) &= \sum_{\vec{R}} \int_{\Omega} d^3x' \Psi^*_{\vec{k}js}(\vec{x}') \Psi_{\vec{k}j's}(\vec{x}') \\ &= N \int_{\Omega} d^3x' \Psi^*_{\vec{k}js}(\vec{x}') \Psi_{\vec{k}j's}(\vec{x}'), \end{aligned} \quad \text{(A31)}$$

where N is the number of units cells in the macrocrystal ; the Bloch functions are orthonormal so we must have

$$\int_{\Omega_0} d^3x' \Psi^*_{\vec{k}js}(\vec{x}') \Psi_{\vec{k}j's}(\vec{x}') = \frac{1}{N} \delta_{j,j'}. \quad \text{(A32)}$$

which gives us the orthogonality condition fulfilled by the Bloch wave functions over the primitive unit cell.

Appendix B Calculation of the Kohn-Sham Response Function

In this appendix we are going to give explicit formulas for the calculation of the density linear response function. We start by deriving the rotational properties of the Bloch States. In Section B.2 we give explicit, detailed expressions for the atomic sphere and Interstitial matrix elements that enter the formula for the non-interacting KS response function. In Section B.3 the formulas for the e_g and t_{2g} decomposition of these matrix elements are presented.

B.1 Rotational Properties of the Bloch Wave Functions

Let us start with the one particle eigenvalue problem:

$$H\Psi_{\vec{k}j}(\vec{x}) = \varepsilon_{\vec{k}j}\Psi_{\vec{k}j}(\vec{x}), \tag{B1}$$

where $\Psi_{\vec{k}j}(\vec{x})$ are Bloch States satisfying the Bloch Theorem. These Bloch states can be written as a plane wave times a function with the periodicity of the Bravais Lattice: $\Psi_{\vec{k}j}(\vec{x}) = e^{i\vec{k}\cdot\vec{x}}u_{\vec{k}j}(\vec{x})$. The one particle Hamiltonian can be written in terms of the kinetic energy and the total potential as $H = -\frac{\hbar^2}{2m}\nabla^2 + V(\vec{x})$.

Let us find the eigenvalue equation for $u_{\vec{k}j}(\vec{x})$:

$$\begin{aligned}\nabla^2\Psi_{\vec{k}j}(\vec{x}) &= \nabla\left\{\nabla\Psi_{\vec{k}j}(\vec{x})\right\} = \nabla\left\{i\vec{k}e^{i\vec{k}\cdot\vec{x}}u_{\vec{k}j}(\vec{x}) + e^{i\vec{k}\cdot\vec{x}}\nabla u_{\vec{k}j}(\vec{x})\right\} \\ &= \left(i\vec{k}\right)^2 e^{i\vec{k}\cdot\vec{x}}u_{\vec{k}j}(\vec{x}) + 2i\vec{k}e^{i\vec{k}\cdot\vec{x}}\nabla u_{\vec{k}j}(\vec{x}) + e^{i\vec{k}\cdot\vec{x}}\nabla^2 u_{\vec{k}j}(\vec{x}) \\ &= \left(\nabla + i\vec{k}\right)^2 u_{\vec{k}j}(\vec{x})e^{i\vec{k}\cdot\vec{x}}.\end{aligned} \tag{B2}$$

Equation (B1) then becomes

$$\left(-\frac{\hbar^2}{2m}\nabla^2-\frac{\hbar}{m}i\vec{k}\cdot\nabla+\frac{\hbar^2k^2}{2m}+V(\vec{x})\right)u_{\vec{k}j}(\vec{x})=\varepsilon_{\vec{k}j}u_{\vec{k}j}(\vec{x}). \tag{B3}$$

$$\left(H+\frac{1}{m}(\hbar\vec{k})\cdot\vec{p}\right)u_{\vec{k}j}(\vec{x})=\left(\varepsilon_{\vec{k}j}-\frac{\hbar^2k^2}{2m}\right)u_{\vec{k}j}(\vec{x}). \tag{B4}$$

If we consider a symmetry transform S such that $\hat{S}^\dagger V(\vec{x})\hat{S}=V(\vec{x})$ and such that it leaves the kinetic energy unchanged then we have the following property for H,

$$\hat{S}^\dagger H\hat{S}=H \quad\Rightarrow\quad \left[\hat{\mathrm{S}},\mathrm{H}\right]=0. \tag{B5}$$

Setting $H_{\vec{k}}=H+\frac{1}{m}(\hbar\vec{k})\cdot\vec{p}$ and $E_{\vec{k}j}=\varepsilon_{\vec{k}j}-\frac{\hbar^2k^2}{2m}$ we have the following symmetry properties for $H_{\vec{k}}$ and $E_{\vec{k}j}$:

1. $\hat{S}^\dagger\left((\hbar\vec{k})\cdot\vec{p}\right)\hat{S}=\hbar\vec{k}\cdot\hat{S}^\dagger\vec{p}\hat{S}=\hbar\vec{k}\cdot\overrightarrow{S}\,\vec{p}=\overrightarrow{S^{-1}}(\hbar\vec{k})\cdot\vec{p}=\hbar\left(\overrightarrow{S^{-1}}\vec{k}\right)\cdot\vec{p}$

From this property it follows that $\hat{S}^\dagger H_{\vec{k}}\hat{S}=H_{S^{-1}\vec{k}}$ (where we have set $\overrightarrow{S^{-1}}=S^{-1}$)

2. $\hat{S}^\dagger\left((\hbar\vec{k})\cdot(\hbar\vec{k})\right)\hat{S}=(\hbar\vec{k})\cdot(\hbar\vec{k})$. This property stems from the fact that a symmetry transformation applied to a scalar quantity leaves this quantity unchanged.

3. $\hat{S}^\dagger\varepsilon_{\vec{k}j}\hat{S}=\varepsilon_{\vec{k}j}$. This property is also due to the fact that the energy eigenvalues are scalar quantities.

Let us consider the action of $\hat{S}^\dagger$ on the ket $\left|u_{\vec{k}j}(\vec{x})\right\rangle$,

$$\hat{S}^\dagger H_{\vec{k}}\left|u_{\vec{k}j}(\vec{x})\right\rangle=\hat{S}^\dagger E_{\vec{k}j}\left|u_{\vec{k}j}(\vec{x})\right\rangle. \tag{B6}$$

but because $\hat{S}^\dagger H_{\vec{k}}\hat{S}=H_{S^{-1}\vec{k}}$ we also have that

$$\hat{S}^\dagger H_{\vec{k}}\left|u_{\vec{k}j}(\vec{x})\right\rangle=H_{S^{-1}\vec{k}}\hat{S}^\dagger\left|u_{\vec{k}j}(\vec{x})\right\rangle, \tag{B7}$$

and

$$\hat{S}^\dagger E_{\vec{k}j}\left|u_{\vec{k}j}(\vec{x})\right\rangle=E_{\vec{k}}\hat{S}^\dagger\left|u_{\vec{k}j}(\vec{x})\right\rangle=E_{S^{-1}\vec{k}}\hat{S}^\dagger\left|u_{\vec{k}j}(\vec{x})\right\rangle. \tag{B8}$$

The last equality follows from the fact that the energy eigenvalues do not change under a symmetry transformation. This can be demonstrated by first considering the following equation

$$H\hat{S}^{\dagger}\left|\vec{k},j\right\rangle=\hat{S}^{\dagger}H\left|\vec{k},j\right\rangle=\hat{S}^{\dagger}E_{\vec{k},j}\left|\vec{k},j\right\rangle=E_{\vec{k},j}\hat{S}^{\dagger}\left|\vec{k},j\right\rangle. \tag{B9}$$

Now, we want to demonstrate that applying a group symmetry operation to the ket $\left|\vec{k},j\right\rangle$ leads to a new ket where $\vec{k}$ is replaced by $S^{-1}\vec{k}$, that is: $\hat{S}^{\dagger}\left|\vec{k},j\right\rangle\propto\left|S^{-1}\vec{k},j\right\rangle$. For this purpose we can use the Bloch Theorem,

$$\Psi_{\vec{k},j}\left(S\left(\vec{x}+\vec{R}\right)\right)=e^{i\vec{k}\cdot S\vec{R}}\Psi_{\vec{k},j}\left(S\vec{x}\right)=e^{iS^{-1}\vec{k}\cdot\vec{R}}\Psi_{\vec{k},j}\left(S\vec{x}\right). \tag{B10}$$

Equation (B10) also holds for $\Psi_{S^{-1}\vec{k},j}\left(\vec{x}\right)$, then if follows that up to a complex phase factor (which we define as C) we have that

$$\left\langle\vec{x}\left|S^{-1}\vec{k},j\right.\right\rangle=\Psi_{S^{-1}\vec{k},j}\left(\vec{x}\right)=C\Psi_{\vec{k},j}\left(S\vec{x}\right)=C\left\langle\vec{x}\left|\hat{S}^{\dagger}\right|\vec{k},j\right\rangle. \tag{B11}$$

From Eq. (B11) it is directly seen that $\hat{S}^{\dagger}\left|\vec{k},j\right\rangle=C\left|S^{-1}\vec{k},j\right\rangle$; now we can replace this equation on both sides of Eq. (B9) to obtain

$$H\left|S^{-1}\vec{k},j\right\rangle=E_{\vec{k},j}\left|S^{-1}\vec{k},j\right\rangle, \tag{B12}$$

(notice that in Eq. 12 the complex phase factor C gets cancelled since it enters both sides of the equation) but we also have that (from the single particle eigenvalue problem)

$$H\left|S^{-1}\vec{k},j\right\rangle=E_{S^{-1}\vec{k},j}\left|S^{-1}\vec{k},j\right\rangle. \tag{B13}$$

From Eq. (B12) and (B13) we conclude that $E_{\vec{k},j}=E_{S^{-1}\vec{k},j}$.

Replacing equations (B7) and (B8) into Eq. (B6) we have that

$$\left(H_{S^{-1}\vec{k}}-E_{S^{-1}\vec{k}}\right)\hat{S}^{\dagger}\left|u_{\vec{k}j}\left(\vec{x}\right)\right\rangle=0\quad\Rightarrow\quad\hat{S}^{\dagger}\left|u_{\vec{k}j}\left(\vec{x}\right)\right\rangle=\left|u_{S^{-1}\vec{k}j}\left(\vec{x}\right)\right\rangle. \tag{B14}$$

Let us now consider the following term:

$$\left\langle \vec{x}\left|\hat{S}^{\dagger}\right|\vec{k},j\right\rangle =\left\langle \vec{k},j\left|\hat{S}\right|\vec{x}\right\rangle ^{*}=\left\langle \vec{k},j\left|R_{\vec{k}}\vec{x}+\vec{\tau}\left(R_{\vec{k}}\right)\right\rangle ^{*}=\left\langle R_{\vec{k}}\vec{x}+\vec{\tau}\left(R_{\vec{k}}\right)\right|\vec{k},j\right\rangle . \quad \text{(B15)}$$

where $R_{\vec{k}}$ is rotation symmetry matrix and $\vec{\tau}$ is a partial lattice translation.

From Eq. (B15) we have that

$$\begin{aligned}\left\langle \vec{x}\left|\hat{S}^{\dagger}\right|\vec{k},j\right\rangle &= e^{i\vec{k}\cdot R_{\vec{k}}\vec{x}+\vec{\tau}\left(R_{\vec{k}}\right)}u_{\vec{k}j}\left(R_{\vec{k}}\vec{x}+\vec{\tau}\left(R_{\vec{k}}\right)\right)\\ &= e^{i\vec{k}\cdot\vec{\tau}\left(R_{\vec{k}}\right)}e^{iR_{\vec{k}}^{-1}\vec{k}\cdot\vec{x}}\left\langle \vec{x}\left|\hat{S}^{\dagger}\right|u_{\vec{k}j}\right\rangle .\end{aligned} \quad \text{(B16)}$$

Replacing Eq. (B14) in the right hand side of Eq. (B16) we have that

$$\begin{aligned}\left\langle \vec{x}\left|\hat{S}^{\dagger}\right|\vec{k},j\right\rangle &= e^{i\vec{k}\cdot\vec{\tau}\left(R_{\vec{k}}\right)}e^{iR_{\vec{k}}^{-1}\vec{k}\cdot\vec{x}}\left\langle \vec{x}\left|u_{R_{\vec{k}}^{-1}\vec{k},j}\right.\right\rangle \\ &= e^{i\vec{k}\cdot\vec{\tau}\left(R_{\vec{k}}\right)}\left\langle \vec{x}\left|R_{\vec{k}}^{-1}\vec{k},j\right.\right\rangle .\end{aligned} \quad \text{(B17)}$$

Finally, we obtain that the action of the operator $\hat{S}^{\dagger}$ on the ket $\left|\vec{k},j\right\rangle$ leads to the following symmetry property,

$$\hat{S}^{\dagger}\left|\vec{k},j\right\rangle = e^{i\vec{k}\cdot\vec{\tau}\left(R_{\vec{k}}\right)}\left|R_{\vec{k}}^{-1}\vec{k},j\right\rangle . \quad \text{(B18)}$$

B.2 Kohn-Sham Density Response Function

The Kohn-Sham density response function is written as

$$\begin{aligned}\chi_{\vec{G}\vec{G}'}^{S}\left(s,s';\vec{q};\omega\right) = \frac{1}{N\Omega_0}\sum_{\vec{k}}^{PZ}\sum_{jj'}\frac{f_{\vec{k},j,s}-f_{\vec{k}+\vec{q},j',s'}}{E_{\vec{k},j,s}-E_{\vec{k}+\vec{q},j',s'}+\hbar\left(\omega+i\eta\right)}\\ \times\left\langle \vec{k},j,s\left|e^{-i\left(\vec{q}+\vec{G}\right)\cdot\hat{\vec{x}}}\right|\vec{k}+\vec{q},j',s'\right\rangle\\ \times\left\langle \vec{k}+\vec{q},j',s'\left|e^{i\left(\vec{q}+\vec{G}'\right)\cdot\hat{\vec{x}}}\right|\vec{k},j,s\right\rangle ,\end{aligned} \quad \text{(B19)}$$

where PZ stands for the parallelepiped zone and small s and s' are spin indices.

We can separate the sum over $\vec{k}$ vectors into a sum over $\vec{k}$'s in the irreducible zone (IZ) (we are going to denote this points as $\vec{\underset{\sim}{k}}$) and a sum over the star of each $\vec{\underset{\sim}{k}}$. The relationship between $\vec{k}$ and its corresponding $\vec{\underset{\sim}{k}}$ in the IZ can be written as

$$\vec{k} = R_{\underset{\sim}{k}}^{-1}\vec{\underset{\sim}{k}} + \vec{H}\left(\vec{k}\right), \tag{B20}$$

in this expression $R_{\underset{\sim}{k}}^{-1}$ is an element of the point group of the crystal and $\vec{H}\left(\vec{k}\right)$ is the unique reciprocal lattice vector which brings $R_{\underset{\sim}{k}}^{-1}\vec{\underset{\sim}{k}}$ back to the PZ. To be able to use the rotational symmetry properties of the Bloch states we have chosen the notation $R_{\underset{\sim}{k}}^{-1}$ instead of $R_{\underset{\sim}{k}}$ in Eq. (B20) (both symmetry operations belong to the star of $\vec{\underset{\sim}{k}}$).

$$\begin{aligned}\chi^{S}_{\vec{G}\vec{G}'}\left(s,s';\vec{q};\omega\right) = \frac{1}{N\Omega_0}\sum_{\vec{\underset{\sim}{k}}}^{IZ}\sum_{R_{\underset{\sim}{k}}}^{\text{star of k}}\sum_{jj'}\frac{f_{R_{\underset{\sim}{k}}^{-1}\vec{\underset{\sim}{k}}+\vec{H}\left(\vec{k}\right),j,s} - f_{R_{\underset{\sim}{k}}^{-1}\vec{\underset{\sim}{k}}+\vec{H}\left(\vec{k}\right)+\vec{q},j',s'}}{E_{R_{\underset{\sim}{k}}^{-1}\vec{\underset{\sim}{k}}+\vec{H}\left(\vec{k}\right),j,s} - E_{R_{\underset{\sim}{k}}^{-1}\vec{\underset{\sim}{k}}+\vec{H}\left(\vec{k}\right)+\vec{q},j',s'} + \hbar\left(\omega+i\eta\right)}\\ \times\left\langle R_{\underset{\sim}{k}}^{-1}\vec{\underset{\sim}{k}}+\vec{H}\left(\vec{k}\right),j,s\left|e^{-i\left(\vec{q}+\vec{G}\right)\cdot\vec{\hat{x}}}\right|R_{\underset{\sim}{k}}^{-1}\vec{\underset{\sim}{k}}+\vec{H}\left(\vec{k}\right)+\vec{q},j',s'\right\rangle\\ \times\left\langle R_{\underset{\sim}{k}}^{-1}\vec{\underset{\sim}{k}}+\vec{H}\left(\vec{k}\right)+\vec{q},j',s'\left|e^{i\left(\vec{q}+\vec{G}'\right)\cdot\vec{\hat{x}}}\right|R_{\underset{\sim}{k}}^{-1}\vec{\underset{\sim}{k}}+\vec{H}\left(\vec{k}\right),j,s\right\rangle.\end{aligned} \tag{B21}$$

The eigenvalues and the occupation numbers do not change under symmetry transformations so we have that,

$$f_{R_{\underset{\sim}{k}}^{-1}\vec{\underset{\sim}{k}}+\vec{H}\left(\vec{k}\right),j,s} = f_{R_{\underset{\sim}{k}}^{-1}\vec{\underset{\sim}{k}},j,s} = f_{\vec{\underset{\sim}{k}},j,s} \tag{B22}$$

$$f_{R_{\underset{\sim}{k}}^{-1}\vec{\underset{\sim}{k}}+\vec{H}\left(\vec{k}\right)+\vec{q},j',s'} = f_{R_{\underset{\sim}{k}}^{-1}\vec{\underset{\sim}{k}}+\vec{H}\left(\vec{k}\right)+\vec{q}+\vec{H}_1\left(\vec{k},\vec{q}\right),j',s'} \tag{B23}$$

$$E_{R_{\underset{\sim}{k}}^{-1}\vec{\underset{\sim}{k}}+\vec{H}\left(\vec{k}\right),j,s} = E_{R_{\underset{\sim}{k}}^{-1}\vec{\underset{\sim}{k}},j,s} = E_{\vec{\underset{\sim}{k}},j,s} \tag{B24}$$

$$E_{R_{\underset{\sim}{k}}^{-1}\vec{\underset{\sim}{k}}+\vec{H}\left(\vec{k}\right)+\vec{q},j',s'} = E_{R_{\underset{\sim}{k}}^{-1}\vec{\underset{\sim}{k}}+\vec{H}\left(\vec{k}\right)+\vec{q}+\vec{H}_1\left(\vec{k},\vec{q}\right),j',s'} \tag{B25}$$

where $\vec{H}_1\left(\vec{k},\vec{q}\right)$ is the unique reciprocal lattice vector which brings $R_{\underset{\sim}{k}}^{-1}\vec{\underset{\sim}{k}}+\vec{H}\left(\vec{k}\right)+\vec{q}$ back to the PZ.

We set

$$R_{\underset{\sim}{k}}^{-1}\vec{\underset{\sim}{k}}+\vec{H}\left(\vec{k}\right)+\vec{q}+\vec{H}_1\left(\vec{k},\vec{q}\right)=R_{\underset{\sim}{k}_1}^{-1}\vec{\underset{\sim}{k}}_1+\vec{H}_2\left(R_{\underset{\sim}{k}_1}^{-1},\vec{\underset{\sim}{k}}_1\right), \tag{B26}$$

$R_{\underset{\sim}{k}_1}^{-1}$ is an operation of the point group used to define a member of the star of $\vec{\underset{\sim}{k}}_1$ ($\vec{\underset{\sim}{k}}_1$ is a vector in the IZ). $\vec{H}_2\left(R_{\underset{\sim}{k}_1}^{-1},\vec{\underset{\sim}{k}}_1\right)$ brings back $R_{\underset{\sim}{k}_1}^{-1}\vec{\underset{\sim}{k}}_1$ to the PZ.

From Eq. (B26) we have the following symmetry properties for the energy eigenvalues and the occupation numbers (Eqs. (B23) and (B25)),

$$\begin{aligned} f_{R_{\underset{\sim}{k}}^{-1}\vec{\underset{\sim}{k}}+\vec{H}\left(\vec{k}\right)+\vec{q}+\vec{H}_1\left(\vec{k},\vec{q}\right),j',s'} &= f_{R_{\underset{\sim}{k}_1}^{-1}\vec{\underset{\sim}{k}}_1+\vec{H}_2\left(R_{\underset{\sim}{k}_1}^{-1},\vec{\underset{\sim}{k}}_1\right),j',s'} \\ &= f_{R_{\underset{\sim}{k}_1}^{-1}\vec{\underset{\sim}{k}}_1,j',s'}=f_{\vec{\underset{\sim}{k}}_1,j',s'} \end{aligned} \tag{B27}$$

$$\begin{aligned} E_{R_{\underset{\sim}{k}}^{-1}\vec{\underset{\sim}{k}}+\vec{H}\left(\vec{k}\right)+\vec{q}+\vec{H}_1\left(\vec{k},\vec{q}\right),j',s'} &= E_{R_{\underset{\sim}{k}_1}^{-1}\vec{\underset{\sim}{k}}_1+\vec{H}_2\left(R_{\underset{\sim}{k}_1}^{-1},\vec{\underset{\sim}{k}}_1\right),j',s'} \\ &= E_{R_{\underset{\sim}{k}_1}^{-1}\vec{\underset{\sim}{k}}_1,j',s'}=E_{\vec{\underset{\sim}{k}}_1,j',s'} \end{aligned} \tag{B28}$$

Replacing Eq. (B27) and (B28) in Eq. (B21) we have that

$$\chi_{\vec{G}\vec{G}'}^{S}\left(s,s';\vec{q};\omega\right)=\frac{1}{N\Omega_0}\sum_{\vec{\underset{\sim}{k}}}^{IZ}\sum_{R_{\underset{\sim}{k}}}^{\text{star of k}}\sum_{jj'}\frac{f_{\vec{\underset{\sim}{k}},j,s}-f_{\vec{\underset{\sim}{k}}_1,j',s'}}{E_{\vec{\underset{\sim}{k}},j,s}-E_{\vec{\underset{\sim}{k}}_1,j',s'}+\hbar\left(\omega+i\eta\right)}$$

$$\times\left\langle R_{\underset{\sim}{k}}^{-1}\vec{\underset{\sim}{k}},j,s\left|e^{-i\left(\vec{q}+\vec{G}\right)\cdot\vec{\hat{x}}}\right|R_{\underset{\sim}{k}}^{-1}\vec{\underset{\sim}{k}}+\vec{H}\left(\vec{k}\right)+\vec{q}+\vec{H}_1\left(\vec{k},\vec{q}\right),j',s'\right\rangle$$

$$\times\left\langle R_{\underset{\sim}{k}}^{-1}\vec{\underset{\sim}{k}}+\vec{H}\left(\vec{k}\right)+\vec{q}+\vec{H}_1\left(\vec{k},\vec{q}\right),j',s'\left|e^{i\left(\vec{q}+\vec{G}'\right)\cdot\vec{\hat{x}}}\right|R_{\underset{\sim}{k}}^{-1}\vec{\underset{\sim}{k}},j,s\right\rangle.$$

$$= \frac{1}{N\Omega_0} \sum_{\vec{\underset{\sim}{k}}}^{IZ} \sum_{R_{\underset{\sim}{k}}}^{\text{star of k}} \sum_{jj'} \frac{f_{\vec{\underset{\sim}{k}},j,s} - f_{\vec{\underset{\sim}{k}}_1,j',s'}}{E_{\vec{\underset{\sim}{k}},j,s} - E_{\vec{\underset{\sim}{k}}_1,j',s'} + \hbar(\omega + i\eta)}$$

$$\times \left\langle R_{\underset{\sim}{k}}^{-1}\vec{\underset{\sim}{k}}, j, s \left| e^{-i(\vec{q}+\vec{G})\cdot\vec{\hat{x}}} \right| R_{\underset{\sim}{k}}^{-1}\left(\vec{\underset{\sim}{k}} + R_{\underset{\sim}{k}}\left(\vec{H}\left(\vec{k}\right) + \vec{q} + \vec{H}_1\left(\vec{k},\vec{q}\right)\right)\right), j', s' \right\rangle$$

$$\times \left\langle R_{\underset{\sim}{k}}^{-1}\left(\vec{\underset{\sim}{k}} + R_{\underset{\sim}{k}}\left(\vec{H}\left(\vec{k}\right) + \vec{q} + \vec{H}_1\left(\vec{k},\vec{q}\right)\right)\right), j', s' \left| e^{i(\vec{q}+\vec{G}')\cdot\vec{\hat{x}}} \right| R_{\underset{\sim}{k}}^{-1}\vec{\underset{\sim}{k}}, j, s \right\rangle. \qquad \text{(B29)}$$

We set

$$\vec{\underset{\sim}{k}} + R_{\underset{\sim}{k}}\left(\vec{H}\left(\vec{k}\right) + \vec{q} + \vec{H}_1\left(\vec{k},\vec{q}\right)\right) = R_{\underset{\sim}{k}'}^{-1}\vec{\underset{\sim}{k}}' + \vec{H}'\left(\vec{k}'\right), \qquad \text{(B30)}$$

where $R_{\underset{\sim}{k}'}^{-1}$ is one of the rotations used to define the star of $\vec{\underset{\sim}{k}}'$ and $\vec{H}'\left(\vec{k}'\right)$ brings $R_{\underset{\sim}{k}'}^{-1}\vec{\underset{\sim}{k}}'$ back to the PZ. We notice here that from Eq. (B26) and (B30) we have that $R_{\underset{\sim}{k}'}^{-1} = R_{\underset{\sim}{k}} R_{\underset{\sim}{k}_1}^{-1}$ and most importantly (since we are going to use it) $\vec{\underset{\sim}{k}}' = \vec{\underset{\sim}{k}}_1$.

Let us consider the first matrix element,

$$\left\langle R_{\underset{\sim}{k}}^{-1}\vec{\underset{\sim}{k}}, j, s \left| e^{-i(\vec{q}+\vec{G})\cdot\vec{\hat{x}}} \right| R_{\underset{\sim}{k}}^{-1}\left(\vec{\underset{\sim}{k}} + R_{\underset{\sim}{k}}\left(\vec{H}\left(\vec{k}\right) + \vec{q} + \vec{H}_1\left(\vec{k},\vec{q}\right)\right)\right), j', s' \right\rangle =$$

$$= \left\langle R_{\underset{\sim}{k}}^{-1}\vec{\underset{\sim}{k}}, j, s \left| e^{-i(\vec{q}+\vec{G})\cdot\vec{\hat{x}}} \right| R_{\underset{\sim}{k}}^{-1}\left[R_{\underset{\sim}{k}'}^{-1}\vec{\underset{\sim}{k}}'\right] + R_{\underset{\sim}{k}}^{-1}\vec{H}'\left(\vec{k}'\right), j', s \right\rangle$$

$$= \left\langle R_{\underset{\sim}{k}}^{-1}\vec{\underset{\sim}{k}}, j, s \left| e^{-i(\vec{q}+\vec{G})\cdot\vec{\hat{x}}} \right| R_{\underset{\sim}{k}}^{-1}\left[R_{\underset{\sim}{k}'}^{-1}\vec{\underset{\sim}{k}}'\right], j', s' \right\rangle, \qquad \text{(B31)}$$

where we have used the property that $\left\langle \vec{x} \middle| \vec{k} + \vec{G}, j, s \right\rangle = \left\langle \vec{x} \middle| \vec{k}, j, s \right\rangle$ when $\vec{G}$ is a reciprocal lattice vector.

From Eq. (B18) we have that,

$$\left| R_{\underset{\sim}{k}}^{-1}\vec{\underset{\sim}{k}}, j, s \right\rangle = e^{-i\vec{\underset{\sim}{k}}\cdot\vec{\tau}\left(R_{\underset{\sim}{k}}\right)} \hat{S}_{R_{\underset{\sim}{k}}}^{\dagger} \left| \vec{\underset{\sim}{k}}, j, s \right\rangle, \qquad \text{(B32)}$$

where $\hat{S}_{R_{\underset{\sim}{k}}}$ is the general symmetry operation of the space group that corresponds to the rotation $R_{\underset{\sim}{k}}$ and partial lattice translation $\vec{\tau}\left(R_{\underset{\sim}{k}}\right)$. So we can re-write the first matrix element as

$$\left\langle R_{\underset{\sim}{k}}^{-1}\vec{\underset{\sim}{k}}, j, s\left| e^{-i\left(\vec{q}+\vec{G}\right)\cdot\vec{\hat{x}}}\right| R_{\underset{\sim}{k}}^{-1}\left[R_{\underset{\sim}{k}'}^{-1}\vec{\underset{\sim}{k}}'\right], j', s'\right\rangle =$$
$$e^{i\vec{\underset{\sim}{k}}\cdot\vec{\tau}\left(R_{\underset{\sim}{k}}\right)}e^{-i\left[R_{\underset{\sim}{k}'}^{-1}\vec{\underset{\sim}{k}}'\right]\cdot\vec{\tau}\left(R_{\underset{\sim}{k}}\right)}\times\left\langle \vec{\underset{\sim}{k}}, j, s\left|\hat{S}_{R_{\underset{\sim}{k}}}e^{-i\left(\vec{q}+\vec{G}\right)\cdot\vec{\hat{x}}}\hat{S}_{R_{\underset{\sim}{k}}}^{\dagger}\right| R_{\underset{\sim}{k}'}^{-1}\vec{\underset{\sim}{k}}', j', s'\right\rangle. \quad \text{(B33)}$$

From elementary quantum mechanics we have that,

$$\hat{S}_{R_{\underset{\sim}{k}}}e^{-i\left(\vec{q}+\vec{G}\right)\cdot\vec{\hat{x}}}\hat{S}_{R_{\underset{\sim}{k}}}^{\dagger} = e^{-i\left(\vec{q}+\vec{G}\right)\cdot\left(\hat{S}_{R_{\underset{\sim}{k}}}\vec{\hat{x}}\hat{S}_{R_{\underset{\sim}{k}}}^{\dagger}\right)}$$
$$= e^{-i\left(\vec{q}+\vec{G}\right)\cdot\left(R_{\underset{\sim}{k}}^{-1}\left(\vec{\hat{x}}-\vec{\tau}\left(R_{\underset{\sim}{k}}\right)\right)\right)}$$
$$= e^{-iR_{\underset{\sim}{k}}\left(\vec{q}+\vec{G}\right)\cdot\vec{\hat{x}}}e^{iR_{\underset{\sim}{k}}\left(\vec{q}+\vec{G}\right)\cdot\vec{\tau}\left(R_{\underset{\sim}{k}}\right)}. \quad \text{(B34)}$$

Finally, Eq. (B33) can be written as,

$$\left\langle R_{\underset{\sim}{k}}^{-1}\vec{\underset{\sim}{k}}, j, s\left| e^{-i\left(\vec{q}+\vec{G}\right)\cdot\vec{\hat{x}}}\right| R_{\underset{\sim}{k}}^{-1}\left[R_{\underset{\sim}{k}'}^{-1}\vec{\underset{\sim}{k}}'\right], j', s'\right\rangle =$$
$$e^{i\vec{\underset{\sim}{k}}\cdot\vec{\tau}\left(R_{\underset{\sim}{k}}\right)}e^{-i\left[R_{\underset{\sim}{k}'}^{-1}\vec{\underset{\sim}{k}}'\right]\cdot\vec{\tau}\left(R_{\underset{\sim}{k}}\right)}e^{iR_{\underset{\sim}{k}}\left(\vec{q}+\vec{G}\right)\cdot\vec{\tau}\left(R_{\underset{\sim}{k}}\right)}\left\langle \vec{\underset{\sim}{k}}, j, s\left| e^{-iR_{\underset{\sim}{k}}\left(\vec{q}+\vec{G}\right)\cdot\vec{\hat{x}}}\right| R_{\underset{\sim}{k}'}^{-1}\vec{\underset{\sim}{k}}', j', s'\right\rangle. \quad \text{(B35)}$$

The second matrix element is written as

$$\left\langle R_{\underset{\sim}{k}}^{-1}\left[R_{\underset{\sim}{k}'}^{-1}\vec{\underset{\sim}{k}}'\right], j', s'\left| e^{i\left(\vec{q}+\vec{G}'\right)\cdot\vec{\hat{x}}}\right| R_{\underset{\sim}{k}}^{-1}\vec{\underset{\sim}{k}}, j, s\right\rangle = \left\langle R_{\underset{\sim}{k}}^{-1}\vec{\underset{\sim}{k}}, j, s\left| e^{-i\left(\vec{q}+\vec{G}'\right)\cdot\vec{\hat{x}}}\right| R_{\underset{\sim}{k}}^{-1}\left[R_{\underset{\sim}{k}'}^{-1}\vec{\underset{\sim}{k}}'\right], j', s'\right\rangle^{*}$$

$$= e^{-i\vec{k}\cdot\vec{\tau}\left(R_{\underset{\sim}{k}}\right)} e^{i\left[R_{\underset{\sim}{k}'}^{-1}\vec{k}'\right]\cdot\vec{\tau}\left(R_{\underset{\sim}{k}}\right)} e^{-iR_{\underset{\sim}{k}}\left(\vec{q}+\vec{G}'\right)\cdot\vec{\tau}\left(R_{\underset{\sim}{k}}\right)}$$

$$\times\left\langle \vec{k},j,s\left|e^{-iR_{\underset{\sim}{k}}\left(\vec{q}+\vec{G}'\right)\cdot\vec{\hat{x}}}\right|R_{\underset{\sim}{k}'}^{-1}\vec{k}',j',s'\right\rangle^{*} \quad . \tag{B36}$$

So we have a final expression for the Kohn-Sham response function:

$$\chi^{S}_{\vec{G}\vec{G}'}\left(s,s';\vec{q};\omega\right)=\frac{1}{N\Omega_0}\sum_{\vec{k}}^{IZ}\sum_{R_{\underset{\sim}{k}}}^{\text{star of k}}\sum_{jj'}\frac{f_{\vec{k},j,s}-f_{\vec{k}',j',s'}}{E_{\vec{k},j,s}-E_{\vec{k}',j',s'}+\hbar\left(\omega+i\eta\right)}\times e^{iR_{\underset{\sim}{k}}\left(\vec{G}-\vec{G}'\right)\cdot\vec{\tau}\left(R_{\underset{\sim}{k}}\right)}$$

$$\times\left\langle \vec{k},j,s\left|e^{-iR_{\underset{\sim}{k}}\left(\vec{q}+\vec{G}\right)\cdot\vec{\hat{x}}}\right|R_{\underset{\sim}{k}'}^{-1}\vec{k}',j',s'\right\rangle$$

$$\times\left\langle \vec{k},j,s\left|e^{-iR_{\underset{\sim}{k}}\left(\vec{q}+\vec{G}'\right)\cdot\vec{\hat{x}}}\right|R_{\underset{\sim}{k}'}^{-1}\vec{k}',j',s'\right\rangle^{*} . \tag{B37}$$

We just need to consider the first matrix element in the following discussions,

$$\left\langle \vec{k},j,s\left|e^{-iR_{\underset{\sim}{k}}\left(\vec{q}+\vec{G}\right)\cdot\vec{\hat{x}}}\right|R_{\underset{\sim}{k}'}^{-1}\vec{k}',j',s'\right\rangle=\int d^3x\ \left\langle \vec{k},j,s\left|\vec{x}\right\rangle\right.\ e^{-iR_{\underset{\sim}{k}}\left(\vec{q}+\vec{G}\right)\cdot\vec{x}}$$

$$\times\left\langle \vec{x}\left|R_{\underset{\sim}{k}'}^{-1}\vec{k}',j',s'\right\rangle\right. \tag{B38}$$

Using the symmetry properties of the Bloch States (Eq. (B32)) we have that

$$\left\langle \vec{x}\left|R_{\underset{\sim}{k}'}^{-1}\vec{k}',j',s'\right\rangle\right.=\Psi_{R_{\underset{\sim}{k}'}^{-1}\vec{k}',j',s'}\left(\vec{x}\right)=e^{-i\vec{k}'\cdot\vec{\tau}\left(R_{\underset{\sim}{k}}'\right)}\Psi_{\vec{k}',j',s'}\left(R_{\underset{\sim}{k}'}\vec{x}+\vec{\tau}\left(R_{\underset{\sim}{k}'}\right)\right). \tag{B39}$$

B.2.1 Contribution from the Atomic Spheres (Muffin Tins) to the First Matrix Element

The contribution from the atomic spheres (or Muffin Tins) to this matrix element is given by

$$\left\langle \vec{\underset{\sim}{k}}, j, s \left| e^{-iR_{\underset{\sim}{k}}\left(\vec{q}+\vec{G}\right)\cdot\hat{\vec{x}}} \right| R_{\underset{\sim}{k}'}^{-1}\vec{\underset{\sim}{k}}', j', s' \right\rangle_{MT} = e^{-i\vec{\underset{\sim}{k}}'\cdot\vec{\tau}\left(R_{\underset{\sim}{k}}'\right)} M_{j,j'}^{MT,s,s'}\left(R_{\underset{\sim}{k}}^{-1}, \vec{\underset{\sim}{k}}, \vec{q}+\vec{G}\right), \quad \text{(B40)}$$

where

$$M_{j,j'}^{MT,s,s'}\left(R_{\underset{\sim}{k}}^{-1}, \vec{\underset{\sim}{k}}, \vec{q}+\vec{G}\right) = \sum_I \int_{\substack{\text{Atomic}\\ \text{sphere I}}} d^3x\ \Psi_{\vec{\underset{\sim}{k}},j,s}^{*,I}\left(\vec{x}\right)\ e^{-iR_{\underset{\sim}{k}}\left(\vec{q}+\vec{G}\right)\cdot\vec{x}}$$

$$\times\Psi_{\vec{\underset{\sim}{k}}',j',s'}^{I}\left(R_{\vec{\underset{\sim}{k}}'}\vec{x}+\vec{\tau}\left(R_{\underset{\sim}{k}'}\right)\right) \quad \text{(B41)}$$

and $\Psi_{\vec{\underset{\sim}{k}}',j',s'}^{I}\left(R_{\vec{\underset{\sim}{k}}'}\vec{x}+\vec{\tau}\left(R_{\underset{\sim}{k}'}\right)\right) = \left\langle R_{\vec{\underset{\sim}{k}}'}\left(\vec{x}_I+\vec{r}\right)+\vec{\tau}\left(R_{\underset{\sim}{k}'}\right)\middle|\vec{\underset{\sim}{k}}', j', s'\right\rangle$. Remember that $\vec{x}=\vec{x}_I+\vec{r}$,where $\vec{x}_I$ is the position of the I[th] atom in the primitive unit cell and $\vec{r}$ is the distance measured from the center of that atom.

In the following we are going to use the following valid relation

$$R_{\vec{\underset{\sim}{k}}'}\vec{x}_I+\vec{\tau}\left(R_{\underset{\sim}{k}'}\right)=\vec{x}_{IR}+\vec{R}_{IR}, \quad \text{(B42)}$$

where $\vec{x}_{IR}$ is the position of an atom in the primitive unit cell and $\vec{R}_{IR}$ is the Bravais lattice vector that brings the new atom position, obtained after applying the symmetry operation $\left\{R_{\vec{\underset{\sim}{k}}'},\vec{\tau}\left(R_{\underset{\sim}{k}'}\right)\right\}$ on $\vec{x}_I$, inside the primitive unit cell (see Fig. B.1).

Making use of Eq. (B42), we have that

$$\Psi_{\vec{\underset{\sim}{k}}',j',s'}^{I}\left(R_{\vec{\underset{\sim}{k}}'}\vec{x}+\vec{\tau}\left(R_{\underset{\sim}{k}'}\right)\right)=\left\langle \vec{x}_{IR}+\vec{R}_{IR}+R_{\vec{\underset{\sim}{k}}'}\vec{r}\middle|\vec{\underset{\sim}{k}}', j', s'\right\rangle = e^{i\vec{\underset{\sim}{k}}'\cdot\vec{R}_{IR}}\left\langle \vec{x}_{IR}+R_{\vec{\underset{\sim}{k}}'}\vec{r}\middle|\vec{\underset{\sim}{k}}', j', s'\right\rangle$$

$$= e^{i\vec{\underset{\sim}{k}}'\cdot\vec{R}_{IR}}\Psi_{\vec{\underset{\sim}{k}}',j',s'}^{IR}\left(\vec{x}_{IR}+R_{\vec{\underset{\sim}{k}}'}\vec{r}\right). \quad \text{(B43)}$$

The Bloch States are written in terms of LAPW basis functions inside the atomic sphere:

$$\Psi_{\vec{\underset{\sim}{k}},j,s}^{*I}\left(\vec{x}\right)=\frac{4\pi\left(R_{MT}^{I}\right)^2}{\sqrt{N}\sqrt{\Omega_0}}\sum_l\sum_m\sum_\beta\left(A_{l,m,s,\beta}^{Ij\vec{\underset{\sim}{k}}}\right)^* u_{l,m,s,\beta}^{*I}\left(\vec{r}\right). \quad \text{(B44)}$$

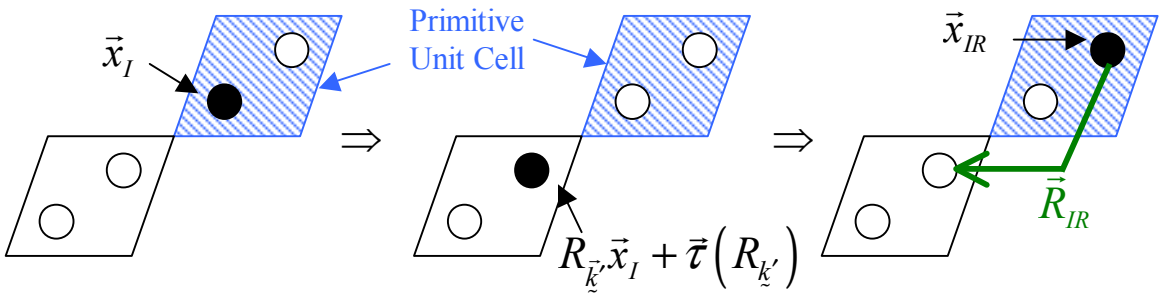

Fig. B.1. Schematic representation of Eq. (B42). After applying the symmetry operation $\left\{R_{\tilde{k}'}, \vec{\tau}\left(R_{\tilde{k}'}\right)\right\}$ to $\vec{x}_I$ we end up in an atomic position which is outside the primitive unit cell. The latter position is related to an atomic position inside the primitive unit cell $\left(\vec{x}_{IR}\right)$ by the Bravais Lattice vector $\vec{R}_{IR}$.

$$\Psi^{IR}_{\underset{\sim}{k}',j',s'}\left(\vec{x}_{IR}+R_{\underset{\sim}{k}'}\vec{r}\right)=\frac{4\pi\left(R^{I}_{MT}\right)^{2}}{\sqrt{N}\sqrt{\Omega_0}}\sum_{l'}\sum_{m'}\sum_{\beta'}A^{IR,j',\vec{k}'}_{l',m',s',\beta'}u^{IR}_{l',m',s',\beta'}\left(R_{\underset{\sim}{k}'}\vec{r}\right). \tag{B45}$$

We can perform the Rayleigh expansion of the exponential in Eq. (B41) in terms of spherical harmonics

$$\begin{aligned}&e^{-iR_{\underset{\sim}{k}}(\vec{q}+\vec{G})\cdot\vec{x}}=e^{-iR_{\underset{\sim}{k}}(\vec{q}+\vec{G})\cdot(\vec{r}+\vec{x}_I)}\\&=e^{-iR_{\underset{\sim}{k}}(\vec{q}+\vec{G})\cdot\vec{x}_I}\left[4\pi\sum_{l''=0}^{\infty}(i)^{l''}j_{l''}\left(\left|R_{\underset{\sim}{k}}\left(\vec{q}+\vec{G}\right)\right|r\right)\sum_{m''=-l''}^{l''}Y^{*}_{l''m''}\left(\Omega_{R_{\underset{\sim}{k}}\left(-\vec{q}-\vec{G}\right)}\right)Y_{l''m''}\left(\Omega_r\right)\right],\end{aligned} \tag{B46}$$

where $j_{l''}\left(\left|R_{\underset{\sim}{k}}\left(\vec{q}+\vec{G}\right)\right|r\right)$ is the spherical Bessel function of order l''.

The contribution to the first matrix element from the atomic spheres is given by

$$\begin{aligned}M^{MT,s}_{j,j'}\left(R^{-1}_{\underset{\sim}{k}},\vec{k},\vec{q}+\vec{G}\right)&=N\sum_{I=1}^{Na}\int_{\substack{\text{Atomic}\\\text{sphere I}}}d^3x\;\Psi^{*,I}_{\underset{\sim}{k},j,s}\left(\vec{x}\right)\;e^{-iR_{\underset{\sim}{k}}\left(\vec{q}+\vec{G}\right)\cdot\vec{x}}\Psi^{I}_{\underset{\sim}{k}',j',s}\left(R_{\underset{\sim}{k}'}\vec{x}+\vec{\tau}\left(R_{\underset{\sim}{k}'}\right)\right)\\&=N\sum_{I=1}^{Na}\frac{(4\pi)^3\left(R^{I}_{MT}R^{IR}_{MT}\right)^{2}}{N\Omega_0}e^{-iR_{\underset{\sim}{k}}(\vec{q}+\vec{G})\cdot\vec{x}_I}e^{i\vec{k}'\cdot\vec{R}_{IR}}\\&\times\sum_{l''=0}^{\infty}(i)^{l''}\sum_{m''=-l''}^{l''}Y^{*}_{l''m''}\left(\Omega_{R_{\underset{\sim}{k}}\left(-\vec{q}-\vec{G}\right)}\right)\\&\times\sum_{l}\sum_{m}\sum_{l'}\sum_{m'}\\&\times\int d\Omega_{\vec{r}}Y^{*}_{lm}\left(\Omega_{\vec{r}}\right)Y_{l''m''}\left(\Omega_{\vec{r}}\right)Y_{l'm'}\left(\Omega_{R_{\underset{\sim}{k}'}\vec{r}}\right)\\&\times\sum_{\beta}\sum_{\beta'}\int_{0}^{R^{I}_{MT}}dr\left\{P^{*I}_{ls\beta}(r)P^{IR}_{l's\beta'}(r)+\alpha^2Q^{*I}_{ls\beta}(r)Q^{IR}_{l's\beta'}(r)\right\}\cdot j_{l''}\left(\left|R_{\underset{\sim}{k}}\left(\vec{q}+\vec{G}\right)\right|r\right)\\&\times\left(A^{Ij\vec{k}}_{l,m,s,\beta}\right)^{*}A^{IR,j',\vec{k}'}_{l',m',s,\beta'},\end{aligned} \tag{B47}$$

where we have used the fact that the product of the spinors from each wave function gives a delta function ($\chi_s^* \chi_{s'} = \delta_{ss'}$).

To calculate the radial integral in Eq. (B47) we need to express it in terms of Gaunt coefficients; for this purpose we can use the rotational properties of the spherical harmonics:

$$Y_{l'm'}\left(\Omega_{R_{\underset{\sim}{k}'}\vec{r}}\right) = \sum_{m''=-l'}^{l'} \left(D^{l'}_{m'm''}\left(R_{\underset{\sim}{k}'}\right)\right)^* Y_{l'm''}\left(\Omega_{\vec{r}}\right), \tag{B48}$$

where $D^{l'}_{m'm''}\left(R_{\underset{\sim}{k}'}\right)$ is the Wigner rotation matrix (see Rose) corresponding to the Euler angles α, β and γ that are associated with the rotation $R_{\underset{\sim}{k}'}$. The Wigner matrix is calculated according to

$$D^{j}_{m'm}(\alpha,\beta,\gamma) = e^{-im'\alpha} d^{j}_{m'm}(\beta) e^{-im\gamma}, \tag{B49}$$

where

$$d^{j}_{m'm}(\beta) = \left\langle jm' \left| e^{-i\beta \hat{J}_y} \right| jm \right\rangle. \tag{B50}$$

A useful expression for the numerical evaluation of Eq. (B50) was given by Rose (Eq. 4.14 in his book):

$$d^{j}_{m'm}(\beta) = \left[\frac{(j-m)!(j+m')!}{(j+m)!(j-m')!}\right]^{\frac{1}{2}} \frac{\left(\cos\frac{\beta}{2}\right)^{2j+m-m'} \left(-\sin\frac{\beta}{2}\right)^{m'-m}}{(m'-m)!},$$
$$\times {}_2F_1\left(m'-j, -m-j; m'-m+1; -\tan^2\frac{\beta}{2}\right); \qquad m' \geq m \tag{B51}$$

where the function ${}_2F_1(a,b;c;z)$ is the hypergeometric function. Since Eq. (B51) is only valid for $m' \geq m$, a useful relation, that will allow us to calculate $d^{j}_{m'm}(\beta)$ for $m' < m$, follows from the unitary relation $d^{j}_{m'm}(\beta) = d^{j}_{mm'}(-\beta)$. Replacing β by $-\beta$ in Eq. (B51) we obtain $d^{j}_{m'm}(\beta) = (-1)^{m'-m} d^{j}_{mm'}(\beta)$.

Replacing Eq. (B48) into Eq. (B47) we obtain:

$$M_{j,j'}^{MT,s}\left(R_{\underset{\sim}{k}}^{-1},\vec{\underset{\sim}{k}},\vec{q}+\vec{G}\right)=N\sum_{I=1}^{Na}\frac{(4\pi)^3\left(R_{MT}^{I}R_{MT}^{IR}\right)^2}{N\Omega_0}e^{-iR_{\underset{\sim}{k}}(\vec{q}+\vec{G})\cdot\vec{x}_I}e^{i\vec{\underset{\sim}{k}}'\cdot\vec{R}_{IR}}$$

$$\times\sum_{l''=0}^{\infty}(i)^{l''}\sum_{m''=-l''}^{l''}Y_{l''m''}^{*}\left(\Omega_{R_{\underset{\sim}{k}}\left(-\vec{q}-\vec{G}\right)}\right)$$

$$\times\sum_{l}\sum_{m}\sum_{l'}\sum_{m'}$$

$$\times\sum_{m'''=-l'}^{l'}\left(D_{m'm'''}^{l'}\left(R_{\underset{\sim}{k}'}\right)\right)^{*}\int d\Omega_{\vec{r}}Y_{lm}^{*}\left(\Omega_{\vec{r}}\right)Y_{l''m''}\left(\Omega_{\vec{r}}\right)Y_{l'm'''}\left(\Omega_{\vec{r}}\right)$$

$$\times\sum_{\beta}\sum_{\beta'}\int_{0}^{R_{MT}^{I}}dr\left\{P_{ls\beta}^{*I}(r)P_{l's\beta'}^{IR}(r)+\alpha^2Q_{ls\beta}^{*I}(r)Q_{l's\beta'}^{IR}(r)\right\}\cdot j_{l''}\left(\left|R_{\underset{\sim}{k}}\left(\vec{q}+\vec{G}\right)\right|r\right)$$

$$\times\left(A_{l,m,s,\beta}^{Ij\vec{k}}\right)^{*}A_{l',m',s,\beta'}^{IR,j',\vec{k}'}. \tag{B52}$$

B.2.2 Contribution of the Interstitial to the First Matrix Element

The contribution from the interstitial to the first matrix element is given by

$$\left\langle\vec{\underset{\sim}{k}},j,s\left|e^{-iR_{\underset{\sim}{k}}\left(\vec{q}+\vec{G}\right)\cdot\hat{\vec{x}}}\right|R_{\underset{\sim}{k}'}^{-1}\vec{\underset{\sim}{k}}',j',s\right\rangle_{INT}=e^{-i\vec{\underset{\sim}{k}}'\cdot\vec{\tau}\left(R_{\underset{\sim}{k}}'\right)}M_{j,j'}^{INT,s}\left(R_{\underset{\sim}{k}}^{-1},\vec{\underset{\sim}{k}},\vec{q}+\vec{G}\right), \tag{B53}$$

where

$$M_{j,j'}^{INT,s}\left(R_{\underset{\sim}{k}}^{-1},\vec{\underset{\sim}{k}},\vec{q}+\vec{G}\right)=N\int_{\substack{\text{Interstitial}\\\text{in unit cell}}}d^3x\;\Psi_{\vec{\underset{\sim}{k}},j,s}^{*,I}\left(\vec{x}\right)e^{-iR_{\underset{\sim}{k}}\left(\vec{q}+\vec{G}\right)\cdot\vec{x}}$$

$$\times\Psi_{\vec{\underset{\sim}{k}}',j',s}^{I}\left(R_{\vec{\underset{\sim}{k}}'}\vec{x}+\vec{\tau}\left(R_{\underset{\sim}{k}'}\right)\right) \tag{B54}$$

The wave functions for the interstitial are written in terms of plane waves as

$$\Psi^{*}_{\underset{\sim}{k},j,s}\left(\vec{x}\right)=\frac{1}{\sqrt{N\Omega_0}}\sum_{\vec{G}''}C^{*}_{j,s}\left(\underset{\sim}{\vec{k}}+\vec{G}''\right)e^{-i\left(\underset{\sim}{\vec{k}}+\vec{G}''\right)\cdot\vec{x}}\chi_s \tag{B55}$$

$$\begin{aligned}\Psi_{\underset{\sim}{\vec{k}}',j',s}\left(R_{\underset{\sim}{k}'}\vec{x}+\vec{\tau}\left(R_{\underset{\sim}{k}'}\right)\right)&=\frac{1}{\sqrt{N\Omega_0}}\sum_{\vec{G}'''}C_{j',s}\left(\underset{\sim}{\vec{k}}'+\vec{G}'''\right)e^{i\left(\underset{\sim}{\vec{k}}'+\vec{G}'''\right)\cdot\left(R_{\underset{\sim}{k}'}\vec{x}+\vec{\tau}\left(R_{\underset{\sim}{k}'}\right)\right)}\chi_s\\&=\frac{1}{\sqrt{N\Omega_0}}\sum_{\vec{G}'''}e^{i\left(\underset{\sim}{\vec{k}}'+\vec{G}'''\right)\cdot\vec{\tau}\left(R_{\underset{\sim}{k}'}\right)}C_{j',s}\left(\underset{\sim}{\vec{k}}'+\vec{G}'''\right)e^{iR^{-1}_{\underset{\sim}{k}'}\left(\underset{\sim}{\vec{k}}'+\vec{G}'''\right)\cdot\vec{x}}\chi_s\end{aligned} \tag{B56}$$

We then can rewrite Eq. (B54) in the following way:

$$\begin{aligned}M^{INT,s}_{j,j'}\left(R^{-1}_{\underset{\sim}{k}},\underset{\sim}{\vec{k}},\vec{q}+\vec{G}\right)&=\frac{N}{N\Omega_0}\sum_{\vec{G}''}\sum_{\vec{G}'''}C^{*}_{j,s}\left(\underset{\sim}{\vec{k}}+\vec{G}''\right)C_{j',s}\left(\underset{\sim}{\vec{k}}'+\vec{G}'''\right)e^{i\left(\underset{\sim}{\vec{k}}'+\vec{G}'''\right)\cdot\vec{\tau}\left(R_{\underset{\sim}{k}'}\right)}\\&\times\int d^3x\;\; e^{-i\left(\underset{\sim}{\vec{k}}+\vec{G}''+R_{\underset{\sim}{k}}\left(\vec{q}+\vec{G}\right)-R^{-1}_{\underset{\sim}{k}'}\left(\underset{\sim}{\vec{k}}'+\vec{G}'''\right)\right)\cdot\vec{x}}\;.\end{aligned} \tag{B57}$$

The integral in Eq. (B57) is equal to the integral over the primitive unit cell minus the integral over each atomic sphere:

$$\begin{aligned}&\int d^3x\;\; e^{-i\left(\underset{\sim}{\vec{k}}+\vec{G}''+R_{\underset{\sim}{k}}\left(\vec{q}+\vec{G}\right)-R^{-1}_{\underset{\sim}{k}'}\left(\underset{\sim}{\vec{k}}'+\vec{G}'''\right)\right)\cdot\vec{x}}\;\;=\\&\int\limits_{unit\;cell}d^3x\;\; e^{-i\left(\underset{\sim}{\vec{k}}+\vec{G}''+R_{\underset{\sim}{k}}\left(\vec{q}+\vec{G}\right)-R^{-1}_{\underset{\sim}{k}'}\left(\underset{\sim}{\vec{k}}'+\vec{G}'''\right)\right)\cdot\vec{x}}\\&-\int\limits_{\substack{atomic\\spheres}}d^3x\;\; e^{-i\left(\underset{\sim}{\vec{k}}+\vec{G}''+R_{\underset{\sim}{k}}\left(\vec{q}+\vec{G}\right)-R^{-1}_{\underset{\sim}{k}'}\left(\underset{\sim}{\vec{k}}'+\vec{G}'''\right)\right)\cdot\vec{x}}\end{aligned} \tag{B58}$$

$$\int d^3x \;\; e^{-i\left(\vec{\underset{\sim}{k}}+\vec{G}''+R_{\underset{\sim}{k}}\left(\vec{q}+\vec{G}\right)-R^{-1}_{\underset{\sim}{k}'}\left(\vec{\underset{\sim}{k}}'+\vec{G}'''\right)\right)\cdot\vec{x}} \;\; =$$

$$\Omega_0\delta_{\vec{\underset{\sim}{k}}+\vec{G}''+R_{\underset{\sim}{k}}\left(\vec{q}+\vec{G}\right),R^{-1}_{\underset{\sim}{k}'}\left(\vec{\underset{\sim}{k}}'+\vec{G}'''\right)}$$

$$-\sum_I \int\limits_{\substack{I^{th}\\ sphere}}^{atomic} d^3x \;\; e^{-i\left(\vec{\underset{\sim}{k}}+\vec{G}''+R_{\underset{\sim}{k}}\left(\vec{q}+\vec{G}\right)-R^{-1}_{\underset{\sim}{k}'}\left(\vec{\underset{\sim}{k}}'+\vec{G}'''\right)\right)\cdot\vec{x}} \;\; . \qquad \text{(B59)}$$

The second term in the LHS of Eq. (B59) can be expanded in spherical harmonics (Raleigh expansion),

$$\int\limits_{\substack{I^{th}\\ sphere}}^{atomic} d^3x \;\; e^{-i\left(\vec{\underset{\sim}{k}}+\vec{G}''+R_{\underset{\sim}{k}}\left(\vec{q}+\vec{G}\right)-R^{-1}_{\underset{\sim}{k}'}\left(\vec{\underset{\sim}{k}}'+\vec{G}'''\right)\right)\cdot\vec{x}} \;\; =$$

$$= e^{-i\left(\vec{\underset{\sim}{k}}+\vec{G}''+R_{\underset{\sim}{k}}\left(\vec{q}+\vec{G}\right)-R^{-1}_{\underset{\sim}{k}'}\left(\vec{\underset{\sim}{k}}'+\vec{G}'''\right)\right)\cdot\vec{x}_I}$$

$$\times 4\pi\sum_{l=0}^{\infty}(-i)^l\sum_m Y_{lm}(\Omega_{\vec{\underset{\sim}{k}}+\vec{G}''+R_{\underset{\sim}{k}}\left(\vec{q}+\vec{G}\right)-R^{-1}_{\underset{\sim}{k}'}\left(\vec{\underset{\sim}{k}}'+\vec{G}'''\right)}$$

$$\times \int\limits_0^{R_{MT}} drr^2 j_l\left(\left|\vec{\underset{\sim}{k}}+\vec{G}''+R_{\underset{\sim}{k}}\left(\vec{q}+\vec{G}\right)-R^{-1}_{\underset{\sim}{k}'}\left(\vec{\underset{\sim}{k}}'+\vec{G}'''\right)\right| r\right)\int d\Omega_r Y^*_{lm}\left(\Omega_r\right). \qquad \text{(B60)}$$

The angular integral can be easily calculated:

$$\int d\Omega_r Y^*_{lm}\left(\Omega_r\right) = \left(4\pi\right)^{1/2}\int d\Omega_r Y_{00}\left(\Omega_r\right)Y^*_{lm}\left(\Omega_r\right)$$

$$= \left(4\pi\right)^{1/2}\delta_{l,0}\delta_{m,0}. \qquad \text{(B61)}$$

Since in Eq. (B60) we only have to consider the $l=0$ term the radial integral can also be calculated analytically,

$$\int_0^{R_{MT}^I} drr^2 j_0\left(\left|\vec{K}\right|r\right) = \begin{cases} \dfrac{\left(R_{MT}^I\right)^3}{3} & ;\ \left|\vec{K}\right| = 0 \\ \int_0^{R_{MT}} drr^2 \dfrac{\sin\left(\left|\vec{K}\right|r\right)}{\left|\vec{K}\right|r} & ;\ \left|\vec{K}\right| \neq 0 \end{cases} \tag{B62}$$

where $\vec{K} = \vec{\underset{\sim}{k}} + \vec{G}'' + R_{\underset{\sim}{k}}\left(\vec{q}+\vec{G}\right) - R^{-1}_{\vec{\underset{\sim}{k}}'}\left(\vec{\underset{\sim}{k}}'+\vec{G}'''\right)$.

We can then calculate the integral in Eq. (B62):

$$\begin{aligned} \int_0^{R_{MT}^I} drr^2 \frac{\sin\left(\left|\vec{K}\right|r\right)}{\left|\vec{K}\right|r} &= \frac{1}{(\left|\vec{K}\right|)^3} \int_0^{\left|\vec{K}\right|\cdot R_{MT}^I} dr' r' \sin\left(r'\right) \\ &= \frac{1}{(\left|\vec{K}\right|)^3}\left\{-\left|\vec{K}\right| r\cos(\left|\vec{K}\right| r)\Big|_0^{R_{MT}^I} + \int_0^{\left|\vec{K}\right|\cdot R_{MT}^I} dr' \cos\left(r'\right)\right\} \\ &= -\frac{R_{MT}^I}{(\left|\vec{K}\right|)^2}\cos(\left|\vec{K}\right| R_{MT}^I) + \frac{1}{(\left|\vec{K}\right|)^3}\sin(\left|\vec{K}\right| R_{MT}^I). \end{aligned} \tag{B63}$$

Equation (B62) becomes,

$$\int_0^{R_{MT}^I} drr^2 j_0\left(\left|\vec{K}\right|r\right) = \begin{cases} \dfrac{\left(R_{MT}^I\right)^3}{3} & ;\ \left|\vec{K}\right| = 0 \\ -\dfrac{R_{MT}^I}{(\left|\vec{K}\right|)^2}\cos(\left|\vec{K}\right| R_{MT}^I) + \dfrac{1}{(\left|\vec{K}\right|)^3}\sin(\left|\vec{K}\right| R_{MT}^I) & ;\ \left|\vec{K}\right| \neq 0 \end{cases} \tag{B64}$$

Using Eqs. (B59), (B60) and (B64) we obtain a final expression for Eq. (B57),

$$M_{j,j'}^{INT,s}\left(R^{-1}_{\underset{\sim}{k}}, \vec{\underset{\sim}{k}}, \vec{q}+\vec{G}\right) = \sum_{\vec{G}''}\sum_{\vec{G}'''} C^*_{j,s}\left(\vec{\underset{\sim}{k}}+\vec{G}''\right) C_{j',s}\left(\vec{\underset{\sim}{k}}'+\vec{G}'''\right) e^{i\left(\vec{\underset{\sim}{k}}'+\vec{G}'''\right)\cdot\vec{\tau}\left(R_{\underset{\sim}{k}'}\right)}$$

$$\times\begin{cases} 1-\dfrac{4\pi}{\Omega_0}\sum_I \dfrac{\left(R_{MT}^I\right)^3}{3} & ;\ |\vec{K}|=0 \\ -\dfrac{4\pi}{\Omega_0}\sum_I e^{-i\vec{K}\cdot\vec{x}_I}\left[-\dfrac{R_{MT}^I}{|\vec{K}|^2}COS\left(|\vec{K}|R_{MT}^I\right)+\dfrac{1}{|\vec{K}|^3}SIN\left(|\vec{K}|R_{MT}^I\right)\right] & ;\ |\vec{K}|\neq 0 \end{cases} \tag{B65}$$

where $\vec{K}=\vec{\underset{\sim}{k}}+\vec{G}''+R_{\underset{\sim}{k}}\left(\vec{q}+\vec{G}\right)-R^{-1}_{\vec{\underset{\sim}{k}}'}\left(\vec{\underset{\sim}{k}}'+\vec{G}'''\right)$.

Eq. (B37) for the Kohn-Sham response function becomes

$$\chi^S_{\vec{G},\vec{G}'}(s;\vec{q};\omega)=\frac{1}{N\Omega_0}\sum_{\vec{\underset{\sim}{k}}}^{IZ}\sum_{R_{\underset{\sim}{k}}}^{\text{star of k}}\sum_{jj'}\frac{f_{\vec{\underset{\sim}{k}},j,s}-f_{\vec{\underset{\sim}{k}}',j',s}}{E_{\vec{\underset{\sim}{k}},j,s}-E_{\vec{\underset{\sim}{k}}',j',s}+\hbar(\omega+i\eta)}\times e^{iR_{\underset{\sim}{k}}\left(\vec{G}-\vec{G}'\right)\cdot\vec{\tau}\left(R_{\underset{\sim}{k}}\right)}$$
$$\times\left[M^{MT,s}_{j,j'}\left(R^{-1}_{\underset{\sim}{k}},\vec{\underset{\sim}{k}},\vec{q}+\vec{G}\right)+M^{INT,s}_{j,j'}\left(R^{-1}_{\underset{\sim}{k}},\vec{\underset{\sim}{k}},\vec{q}+\vec{G}\right)\right]$$
$$\times\left[M^{MT,s}_{j,j'}\left(R^{-1}_{\underset{\sim}{k}},\vec{\underset{\sim}{k}},\vec{q}+\vec{G}'\right)+M^{INT,s}_{j,j'}\left(R^{-1}_{\underset{\sim}{k}},\vec{\underset{\sim}{k}},\vec{q}+\vec{G}'\right)\right]^*. \tag{B66}$$

B.3 E_g and T_{2g} Decomposition Inside the Atomic Spheres

B.3.1 E_g and T_{2g} Decomposition of the Bloch States

The e_g and t_{2g} orthonormal basis is formed by performing linear combinations of Spherical Harmonics,

$$\Phi_1=\Phi^{(1)}_{e_g}=\frac{1}{\sqrt{2}}\left(Y_{2,2}+Y_{2,-2}\right)\ \rightarrow\ (x^2\text{-}y^2), \tag{B67}$$

$$\Phi_2=\Phi^{(2)}_{e_g}=Y_{2,0}\ \rightarrow\ (3z^2\text{-}r^2), \tag{B68}$$

$$\Phi_3=\Phi^{(1)}_{t_{2g}}=\frac{i}{\sqrt{2}}\left(Y_{2,2}-Y_{2,-2}\right)\ \rightarrow\ (xy), \tag{B69}$$

$$\Phi_4 = \Phi_{t_{2g}}^{(2)} = \frac{i}{\sqrt{2}}\left(Y_{2,1} + Y_{2,-1}\right) \;\rightarrow\; (\mathrm{zy}), \tag{B70}$$

$$\Phi_5 = \Phi_{t_{2g}}^{(3)} = \frac{1}{\sqrt{2}}\left(Y_{2,1} - Y_{2,-1}\right) \;\rightarrow\; (\mathrm{zx}). \tag{B71}$$

Inside the atomic spheres the Bloch States are expanded in the LAPW basis:

$$\Psi_{\vec{k},j,s}^{I}(\vec{x}) = \frac{4\pi\left(R_{MT}^{I}\right)^2}{\sqrt{N\Omega_0}} \sum_{l}\sum_{m}\sum_{\beta} A_{l,m,s,\beta}^{I\vec{jk}}\, u_{l,s,\beta}^{I}(\vec{r})\, Y_{lm}(\Omega_{\vec{r}}). \tag{B72}$$

In general there is no guarantee that the global system of coordinates will be the same as the local system of coordinates needed to describe the splitting into e_g and t_{2g} states induced by the octahedral symmetry. An appropriate local system of coordinates for each cation would be such that the $\hat{x}$ and $\hat{y}$ unit vectors lie in the base plane of the cation-anion octahedral structure; the $\hat{z}$ unit vector should point towards one of the anions at the apex of the octahedron.

If the global system of coordinates does not correspond to the one depicted in Fig. B.2 then we need to change our basis to the local system of coordinates appropriate for each cation. First we find the rotation matrix (R_I) that will allows us to make the transformation from the global system of coordinates to the local one (basically we need to find the appropriate euler angles for this basis transformation). Subsequently we use the rotation properties for the spherical harmonics,

$$Y_{lm}(\Omega_{\vec{r}}) = \sum_{m_1=l}^{l}\left(D_{mm_1}^{l}(R_I)\right)^{*} Y_{lm_1}\left(\Omega_{R^{-1}\vec{r}}\right). \tag{B73}$$

Having Eq. (B73) allows a correct description of the e_g and t_{2g} subspaces; we can then substitute this equation in Eq. (B72) for the Bloch States,

$$\Psi_{\vec{k},j,s}^{I}(\vec{x}) = \frac{4\pi\left(R_{MT}^{I}\right)^2}{\sqrt{N\Omega_0}} \sum_{l}\sum_{m=-l}^{l}\sum_{\beta} A_{l,m,s,\beta}^{I\vec{jk}}\, u_{l,s,\beta}^{I}(\vec{r}) \sum_{m_1=-l}^{l}\left(D_{mm_1}^{l}(R_I)\right)^{*} Y_{lm_1}\left(\Omega_{R^{-1}\vec{r}}\right)$$

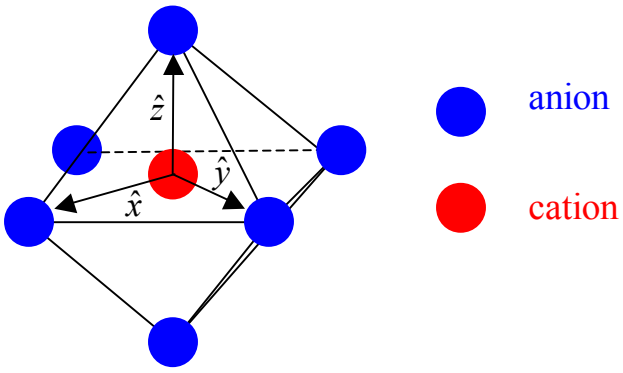

Fig. B.2. Schematic representation of the octahedral symmetry and the appropriate local symmetry axes to be used in the e_g and t_{2g} decomposition of the Bloch States.

$$= \frac{4\pi\left(R_{MT}^{I}\right)^{2}}{\sqrt{N\Omega_0}} \sum_{l} \sum_{m_1=-l}^{l} \left(\sum_{m=-l}^{l} \sum_{\beta} A_{l,m,s,\beta}^{Ij\vec{k}} u_{l,s,\beta}^{I}(\vec{r}) \left(D_{mm_1}^{l}(R_I) \right)^{*} \right) Y_{lm_1}\left(\Omega_{R^{-1}\vec{r}}\right). \tag{B74}$$

Switching the index labels $m_1 \leftrightarrow m$ we have that

$$\begin{aligned} \Psi_{\vec{k},j,s}^{I}(\vec{x}) = & \frac{4\pi\left(R_{MT}^{I}\right)^{2}}{\sqrt{N\Omega_0}} \sum_{l} \\ & \times \sum_{m=-l}^{l} \left(\sum_{m_1=-l}^{l} \sum_{\beta} A_{l,m_1,s,\beta}^{Ij\vec{k}} u_{l,s,\beta}^{I}(\vec{r}) \left(D_{m_1 m}^{l}(R_I) \right)^{*} \right) Y_{lm}\left(\Omega_{R^{-1}\vec{r}}\right) \end{aligned} \tag{B75}$$

To clarify the notation we are going to make the following definition $\Lambda_{l,m,s}^{Ij\vec{k}}(\vec{r}) = \sum_{m_1=-l}^{l} \sum_{\beta} A_{l,m_1,s,\beta}^{Ij\vec{k}} u_{l,s,\beta}^{I}(\vec{r}) \left(D_{m_1 m}^{l}(R_I) \right)^{*} = \sum_{\beta} \left(\sum_{m_1=-l}^{l} \left(D_{m_1 m}^{l}(R_I) \right)^{*} A_{l,m_1,s,\beta}^{Ij\vec{k}} \right) u_{l,s,\beta}^{I}(\vec{r})$ with this definition Eq. (B75) becomes,

$$\Psi_{\vec{k},j,s}^{I}(\vec{x}) = \frac{4\pi\left(R_{MT}^{I}\right)^{2}}{\sqrt{N\Omega_0}} \sum_{l} \sum_{m=-l}^{l} \Lambda_{l,m,s}^{Ij\vec{k}}(\vec{r}) Y_{lm}\left(\Omega_{R^{-1}\vec{r}}\right). \tag{B76}$$

Let us now calculate the inverse relations relating the spherical harmonics to the e_g and t_{2g} basis functions:

$$\Phi_{t_{2g}}^{(2)} + i\Phi_{t_{2g}}^{(3)} = i\sqrt{2}Y_{2,1} \;\rightarrow\; Y_{2,1} = \frac{1}{\sqrt{2}}\left(-i\Phi_{t_{2g}}^{(2)} + \Phi_{t_{2g}}^{(3)} \right), \tag{B77}$$

$$\Phi_{t_{2g}}^{(2)} - i\Phi_{t_{2g}}^{(3)} = i\sqrt{2}Y_{2,-1} \;\rightarrow\; Y_{2,-1} = \frac{1}{\sqrt{2}}\left(-i\Phi_{t_{2g}}^{(2)} - \Phi_{t_{2g}}^{(3)} \right), \tag{B78}$$

$$\Phi_{t_{2g}}^{(1)} + i\Phi_{e_g}^{(1)} = i\sqrt{2}Y_{2,2} \;\rightarrow\; Y_{2,2} = \frac{1}{\sqrt{2}}\left(-i\Phi_{t_{2g}}^{(1)} + \Phi_{e_g}^{(1)} \right), \tag{B79}$$

$$\Phi_{t_{2g}}^{(1)} - i\Phi_{e_g}^{(1)} = -i\sqrt{2}Y_{2,-2} \;\rightarrow\; Y_{2,-2} = \frac{-1}{\sqrt{2}}\left(-i\Phi_{t_{2g}}^{(1)} - \Phi_{e_g}^{(1)} \right), \tag{B80}$$

$$Y_{2,0} = \Phi_{e_g}^{(2)}. \tag{B81}$$

So, for l=2 we have that,

$$\sum_{m=-2}^{2}\Lambda_{l=2,m,s}^{Ij\vec{k}}(\vec{r})\,Y_{2,m}\left(\Omega_{R^{-1}\vec{r}}\right)=\Lambda_{2,0,s}^{Ij\vec{k}}(\vec{r})\,\Phi_{e_g}^{(2)}$$
$$+\Lambda_{2,-1,s}^{Ij\vec{k}}(\vec{r})\frac{1}{\sqrt{2}}\left(-i\Phi_{t_{2g}}^{(2)}-\Phi_{t_{2g}}^{(3)}\right)$$
$$+\Lambda_{2,1,s}^{Ij\vec{k}}(\vec{r})\frac{1}{\sqrt{2}}\left(-i\Phi_{t_{2g}}^{(2)}+\Phi_{t_{2g}}^{(3)}\right)$$
$$+\Lambda_{2,-2,s}^{Ij\vec{k}}(\vec{r})_{2,-2}\frac{-1}{\sqrt{2}}\left(-i\Phi_{t_{2g}}^{(1)}-\Phi_{e_g}^{(1)}\right)$$
$$+\Lambda_{2,2,s}^{Ij\vec{k}}(\vec{r})\frac{1}{\sqrt{2}}\left(-i\Phi_{t_{2g}}^{(1)}+\Phi_{e_g}^{(1)}\right) \qquad \text{(B82)}$$

$$\sum_{m=-2}^{2}\Lambda_{2,m,s}^{Ij\vec{k}}(\vec{r})\,Y_{2,m}\left(\Omega_{R^{-1}\vec{r}}\right)=\frac{1}{\sqrt{2}}\left(\Lambda_{2,-2,s}^{Ij\vec{k}}(\vec{r})+\Lambda_{2,2,s}^{Ij\vec{k}}(\vec{r})\right)\Phi_1$$
$$+\Lambda_{2,0,s}^{Ij\vec{k}}(\vec{r})\Phi_2$$
$$+\frac{i}{\sqrt{2}}\left(\Lambda_{2,-2,s}^{Ij\vec{k}}(\vec{r})-\Lambda_{2,2,s}^{Ij\vec{k}}(\vec{r})\right)\Phi_3$$
$$-\frac{i}{\sqrt{2}}\left(\Lambda_{2,-1,s}^{Ij\vec{k}}(\vec{r})+\Lambda_{2,1,s}^{Ij\vec{k}}(\vec{r})\right)\Phi_4$$
$$-\frac{1}{\sqrt{2}}\left(\Lambda_{2,-1,s}^{Ij\vec{k}}(\vec{r})-\Lambda_{2,1,s}^{Ij\vec{k}}(\vec{r})\right)\Phi_5 \qquad \text{(B83)}$$

where we have replaced $\Phi_{\{e_g,t_{2g}\}}^{i}$ by Φ_i according to Eqs. (B67)-(B71). Eq. (B76) along with Eq. (B83) constitutes the final formulas for the e_g and t_{2g} decomposition of the Bloch States.

B.3.2 E_g and T_{2g} Decomposition of the Matrix Elements

Applying the results of the previous section to the calculation of the atomic spheres Matrix elements we wind up with a new expression for Eq. (B52):

$$M_{j,j'}^{MT,s}\left(R_{\underset{\sim}{k}}^{-1},\vec{\underset{\sim}{k}},\vec{q}+\vec{G}\right)=N\sum_{I=1}^{Na}\frac{(4\pi)^3\left(R_{MT}^{I}R_{MT}^{IR}\right)^2}{N\Omega_0}e^{-iR_{\underset{\sim}{k}}(\vec{q}+\vec{G})\cdot\vec{x}_I}e^{i\vec{\underset{\sim}{k}}'\cdot\vec{R}_{IR}}$$

$$\times\sum_{l''=0}^{\infty}(i)^{l''}\sum_{m''=-l''}^{l''}\left(\sum_{M=-l}^{l}Y_{l''M}^{*}\left(\Omega_{R_{\underset{\sim}{k}}\left(-\vec{q}-\vec{G}\right)}\right)\left(D_{Mm''}^{l}\left(R_I\right)\right)\right)$$

$$\times\sum_{l}\sum_{m}\sum_{l'}$$

$$\times\sum_{m'''=-l'}^{l'}\int d\Omega_{\vec{r}}\Phi_{lm}^{*}\left(\Omega_{\vec{r}}\right)Y_{l''m''}\left(\Omega_{\vec{r}}\right)\Phi_{l'm'''}\left(\Omega_{\vec{r}}\right)$$

$$\times\sum_{\beta}\sum_{\beta'}\int_{0}^{R_{MT}^{I}}dr\left\{P_{ls\beta}^{*I}(r)P_{l's\beta'}^{IR}(r)+\alpha^{2}Q_{ls\beta}^{*I}(r)Q_{l's\beta'}^{IR}(r)\right\}\cdot j_{l''}\left(\left|R_{\underset{\sim}{k}}\left(\vec{q}+\vec{G}\right)\right|r\right)$$

$$\times\left((a)_{l,m,s,\beta}^{Ij\vec{k}}\right)^{*}\left(a_p\right)_{l',m',s,\beta'}^{IR,j',\vec{k}'}. \tag{B84}$$

where we have made the following definitions,

$$\Phi_{lm}\left(\Omega_{\vec{r}}\right)=\begin{cases}Y_{lm}\left(\Omega_{\vec{r}}\right) & ;\, l\neq 2\\ \Phi_i \quad \left(i=1...5\right) & ;\, l=2\end{cases} \tag{B85}$$

$$(a)_{l,m,s,\beta}^{Ij\vec{k}}=\begin{cases}\sum_{m_1=-l}^{l}\left(D_{m_1m}^{l}\left(R_I\right)\right)^{*}A_{l,m_1,s,\beta}^{Ij\vec{k}} & ;\; l\neq 2\\ a_i \quad \left(i=1...5\right) & ;\, l=2\end{cases} \tag{B86}$$

and

$$\left(a_p\right)_{l,m,s,\beta}^{Ij\vec{k}}=\begin{cases}\sum_{m_1=-l}^{l}\left(D_{m_1m}^{l}\left(R_I\right)\right)^{*}\sum_{m_2=-l}^{l}\left(D_{m_2m_1}^{l}\left(R_{\underset{\sim}{k}'}\right)\right)^{*}A_{l,m_2,s,\beta}^{IR,j,\vec{k}} & ;\; l\neq 2\\ \left(a_p\right)_i \quad \left(i=1...5\right) & ;\, l=2\end{cases} \tag{B87}$$

where a_i is defined as follows,

$$a_1 = \frac{1}{\sqrt{2}}\left(\left[\sum_{m_1=-l}^{l}\left(D^l_{m_1 m=-2}(R_I)\right)^* A^{Ij\vec{k}}_{l,m_1,s,\beta}\right]+\left[\sum_{m_1=-l}^{l}\left(D^l_{m_1 m=2}(R_I)\right)^* A^{Ij\vec{k}}_{l,m_1,s,\beta}\right]\right). \quad \text{(B88)}$$

$$a_2 = \sum_{m_1=-l}^{l}\left(D^l_{m_1 m=0}(R_I)\right)^* A^{Ij\vec{k}}_{l,m_1,s,\beta}. \quad \text{(B89)}$$

$$a_3 = \frac{i}{\sqrt{2}}\left(\left[\sum_{m_1=-l}^{l}\left(D^l_{m_1 m=-2}(R_I)\right)^* A^{Ij\vec{k}}_{l,m_1,s,\beta}\right]-\left[\sum_{m_1=-l}^{l}\left(D^l_{m_1 m=2}(R_I)\right)^* A^{Ij\vec{k}}_{l,m_1,s,\beta}\right]\right). \quad \text{(B90)}$$

$$a_4 = \frac{-i}{\sqrt{2}}\left(\left[\sum_{m_1=-l}^{l}\left(D^l_{m_1 m=-1}(R_I)\right)^* A^{Ij\vec{k}}_{l,m_1,s,\beta}\right]+\left[\sum_{m_1=-l}^{l}\left(D^l_{m_1 m=1}(R_I)\right)^* A^{Ij\vec{k}}_{l,m_1,s,\beta}\right]\right). \quad \text{(B91)}$$

$$a_5 = \frac{-1}{\sqrt{2}}\left(\left[\sum_{m_1=-l}^{l}\left(D^l_{m_1 m=-1}(R_I)\right)^* A^{Ij\vec{k}}_{l,m_1,s,\beta}\right]-\left[\sum_{m_1=-l}^{l}\left(D^l_{m_1 m=1}(R_I)\right)^* A^{Ij\vec{k}}_{l,m_1,s,\beta}\right]\right). \quad \text{(B92)}$$

The definitions of $\left(a_p\right)_i$ follow by simply replacing $\left[\sum_{m_1=-l}^{l}\left(D^l_{m_1 m}(R_I)\right)^* A^{Ij\vec{k}}_{l,m_1,s,\beta}\right]$ by $\left[\sum_{m_1=-l}^{l}\left(D^l_{m_1 m}(R_I)\right)^* \sum_{m_2=-l}^{l}\left(D^l_{m_2 m_1}\left(R_{\tilde{k}'}\right)\right)^* A^{IR,j,\vec{k}}_{l,m_2,s,\beta}\right]$ in Eqs. (B88)-(B92).

To calculate the angular integral in Eq. (B84) we need to express it in terms of gaunt coefficients.

Setting the new Gaunt coefficients as

$$G_A\left(lm,l''m'',l'm'''\right) = \int d\Omega_{\vec{r}}\,\Phi^*_{lm}\left(\Omega_{\vec{r}}\right) Y_{l''m''}\left(\Omega_{\vec{r}}\right)\Phi_{l'm'''}\left(\Omega_{\vec{r}}\right), \quad \text{(B93)}$$

we then consider the different possible values for l and l'; when $l \neq 2$ and $l' \neq 2$ Eq. (B93) is equal to the usual Gaunt coefficients,

$$G_A\left(lm,l''m'',l'm'''\right) = G\left(lm,l''m'',l'm'''\right) = \int d\Omega_{\vec{r}}\, Y^*_{lm}\left(\Omega_{\vec{r}}\right) Y_{l''m''}\left(\Omega_{\vec{r}}\right) Y_{l'm'''}\left(\Omega_{\vec{r}}\right). \quad \text{(B94)}$$

It is important to notice that the Gaunt coefficients are equal to zero unless the sum $l+l'+l''$ is even; $\left|l''-l'\right| \leq l \leq l''+l'$, or $m = m''+m'$.

If $l=2$ and $l'\neq 2$ we have that

$$G_A\left(lm=-2,l''m'',l'm'''\right)=\frac{1}{\sqrt{2}}\left(G\left(lm=2,l''m'',l'm'''\right)+G\left(lm=-2,l''m'',l'm'''\right)\right), \tag{B95}$$

$$G_A\left(lm=-1,l''m'',l'm'''\right)=G\left(lm=0,l''m'',l'm'''\right), \tag{B96}$$

$$G_A\left(lm=0,l''m'',l'm'''\right)=\frac{-i}{\sqrt{2}}\left(G\left(lm=2,l''m'',l'm'''\right)-G\left(lm=-2,l''m'',l'm'''\right)\right), \tag{B97}$$

$$G_A\left(lm=1,l''m'',l'm'''\right)=\frac{-i}{\sqrt{2}}\left(G\left(lm=1,l''m'',l'm'''\right)+G\left(lm=-1,l''m'',l'm'''\right)\right), \tag{B98}$$

$$G_A\left(lm=2,l''m'',l'm'''\right)=\frac{1}{\sqrt{2}}\left(G\left(lm=1,l''m'',l'm'''\right)-G\left(lm=-1,l''m'',l'm'''\right)\right). \tag{B99}$$

If $l\neq 2$ and $l'=2$ we have that

$$G_A\left(lm,l''m'',l'm'''=-2\right)=\frac{1}{\sqrt{2}}\left(G\left(lm,l''m'',l'm'''=2\right)+G\left(lm,l''m'',l'm'''=-2\right)\right). \tag{B100}$$

$$G_A\left(lm,l''m'',l'm'''=-1\right)=G\left(lm,l''m'',l'm'''=0\right), \tag{B101}$$

$$G_A\left(lm,l''m'',l'm'''=0\right)=\frac{i}{\sqrt{2}}\left(G\left(lm,l''m'',l'm'''=2\right)-G\left(lm,l''m'',l'm'''=-2\right)\right), \tag{B102}$$

$$G_A\left(lm,l''m'',l'm'''=1\right)=\frac{i}{\sqrt{2}}\left(G\left(lm,l''m'',l'm'''=1\right)+G\left(lm,l''m'',l'm'''=-1\right)\right), \tag{B103}$$

$$G_A\left(lm,l''m'',l'm'''=2\right)=\frac{1}{\sqrt{2}}\left(G\left(lm,l''m'',l'm'''=1\right)-G\left(lm,l''m'',l'm'''=-1\right)\right). \tag{B104}$$

When $l=2$ and $l'=2$ it is simpler if we define the following matrix

$$\mathrm{M} = \begin{bmatrix} \frac{1}{\sqrt{2}} & 2 & 1 & -2 \\ 1 & 0 & 0 & 0 \\ \frac{i}{\sqrt{2}} & 2 & -1 & -2 \\ \frac{i}{\sqrt{2}} & 1 & +1 & -1 \\ \frac{1}{\sqrt{2}} & 1 & -1 & -1 \end{bmatrix}, \tag{B105}$$

then the new Gaunt coefficients can be written in terms of the rows (i) and columns (j) of the M matrix as

$$\begin{aligned} G_A(lm, l''m'', l'm''') = \sum_{j=1}^{*} M_{i=3+m} \sum_{j=1} M_{i=3+m'''} \Bigg[& G\left(lm = M_{\substack{i=3+m \\ j=2}}, l''m'', l'm''' = M_{\substack{i=3+m''' \\ j=2}} \right) \\ & + \sum_{j=3} M_{i=3+m'''} G\left(lm = M_{\substack{i=3+m \\ j=2}}, l''m'', l'm''' = M_{\substack{i=3+m''' \\ j=4}} \right) \\ & + \sum_{j=3} M_{i=3+m} G\left(lm = M_{\substack{i=3+m \\ j=4}}, l''m'', l'm''' = M_{\substack{i=3+m''' \\ j=2}} \right) \\ & + \sum_{j=3} M_{i=3+m} \sum_{j=3} M_{i=3+m'''} G\left(lm = M_{\substack{i=3+m \\ j=4}}, l''m'', l'm''' = M_{\substack{i=3+m''' \\ j=4}} \right) \Bigg] \end{aligned} \tag{B106}$$

Appendix C Crystal Local Field Effects in the Charge Density Response Function: Case of MgB_2

In this appendix we derive (3.6). This equation is exact and valid for an *N x N* dielectric matrix, thus permitting a valuable insight into the low energy excitation of MgB_2 for large momentum transfers.

The charge density response function can be written in the following way:

$$\mathrm{Im}\,\chi(\vec{q},\omega)=\frac{1}{v}\mathrm{Im}\left[-\varepsilon\left(\vec{q}-\vec{G}_q;\omega\right)\right]^{-1}_{\vec{G}_q,\vec{G}_q}, \tag{C1}$$

where v is the coulomb factor, $\varepsilon\left(\vec{q}-\vec{G}_q;\omega\right)$ is the dielectric matrix, $\vec{q}$ is the experimental wave vector and $\vec{G}_q$ is the unique reciprocal vector that brings $\vec{q}$ back to the first Brillouin Zone.

The $\left\{\vec{G}_q,\vec{G}_q\right\}$ element of the inverse of the dielectric matrix is given by

$$\left[-\varepsilon\left(\vec{q}-\vec{G}_q;\omega\right)\right]^{-1}_{\vec{G}_q,\vec{G}_q}=\frac{-M_{\vec{G}_q\vec{G}_q}\left(\vec{q}-\vec{G}_q;\omega\right)}{Det\left(\varepsilon\left(\vec{q}-\vec{G}_q;\omega\right)\right)}, \tag{C2}$$

where $M_{\vec{G}_q\vec{G}_q}\left(\vec{q}-\vec{G}_q;\omega\right)$ is the minor for the $\left\{\vec{G}_q,\vec{G}_q\right\}$ element of ε. Eq. (C2) can be written in the following way (In the following it is understood that all functions depend on $\vec{q}-\vec{G}_q$ and ω; I have not written explicitly these dependences to make the algebra as clear as possible),

$$\left[-\varepsilon\right]^{-1}_{\vec{G}_q,\vec{G}_q}=\frac{-1}{\dfrac{Det(\varepsilon)}{M_{\vec{G}_q\vec{G}_q}}}=\frac{-1}{\varepsilon_{\vec{G}_q\vec{G}_q}+\dfrac{Det(\varepsilon)}{M_{\vec{G}_q\vec{G}_q}}-\varepsilon_{\vec{G}_q\vec{G}_q}}=\frac{-1}{\varepsilon_{\vec{G}_q\vec{G}_q}+a_{\vec{G}_q\vec{G}_q}}, \tag{C3}$$

where $a_{\vec{G}_q\vec{G}_q}$ is defined as

$$a_{\vec{G}_q\vec{G}_q} = \frac{Det(\varepsilon)}{M_{\vec{G}_q\vec{G}_q}} - \varepsilon_{\vec{G}_q\vec{G}_q}. \tag{C4}$$

We can rearrange Eq. (C3) and we have that,

$$\left[-\varepsilon\right]^{-1}_{\vec{G}_q,\vec{G}_q} = \frac{-\varepsilon_{\vec{G}_q\vec{G}_q} + a_{\vec{G}_q\vec{G}_q} - a_{\vec{G}_q\vec{G}_q}}{\varepsilon_{\vec{G}_q\vec{G}_q}\left(\varepsilon_{\vec{G}_q\vec{G}_q} + a_{\vec{G}_q\vec{G}_q}\right)} = -\frac{1}{\varepsilon_{\vec{G}_q\vec{G}_q}} + \frac{1}{\varepsilon^2_{\vec{G}_q\vec{G}_q}} \frac{a_{\vec{G}_q\vec{G}_q}}{\left(1 + \frac{a_{\vec{G}_q\vec{G}_q}}{\varepsilon_{\vec{G}_q\vec{G}_q}}\right)}. \tag{C5}$$

It will be convenient to multiply the second term in Eq. (C5) by $M_{\vec{G}_q\vec{G}_q}$,

$$\left[-\varepsilon\right]^{-1}_{\vec{G}_q,\vec{G}_q} = -\frac{1}{\varepsilon_{\vec{G}_q\vec{G}_q}} + \frac{1}{\varepsilon^2_{\vec{G}_q\vec{G}_q}} \frac{M_{\vec{G}_q\vec{G}_q} a_{\vec{G}_q\vec{G}_q}}{\left(M_{\vec{G}_q\vec{G}_q} + \frac{M_{\vec{G}_q\vec{G}_q} a_{\vec{G}_q\vec{G}_q}}{\varepsilon_{\vec{G}_q\vec{G}_q}}\right)}. \tag{C6}$$

From Eq. (C4) we have that for an arbitrary $\vec{G}$ vector,

$$a_{\vec{G}\vec{G}} = \frac{Det(\varepsilon)}{M_{\vec{G}\vec{G}}} - \varepsilon_{\vec{G}\vec{G}}. \tag{C7}$$

In this case $a_{\vec{G}\vec{G}}$ plays the same role as $a_{\vec{G}_q\vec{G}_q}$ but in the calculation of $\left[-\varepsilon\left(\vec{q}-\vec{G}_q;\omega\right)\right]^{-1}_{\vec{G},\vec{G}}$. More precisely,

$$\left[-\varepsilon\left(\vec{q}-\vec{G}_q;\omega\right)\right]^{-1}_{\vec{G},\vec{G}} = \frac{-1}{\varepsilon_{\vec{G}\vec{G}}\left(\vec{q}-\vec{G}_q;\omega\right) + a_{\vec{G}\vec{G}}\left(\vec{q}-\vec{G}_q;\omega\right)}. \tag{C8}$$

Combining Eqs. (C4) and (C7) we obtain,

$$M_{\vec{G}_q\vec{G}_q} a_{\vec{G}_q\vec{G}_q} = M_{\vec{G}\vec{G}} a_{\vec{G}\vec{G}} + \varepsilon_{\vec{G}\vec{G}} M_{\vec{G}\vec{G}} - \varepsilon_{\vec{G}_q\vec{G}_q} M_{\vec{G}_q\vec{G}_q}. \tag{C9}$$

Replacing Eq. (C9) in the denominator of the second term of Eq. (C6) we find,

$$\left[-\varepsilon\right]^{-1}_{\vec{G}_q,\vec{G}_q} = -\frac{1}{\varepsilon_{\vec{G}_q\vec{G}_q}} + \frac{1}{\varepsilon^2_{\vec{G}_q\vec{G}_q}} \frac{M_{\vec{G}_q\vec{G}_q} a_{\vec{G}_q\vec{G}_q}}{\left(M_{\vec{G}_q\vec{G}_q} + \frac{M_{\vec{G}\vec{G}} a_{\vec{G}\vec{G}}}{\varepsilon_{\vec{G}_q\vec{G}_q}} + \frac{\varepsilon_{\vec{G}\vec{G}} M_{\vec{G}\vec{G}}}{\varepsilon_{\vec{G}_q\vec{G}_q}} - M_{\vec{G}_q\vec{G}_q} \right)} . \quad \text{(C10)}$$

Replacing Eq. (C4) in the numerator of the second term of Eq. (C10) we have that,

$$\left[-\varepsilon\right]^{-1}_{\vec{G}_q,\vec{G}_q} = -\frac{1}{\varepsilon_{\vec{G}_q\vec{G}_q}} + \frac{\left(Det(\varepsilon) - \varepsilon_{\vec{G}_q\vec{G}_q} M_{\vec{G}_q\vec{G}_q} \right)}{\varepsilon_{\vec{G}_q\vec{G}_q} M_{\vec{G}\vec{G}}} \frac{1}{\left(\varepsilon_{\vec{G}\vec{G}} + a_{\vec{G}\vec{G}} \right)} . \quad \text{(C11)}$$

Replacing Eq. (C8) in Eq. (C11) we finally obtain,

$$\left[-\varepsilon\right]^{-1}_{\vec{G}_q,\vec{G}_q} = -\frac{1}{\varepsilon_{\vec{G}_q\vec{G}_q}} - \frac{\left(Det(\varepsilon) - \varepsilon_{\vec{G}_q\vec{G}_q} M_{\vec{G}_q\vec{G}_q} \right)}{\varepsilon_{\vec{G}_q\vec{G}_q} M_{\vec{G}\vec{G}}} \left[-\varepsilon\right]^{-1}_{\vec{G},\vec{G}} . \quad \text{(C12)}$$

Setting

$$F\left(\vec{q}-\vec{G},\vec{q}-\vec{G}_q;\omega\right) = -\frac{\left(Det\left(\varepsilon\left(\vec{q}-\vec{G}_q;\omega\right)\right) - \varepsilon_{\vec{G}_q\vec{G}_q}\left(\vec{q}-\vec{G}_q;\omega\right) M_{\vec{G}_q\vec{G}_q}\left(\vec{q}-\vec{G}_q;\omega\right) \right)}{\varepsilon_{\vec{G}_q\vec{G}_q}\left(\vec{q}-\vec{G}_q;\omega\right) M_{\vec{G}\vec{G}}\left(\vec{q}-\vec{G}_q;\omega\right)} , \quad \text{(C13)}$$

and putting back the $\vec{q}-\vec{G}_q$ and ω dependence in all functions, Eq. (C12) becomes

$$\left[-\varepsilon\left(\vec{q}-\vec{G}_q;\omega\right)\right]^{-1}_{\vec{G}_q,\vec{G}_q} = -\frac{1}{\varepsilon_{\vec{G}_q\vec{G}_q}\left(\vec{q}-\vec{G}_q;\omega\right)} + F\left(\vec{q}-\vec{G},\vec{q}-\vec{G}_q;\omega\right)\left[-\varepsilon\left(\vec{q}-\vec{G}_q;\omega\right)\right]^{-1}_{\vec{G},\vec{G}} \quad \text{(C14)}$$

This result is valid for any $N \times N$ dielectric matrix.

In particular, when $\vec{q}$ belongs to higher BZ's than the first one it is convenient to set $\vec{G} = \vec{0}$,

$$\left[-\varepsilon\left(\vec{q}-\vec{G}_q;\omega\right)\right]^{-1}_{\vec{G}_q,\vec{G}_q} = -\frac{1}{\varepsilon_{\vec{G}_q\vec{G}_q}\left(\vec{q}-\vec{G}_q;\omega\right)}$$
$$+F\left(\vec{q},\vec{q}-\vec{G}_q;\omega\right)\left[-\varepsilon\left(\vec{q}-\vec{G}_q;\omega\right)\right]^{-1}_{\vec{G}=\vec{0},\vec{G}=\vec{0}} \qquad \text{(C15)}$$

in this case, $F\left(\vec{q},\vec{q}-\vec{G}_q;\omega\right)$ acts as a coupling constant relating the physics of large q's, namely $\left[-\varepsilon\left(\vec{q}-\vec{G}_q;\omega\right)\right]^{-1}_{\vec{G}_q,\vec{G}_q}$, with the physics of small q's given by $\left[-\varepsilon\left(\vec{q}-\vec{G}_q;\omega\right)\right]^{-1}_{\vec{G}=\vec{0},\vec{G}=\vec{0}}$.

Appendix D Epsilon Effective

We are going to present a derivation of Eq. (4.2) for ε_{eff} needed in for the correct explanation of the nature of the collective mode observed in manganites and rutiles systems. There are no approximations in this derivation, the resulting formula is exact.

Epsilon effective is defined as

$$\varepsilon_{eff}\left(\vec{q};\vec{\omega}\right)=\frac{1}{\varepsilon^{-1}_{\vec{G}_q,\vec{G}_q}\left(\vec{q}-\vec{G}_q;\omega\right)}, \tag{D1}$$

where the vector $\vec{k}=\vec{q}-\vec{G}_q$ lies in the First Brillouin Zone (1BZ) and $\varepsilon^{-1}_{\vec{G}_q,\vec{G}_q}\left(\vec{q}-\vec{G}(\vec{q});\omega\right)$ is the $\left\{\vec{G}_q,\vec{G}_q\right\}$ element of the inverse of the dielectric matrix. The $\vec{G}_q$ vector specifies the element in the dielectric matrix one has to invert in a scalar calculation of the response function. Remember that $S\left(\vec{q}\,|\,\omega\right)=-2\hbar V\,\mathrm{Im}\,\chi_{\vec{G}_q,\vec{G}_q}\left(\vec{q}-\vec{G}_q\,|\,\omega\right)$ (if $\vec{q}$ is in the first BZ then $\vec{G}_q=0$).

The formula to calculate $\varepsilon^{-1}_{\vec{G}_q,\vec{G}_q}\left(\vec{q}-\vec{G}_q;\omega\right)$ is given by

$$\varepsilon^{-1}_{\vec{G}_q,\vec{G}_q}\left(\vec{q}-\vec{G}_q;\omega\right)=\frac{(-1)^{q+q}\,M_{q,q}}{\left|\varepsilon\left(\vec{q}-\vec{G}_q;\omega\right)\right|}, \tag{D2}$$

where $M_{q,q}$ is the "minor" of the dielectric matrix corresponding to the determinant of the matrix formed by omitting the qth row and the qth column of the dielectric matrix , we are going to call this reduced matrix ε'. $\left|\varepsilon\left(\vec{q}-\vec{G}_q;\omega\right)\right|$ is the determinant of the dielectric matrix $\varepsilon\left(\vec{q}-\vec{G}_q;\omega\right)$.

If we calculate $\left|\varepsilon\left(\vec{q}-\vec{G}_q;\omega\right)\right|$ by expanding the qth row we have that

$$\left|\varepsilon\left(\vec{q}-\vec{G}_q;\omega\right)\right|=\sum_{i=0}(-1)^{q+i}\varepsilon_{\vec{G}_q,\vec{G}_i}\left(\vec{q}-\vec{G}_q;\omega\right)M_{qi}, \tag{D3}$$

where M_{qi} is the minor that we obtain by taking out the q[th] row and the i[th] column of $\varepsilon\left(\vec{q}-\vec{G}_q;\omega\right)$.

It will be useful to rewrite Eq. (D3) in the following way

$$\left|\varepsilon\left(\vec{q}-\vec{G}_q;\omega\right)\right| = (-1)^{2q}\,\varepsilon_{\vec{G}_q,\vec{G}_q}\left(\vec{q}-\vec{G}_q;\omega\right)M_{qq} + \sum_{i\neq q}(-1)^{q+i}\,\varepsilon_{\vec{G}_q,\vec{G}_i}\left(\vec{q}-\vec{G}_q;\omega\right)M_{qi} \tag{D4}$$

Eq. (D4) can be further expanded as (where we are going to omit the $\vec{q}-\vec{G}_q$ and ω dependence for clearer notation),

$$\begin{aligned}|\varepsilon| &= \varepsilon_{\vec{G}_q,\vec{G}_q}M_{qq} + \sum_{\substack{i\neq q\\ i<q}}(-1)^{q+i}\,\varepsilon_{\vec{G}_q,\vec{G}_i} \\ &\times\left\{\sum_{\substack{j\neq q\\ j<q}}(-1)^{j+q-1}\,\varepsilon_{\vec{G}_j,\vec{G}_q}M_{\{q,j\},\{q,i\}} + \sum_{\substack{j\neq q\\ j>q}}(-1)^{j+q}\,\varepsilon_{\vec{G}_j,\vec{G}_q}M_{\{q,j\},\{q,i\}}\right\} \\ &+\sum_{\substack{i\neq q\\ i>q}}(-1)^{q+i}\,\varepsilon_{\vec{G}_q,\vec{G}_i} \\ &\times\left\{\sum_{\substack{j\neq q\\ j<q}}(-1)^{j+q}\,\varepsilon_{\vec{G}_j,\vec{G}_q}M_{\{q,j\},\{q,i\}} + \sum_{\substack{j\neq q\\ j>q}}(-1)^{j+q-1}\,\varepsilon_{\vec{G}_j,\vec{G}_q}M_{\{q,j\},\{q,i\}}\right\}\end{aligned} \tag{D5}$$

where we have expressed M_{qi} in terms of an expansion of the q[th] column. $M_{\{q,j\},\{q,i\}}$ is the minor corresponding to the reduced matrix obtained after having taking out the q[th] and j[th] rows and the q[th] and i[th] columns from the dielectric matrix $\varepsilon\left(\vec{q}-\vec{G}_q;\omega\right)$.

Epsilon effective can then be written as

$$\varepsilon_{eff}\left(\vec{q}\,|\,\omega\right)=\frac{1}{\varepsilon^{-1}_{\vec{G}_q,\vec{G}_q}\left(\vec{q}-\vec{G}_q\,|\,\omega\right)}=\frac{\left|\varepsilon\left(\vec{q}-\vec{G}_q;\omega\right)\right|}{M_{qq}}=$$

$$=\varepsilon_{\vec{G}_q,\vec{G}_q}+\sum_{\substack{i,j\neq q\\ \{i,j<q \text{ or}\\ i,j>q\}}}(-1)^{q+i+j+q-1}\varepsilon_{\vec{G}_q,\vec{G}_i}\frac{M_{\{q,j\},\{q,i\}}}{M_{qq}}\varepsilon_{\vec{G}_j,\vec{G}_q}$$

$$+\sum_{\substack{i,j\neq q\\ \{i<q,j>q \text{ or}\\ i>q,j<q\}}}(-1)^{q+i+j+q}\varepsilon_{\vec{G}_q,\vec{G}_i}\frac{M_{\{q,j\},\{q,i\}}}{M_{qq}}\varepsilon_{\vec{G}_j,\vec{G}_q} \qquad \text{(D6)}$$

We also have, from the definition of inverse matrix, that

$$\left[\varepsilon'\right]^{-1}_{\vec{G}_i,\vec{G}_{j\neq q}}=\frac{M_{\{q,j\},\{q,i\}}}{M_{qq}}\begin{cases}\times(-1)^{i+j} & \text{if } i,j<q \text{ or } i,j>q\\ \times(-1)^{i+j-1} & \text{if } i<q \text{ and } j>q \text{ or}\\ & i>q \text{ and } j<q\end{cases} \qquad \text{(D7)}$$

where, by definition, M_{qq} is the determinant of the reduced matrix ε' (defined previously) and $M_{\{q,i\},\{q,i\}}$ is a minor in the subspace of ε'. The index notation in Eq. (D7) refers to the original matrix ε (by definition, ε' is constructed from ε, by taking out the qth row and the qth column).

Inserting Eq. (D7) into Eq. (D6) we have that

$$\varepsilon_{eff}\left(\vec{q}\,|\,\omega\right)=\varepsilon_{\vec{G}_q,\vec{G}_q}\left(\vec{q}-\vec{G}_q\,|\,\omega\right)$$

$$-\sum_{i,j\neq q}\varepsilon_{\vec{G}_q,\vec{G}_i}\left(\vec{q}-\vec{G}_q\,|\,\omega\right)\left[\varepsilon'\right]^{-1}_{\vec{G}_i,\vec{G}_j}\varepsilon_{\vec{G}_j,\vec{G}_q}\left(\vec{q}-\vec{G}_q\,|\,\omega\right) \qquad \text{(D8)}$$

Appendix E "Star of k" and Basis Transformations

E.1 Introduction

To calculate physical properties of a periodic solid it is necessary to sum over vectors in reciprocal space. The choice of these vectors is done by taking into account the symmetry properties of the crystal along with the Born-Von Karman boundary conditions. These two settings lead to the definition of the Irreducible wedge (IW) of the first Brillouin zone (BZ) in which all the summations are going to take place.

A vector in real or reciprocal space is expanded in a basis that is convenient for the calculation we have in mind. In this appendix we give the expansion coefficients of a vector (in real or reciprocal space) in three different bases (the definition of these three bases is necessary for the calculation of the density response function). The relationship between the coefficients of these different bases is found for various structures (fcc, bcc, hcp) in the form of 3x3 matrices.

E.2 Use of Symmetry

Let us consider a two-dimensional periodic square lattice composed of sixteen atoms, with lattice constant a, Fig. E.1 gives a representation of this lattice in real and reciprocal space. According to the Born-Von Karman boundary conditions the allowed k vectors $\vec{k} = \left(\vec{k}_x, \vec{k}_y\right)$ are determined by the formulas: $\vec{k}_x = \frac{2\pi}{N_1 a} n\hat{x}$ and $\vec{k}_y = \frac{2\pi}{N_2 a} m\hat{y}$, where N_1 and N_2 are the number of atoms in the $\hat{x}$ and $\hat{y}$ directions respectively, four in each direction in Fig. E.1, n and m are integers $\left(n, m = 0, \pm 1, \pm 2, \ldots\right)$. The sides of the first BZ bisect the lines joining the central point (or Γ point) to every one of its nearest neighboring points.

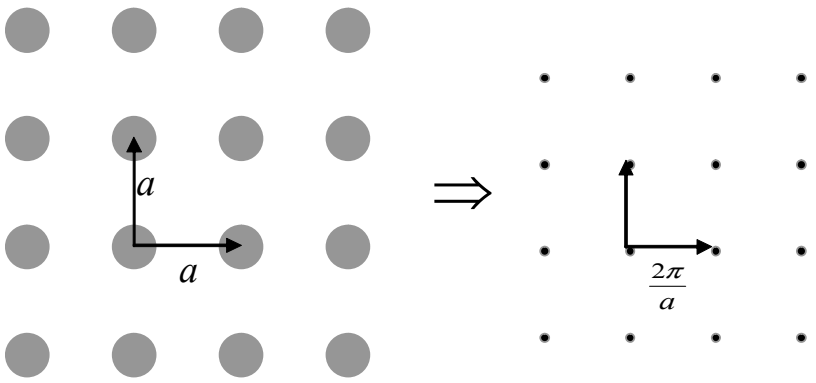

Fig. E.1. Real and reciprocal space representation of a periodic square lattice. The black circles in reciprocal space correspond to reciprocal lattice vectors.

E.2.1 Star of k and Wedge of the First BZ

By using rotational symmetries one can obtain all the vectors in the BZ by considering only the ones in the IW. The IW corresponds to the smallest number of points in the first BZ from which (after applying all the symmetry operations to them) all the linear independent points in the first BZ are produced. To every point $\vec{k}$ in the IW there corresponds a certain weight which accounts for the number of linearly independent points, also called the star of $\vec{k}$, in the first BZ generated by that single point in the IW. In Fig. E.2 we construct the different stars for the model we have consider so far. A weight is assigned to each one of the stars. The "1", "2", and "4" stars have weight 4; the star "3" has weight 2 and the "5" and "Γ" star have weight 1. All the points in the BZ are constructed by applying rotations to the points in the IW. As an example, in Fig. E.3 we reproduced the star of "1".

In Fig. E.3 the point which belongs to the IW has coordinates $\left(k_x, k_y\right) = \left(\frac{\pi}{2a}, \frac{\pi}{2a}\right)$; we can generate the coordinates for the other four points by applying rotations:

$$\begin{pmatrix} k_{-x} \\ k_y \end{pmatrix} = \begin{pmatrix} -1 & 0 \\ 0 & 1 \end{pmatrix} \begin{pmatrix} k_x \\ k_y \end{pmatrix}, \tag{E1}$$

$\left(k_{-x}, k_y\right)$ are the coordinates of the point whose coordinates are in the –x and y directions, for the other points we have:

$$\begin{pmatrix} k_{-x} \\ k_{-y} \end{pmatrix} = \begin{pmatrix} 1 & 0 \\ 0 & -1 \end{pmatrix} \begin{pmatrix} k_{-x} \\ k_y \end{pmatrix} = \begin{pmatrix} -1 & 0 \\ 0 & -1 \end{pmatrix} \begin{pmatrix} k_x \\ k_y \end{pmatrix}, \tag{E2}$$

$$\begin{pmatrix} k_x \\ k_{-y} \end{pmatrix} = \begin{pmatrix} -1 & 0 \\ 0 & 1 \end{pmatrix} \begin{pmatrix} k_{-x} \\ k_{-y} \end{pmatrix} = \begin{pmatrix} 1 & 0 \\ 0 & -1 \end{pmatrix} \begin{pmatrix} k_x \\ k_y \end{pmatrix}. \tag{E3}$$

One can also relate any point in the reciprocal lattice to one point of the star by using translations, for example let's take the point $\vec{k}_1$ in the graph with coordinates $\left(\frac{3\pi}{2a}, \frac{3\pi}{2a}\right)$. This point can be mapped one of the points in the star of 1 by applying the translation $\vec{k} - \vec{G}$, where G is a vector of the reciprocal lattice (in this case $G = \left(\frac{2\pi}{a}, \frac{2\pi}{a}\right)$).

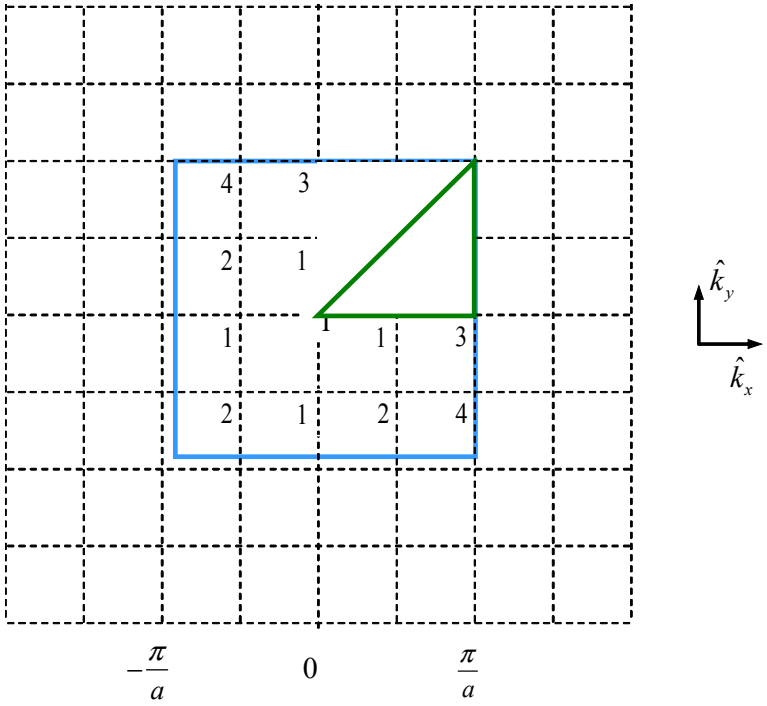

Fig. E.2. The first BZ is denoted by the blue rectangle. The IW corresponds to the green triangle.

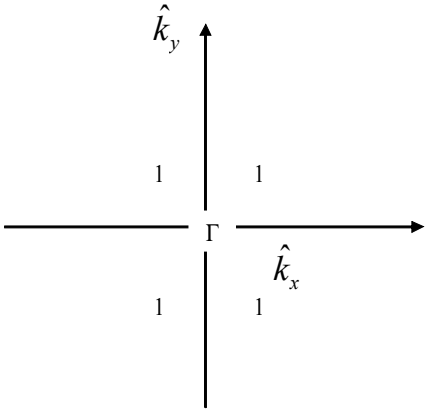

Fig. E.3. Star of "1".

In Fig. E.4 it is shown the areas spanned by the first two reciprocal vectors, $G=\left(\frac{2\pi}{a},\frac{2\pi}{a}\right)$ and $G=\left(\frac{4\pi}{a},\frac{4\pi}{a}\right)$, we see how the $\vec{k}_1$ is within the region covered by the second primitive vector. The momentum transfer $\vec{q}$ in non-resonant Inelastic Scattering experiments is usually not confined to the first BZ; for these large momentum transfers we are required to map $\vec{q}$ to one of the members of the star of one the vectors in the IW (since only for the latter we are able to obtain the relevant physical information: eigenvalues, eigenvectors, etc…).

E.2.2. Parallelepiped Zone

One can also construct a parallelepiped primitive zone with the same physical information as in the BZ, that is we can construct the Bloch States $\Psi_{\vec{k}_{par.}}(\vec{x})=\Psi_{\vec{k}_{BZ}+\vec{G}}(\vec{x})=\Psi_{\vec{k}_{BZ}}(\vec{x})$, where $\vec{k}_{par.}$ is inside the parallelepiped but not necessarily inside the BZ, $\vec{k}_{BZ}$ is inside the BZ and $\vec{G}$ is a reciprocal lattice vector.

This zone will have as primitive vectors the vectors of the reciprocal lattice. The IW of the BZ can be mapped inside the parallepiped zone. Although the BZ is useful for numerical work, the parallelepiped allows us to treat all structures with the same algorithm if case we want to recognize if a $\vec{k}$ vector belongs or not to the parallepiped zone. This is useful because in the formula to calculate the response we encounter in some cases that $\vec{k}'=\vec{k}+\vec{q}$ (where $\vec{k}'$, $\vec{k}$ and $\vec{q}$ are in the parallelepiped zone) is outside our primitive zone and we want to bring it back because we only have the information from the ground state in that zone. Then, the translational symmetry of the lattice allows us to write: $\vec{k}'=\vec{k}+\vec{q}-\vec{G}$, $\vec{G}$ is the reciprocal lattice vector that brings $\vec{k}+\vec{q}$ back into the parallelepiped zone. For complicated shapes of the BZ, the parallelepiped zone represents a simpler form of summing over points of the IW.

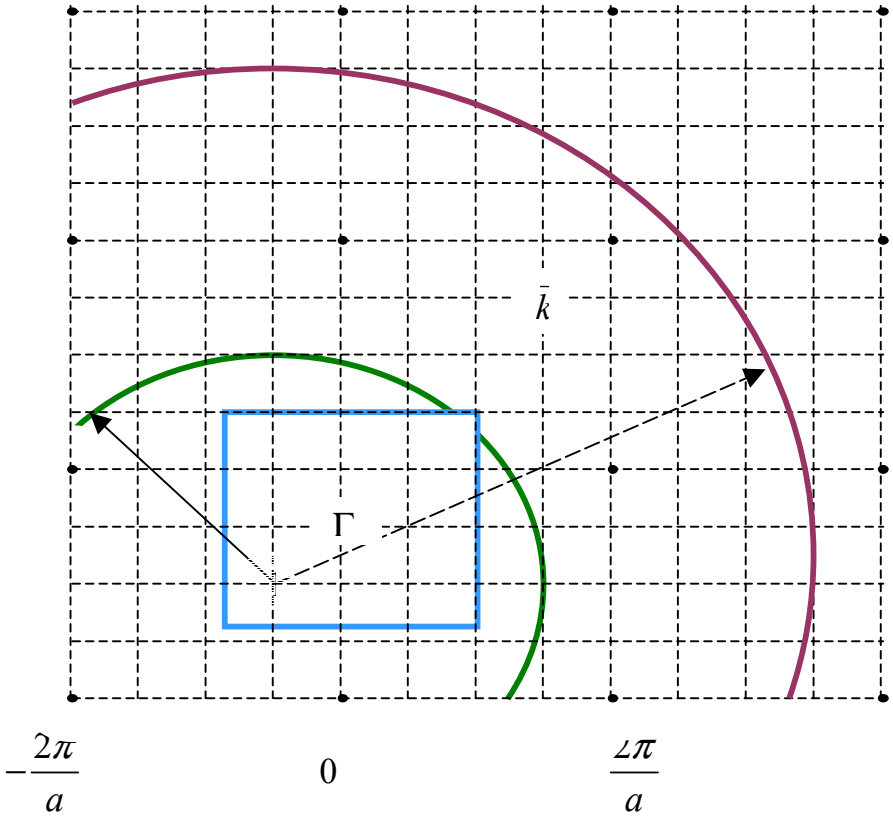

Fig. E.4. Mapping of $\vec{k}_1$ to the first BZ requires use of the reciprocal lattice vector $G = \left(\frac{2\pi}{a}, \frac{2\pi}{a}\right)$.

As shown in the Fig. E.5, all the points in the IW also belong to the parallelepiped zone.

Let's consider the case of a hexagonal lattice of Fig. E.6 with Primitive lattice vectors: $\vec{a}_1 = a\hat{x}$ and $\vec{a}_2 = \frac{a}{2}\hat{x} + \frac{\sqrt{3}}{2}a\hat{y}$.

The unit reciprocal lattice vectors are given by $\vec{b}_1 = \frac{2\pi}{a}\hat{x} - \frac{2\pi}{\sqrt{3}a}\hat{y}$ and $\vec{b}_2 = \frac{4\pi}{\sqrt{3}a}\hat{y}$ (see Fig. E.7).

The corresponding BZ is the area defined by the bisectors to the lines joining the central point to its nearest neighbors (see Fig. E.8). The parallelepiped zone is defined as the region spanned by the two reciprocal lattice vectors.

We see that the IW is shared by the two zones but it is easier to work with the PZ than the hexagonal BZ.

E.3.Vector Representation in Real and Reciprocal Space

In practice since the ground state information extracted from the WIEN package is given in certain specific bases, we need to consider the representation of vectors of the reciprocal lattice in three different coordinate systems:

$$\vec{k} = k_x\hat{x} + k_y\hat{y} + k_z\hat{z} = \beta_1\vec{b}_1 + \beta_2\vec{b}_2 + \beta_3\vec{b}_3 = \beta'_1\vec{b}'_1 + \beta'_2\vec{b}'_2 + \beta'_3\vec{b}'_3 \qquad \text{(E4)}$$

where $\{\hat{x}, \hat{y}, \hat{z}\}$ are orthogonal unit vectors. The basis $\{\vec{b}_1, \vec{b}_2, \vec{b}_3\}$ are the usual reciprocal lattice vectors obtained from the lattice vectors $\{\vec{a}_1, \vec{a}_2, \vec{a}_3\}$ in real space. The basis formed by $\{\vec{b}'_1, \vec{b}'_2, \vec{b}'_3\}$ is orthogonal for the FCC and BCC structures but for some other structures (like HCP) it is actually the same as $\{\vec{b}_1, \vec{b}_2, \vec{b}_3\}$.

We also need to consider the real space vector $\vec{x}$ in three different bases,

$$\vec{x} = x\hat{x} + y\hat{y} + z\hat{z} = \alpha_1\vec{a}_1 + \alpha_2\vec{a}_2 + \alpha_3\vec{a}_3 = \alpha'_1\vec{a}'_1 + \alpha'_2\vec{a}'_2 + \alpha'_3\vec{a}'_3 \qquad \text{(E5)}$$

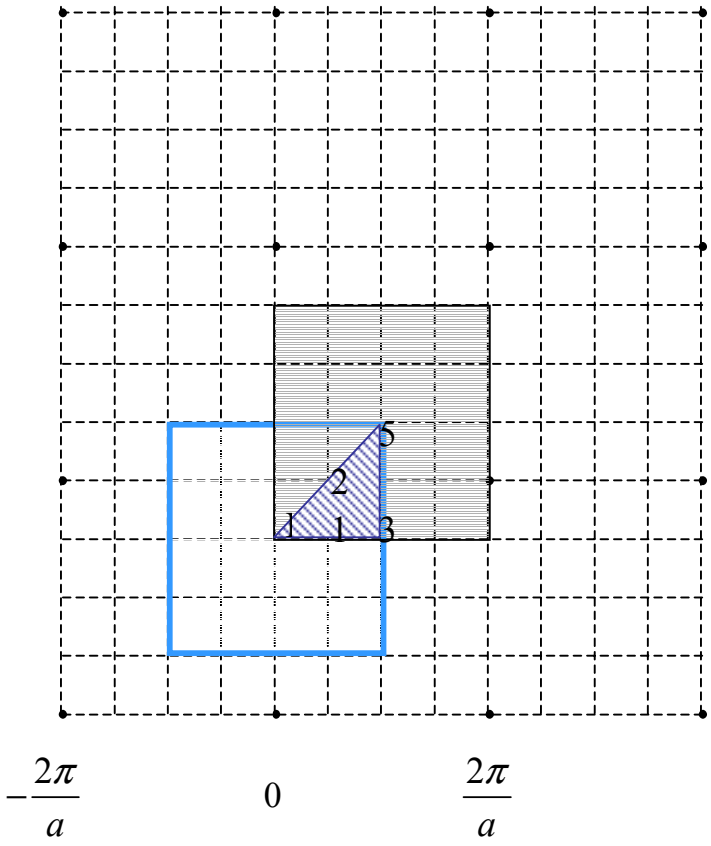

Fig. E.5. Representation of the BZ and PZ.

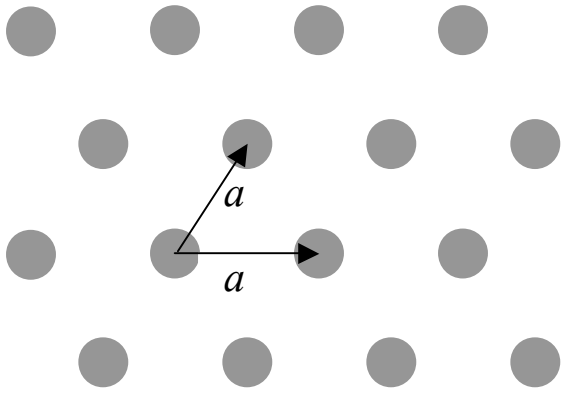

Fig. E.6. Hexagonal lattice.

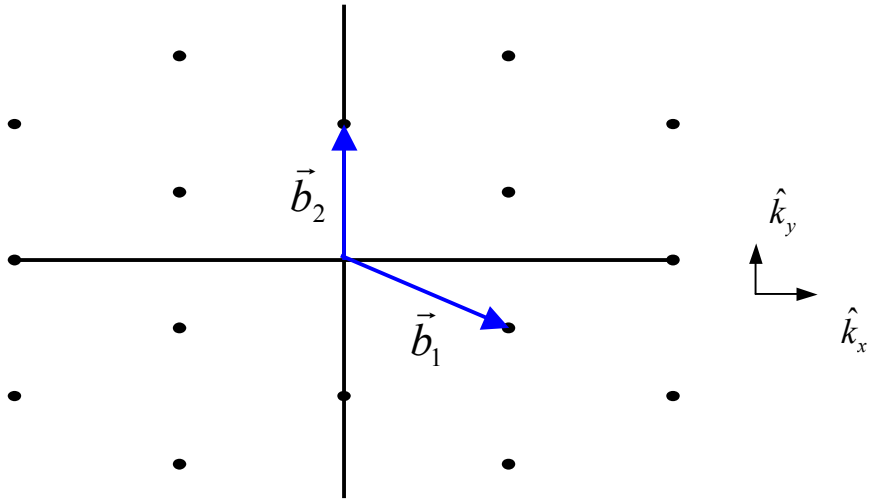

Fig. E.7. Reciprocal Hexagonal lattice.

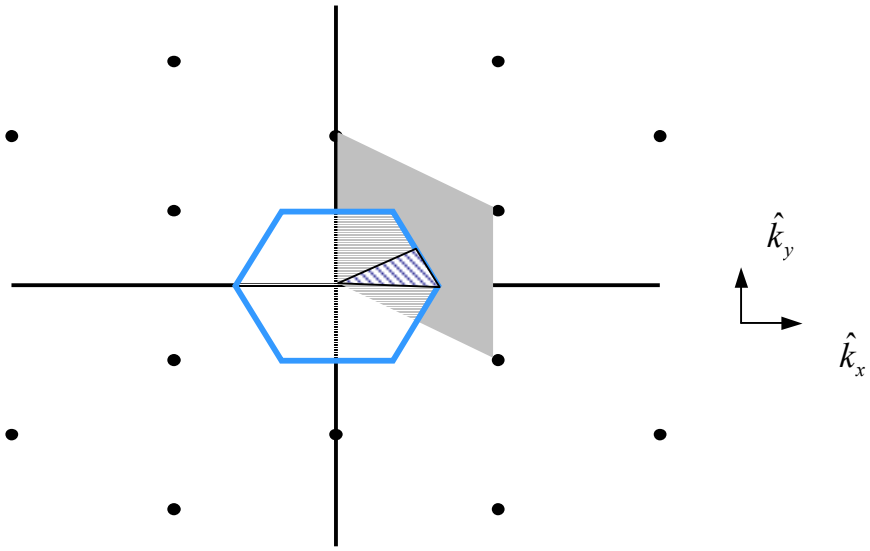

Fig. E.8. BZ and PZ of the Hexagonal lattice.

where $\{\hat{x},\hat{y},\hat{z}\}$ are orthogonal unit vectors. The basis $\{\vec{a}_1,\vec{a}_2,\vec{a}_3\}$ corresponds to the primitive lattice vectors and $\{\vec{a}_1',\vec{a}_2',\vec{a}_3'\}$ is an orthogonal basis from which we obtain the $\{\vec{b}_1',\vec{b}_2',\vec{b}_3'\}$ basis.

Our task will be to obtain the matrices that relate the coefficients of these different bases for vectors in real and reciprocal space. For this purpose in this section we will consider three crystal structures: FCC, BCC and HCP.

E.3.1. FCC Structure

The FCC primitive Lattice vectors are

$$\vec{a}_1 = \frac{a_y}{2}\hat{y} + \frac{a_z}{2}\hat{z}, \tag{E6}$$

$$\vec{a}_2 = \frac{a_x}{2}\hat{x} + \frac{a_z}{2}\hat{z}, \tag{E7}$$

$$\vec{a}_3 = \frac{a_x}{2}\hat{x} + \frac{a_y}{2}\hat{y}, \tag{E8}$$

a_x, a_y, a_z correspond to the vectors that span the unit cell (see Fig. E.9).

The reciprocal lattice vectors are

$$\vec{b}_1 = 2\pi\frac{\vec{a}_2\times\vec{a}_3}{\vec{a}_1\cdot(\vec{a}_2\times\vec{a}_3)} = 2\pi\left[\frac{-1}{a_x}\hat{x} + \frac{1}{a_y}\hat{y} + \frac{1}{a_z}\hat{z}\right]. \tag{E9}$$

$$\overrightarrow{b_2} = 2\pi\frac{\vec{a}_3\times\vec{a}_1}{\vec{a}_1(\vec{a}_2\times\vec{a}_3)} = 2\pi\left[\frac{1}{a_x}\hat{x} - \frac{1}{a_y}\hat{y} + \frac{1}{a_z}\hat{z}\right]. \tag{E10}$$

$$\vec{b}_3 = 2\pi\frac{\vec{a}_1\times\vec{a}_2}{\vec{a}_1(\vec{a}_2\times\vec{a}_3)} = 2\pi\left[\frac{1}{a_x}\hat{x} + \frac{1}{a_y}\hat{y} - \frac{1}{a_z}\hat{z}\right]. \tag{E11}$$

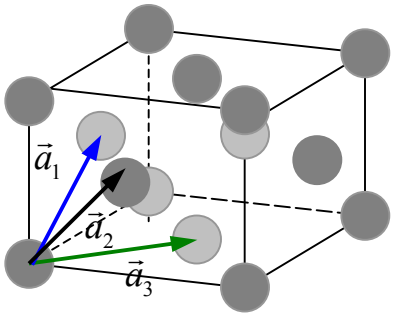

Fig. E.9. FCC crystal structure.

We can perform a mapping between the $\vec{b}$ vectors and the unit vectors by considering the following matrix:

$$\begin{pmatrix} \vec{b}_1 \\ \vec{b}_2 \\ \vec{b}_3 \end{pmatrix} = \begin{pmatrix} -\frac{2\pi}{a_x} & \frac{2\pi}{a_y} & \frac{2\pi}{a_z} \\ \frac{2\pi}{a_x} & -\frac{2\pi}{a_y} & \frac{2\pi}{a_z} \\ \frac{2\pi}{a_x} & \frac{2\pi}{a_y} & -\frac{2\pi}{a_z} \end{pmatrix} \begin{pmatrix} \hat{x} \\ \hat{y} \\ \hat{z} \end{pmatrix}. \tag{E12}$$

A vector in reciprocal space can be written in two different bases as

$$\vec{k} = \beta_1\vec{b}_1 + \beta_2\vec{b}_2 + \beta_3\vec{b}_3 \ , \tag{E13}$$

$$\vec{k} = k_x\hat{x} + k_y\hat{y} + k_z\hat{z} \, . \tag{E14}$$

Now, replacing Eq. (E12) in Eq. (E13) we obtain

$$\vec{k} = \frac{2\pi}{a_x}\left(-\beta_1 + \beta_2 + \beta_3\right)\hat{x} + \frac{2\pi}{a_y}\left(\beta_1 - \beta_2 + \beta_3\right)\hat{y} + \frac{2\pi}{a_z}\left(\beta_1 + \beta_2 - \beta_3\right)\hat{z} \, . \tag{E15}$$

The coefficients of equations (E14) and (E15) are related by the following matrix:

$$\begin{pmatrix} k_x \\ k_y \\ k_z \end{pmatrix} = \begin{pmatrix} -\frac{2\pi}{a_x} & \frac{2\pi}{a_x} & \frac{2\pi}{a_x} \\ \frac{2\pi}{a_y} & -\frac{2\pi}{a_y} & \frac{2\pi}{a_y} \\ \frac{2\pi}{a_z} & \frac{2\pi}{a_z} & -\frac{2\pi}{a_z} \end{pmatrix} \begin{pmatrix} \beta_1 \\ \beta_2 \\ \beta_3 \end{pmatrix}. \tag{E16}$$

For a FCC structure we have $a_x = a_y = a_z = a$,

$$\begin{pmatrix} k_x \\ k_y \\ k_z \end{pmatrix} = \frac{2\pi}{a} \begin{pmatrix} -1 & 1 & 1 \\ 1 & -1 & 1 \\ 1 & 1 & -1 \end{pmatrix} \begin{pmatrix} \beta_1 \\ \beta_2 \\ \beta_3 \end{pmatrix}. \tag{E17}$$

Let's now consider the primitive unit cell in real space for an fcc structure described by the vectors $\vec{a}'_x \perp \vec{a}'_y \perp \vec{a}'_z$. Definition: $\vec{a}'_1 = a_x \hat{x}$, $\vec{a}'_2 = a_y \hat{y}$, and $\vec{a}'_3 = a_z \hat{z}$. These are our new rescaled primitive vectors in real space. We can find now the Reciprocal Lattice vectors:

$$\vec{b}'_1 = \frac{2\pi}{a_x} \hat{x}, \tag{E18}$$

$$\vec{b}'_2 = \frac{2\pi}{a_y} \hat{y}, \tag{E19}$$

$$\vec{b}'_3 = \frac{2\pi}{a_z} \hat{z}. \tag{E20}$$

The transformation between the coefficients of the b' basis and the unitary basis is performed via the matrix:

$$\begin{pmatrix} k_x \\ k_y \\ k_z \end{pmatrix} = \begin{pmatrix} \frac{2\pi}{a_x} & 0 & 0 \\ 0 & \frac{2\pi}{a_y} & 0 \\ 0 & 0 & \frac{2\pi}{a_z} \end{pmatrix} \begin{pmatrix} \beta'_1 \\ \beta'_2 \\ \beta'_3 \end{pmatrix}. \tag{E21}$$

Inserting Eq. (E17) into Eq. (E21) we have that,

$$2\pi\begin{pmatrix} -\frac{1}{a_x} & \frac{1}{a_x} & \frac{1}{a_x} \\ \frac{1}{a_y} & -\frac{1}{a_y} & \frac{1}{a_y} \\ \frac{1}{a_z} & \frac{1}{a_z} & -\frac{1}{a_z} \end{pmatrix}\begin{pmatrix} \beta_1 \\ \beta_2 \\ \beta_3 \end{pmatrix} = \begin{pmatrix} \frac{2\pi}{a_x} & 0 & 0 \\ 0 & \frac{2\pi}{a_y} & 0 \\ 0 & 0 & \frac{2\pi}{a_z} \end{pmatrix}\begin{pmatrix} \beta'_1 \\ \beta'_2 \\ \beta'_3 \end{pmatrix}. \tag{E22}$$

We can solve this equation for the coefficients β_1, β_2 and β_3:

$$\begin{pmatrix} \beta_1 \\ \beta_2 \\ \beta_3 \end{pmatrix} = \begin{pmatrix} 0 & \frac{1}{2} & \frac{1}{2} \\ \frac{1}{2} & 0 & \frac{1}{2} \\ \frac{1}{2} & \frac{1}{2} & 0 \end{pmatrix}\begin{pmatrix} \beta'_1 \\ \beta'_2 \\ \beta'_3 \end{pmatrix}. \tag{E23}$$

Inverting this matrix we are lead to the following result:

$$\begin{pmatrix} \beta'_1 \\ \beta'_2 \\ \beta'_3 \end{pmatrix} = \begin{pmatrix} -1 & 1 & 1 \\ 1 & -1 & 1 \\ 1 & 1 & -1 \end{pmatrix}\begin{pmatrix} \beta_1 \\ \beta_2 \\ \beta_3 \end{pmatrix}. \tag{E24}$$

In summary, for an FCC structure (say for Al) we have $a_x = a_y = a_z = a$ and the matrices to change bases in reciprocal space become

$$M_{k\leftarrow\beta} = \frac{2\pi}{a}\begin{pmatrix} -1 & 1 & 1 \\ 1 & -1 & 1 \\ 1 & 1 & -1 \end{pmatrix}. \tag{E25}$$

$$M_{k\leftarrow\beta'} = \frac{2\pi}{a}\begin{pmatrix} 1 & 0 & 0 \\ 0 & 1 & 0 \\ 0 & 0 & 1 \end{pmatrix}. \tag{E26}$$

$$M_{\beta'\leftarrow\beta} = \begin{pmatrix} -1 & 1 & 1 \\ 1 & -1 & 1 \\ 1 & 1 & -1 \end{pmatrix}. \tag{E27}$$

$$M_{\beta\leftarrow\beta'}=\begin{pmatrix}0 & \frac{1}{2} & \frac{1}{2}\\ \frac{1}{2} & 0 & \frac{1}{2}\\ \frac{1}{2} & \frac{1}{2} & 0\end{pmatrix}. \tag{E28}$$

Let's now consider the vector $\vec{x}$ in real space

$$\vec{x}=x\hat{x}+y\hat{y}+z\hat{z}=\alpha_1\vec{a}_1+\alpha_2\vec{a}_2+\alpha_3\vec{a}_3$$

$$=\alpha_1\left(\frac{a_y}{2}\hat{y}+\frac{a_z}{2}\hat{z}\right)+\alpha_2\left(\frac{a_x}{2}\hat{x}+\frac{a_z}{2}\hat{z}\right)+\alpha_3\left(\frac{a_x}{2}\hat{x}+\frac{a_y}{2}\hat{y}\right)$$

$$=\left(\frac{a_x}{2}\alpha_2+\frac{a_x}{2}\alpha_3\right)\hat{x}+\left(\frac{a_y}{2}\alpha_1+\frac{a_y}{2}\alpha_3\right)\hat{y}+\left(\frac{a_z}{2}\alpha_1+\frac{a_z}{2}\alpha_2\right)\hat{z}. \tag{E29}$$

where we have used the definitions (E6)-(E8). The coefficients of these two bases are related by the following matrix,

$$\begin{pmatrix}x\\ y\\ z\end{pmatrix}=\begin{pmatrix}0 & \frac{a_x}{2} & \frac{a_x}{2}\\ \frac{a_y}{2} & 0 & \frac{a_y}{2}\\ \frac{a_z}{2} & \frac{a_z}{2} & 0\end{pmatrix}\begin{pmatrix}\alpha_1\\ \alpha_2\\ \alpha_3\end{pmatrix}. \tag{E30}$$

This last matrix represents $M_{x\leftarrow\alpha}$, inverting this matrix we obtain

$$M_{\alpha\leftarrow x}=\begin{pmatrix}-\frac{1}{a_x} & \frac{1}{a_y} & \frac{1}{a_z}\\ \frac{1}{a_x} & -\frac{1}{a_y} & \frac{1}{a_z}\\ \frac{1}{a_x} & \frac{1}{a_y} & -\frac{1}{a_z}\end{pmatrix}. \tag{E31}$$

The vector $\vec{x}$ can also be expanded in the $\vec{a}'$ basis

$$\vec{x} = \alpha_1'\vec{a}_1' + \alpha_2'\vec{a}_2' + \alpha_3'\vec{a}_3' = \alpha_1' a_x\hat{x} + \alpha_2' a_y\hat{y} + \alpha_3' a_z\hat{z}$$

$$= \left(\frac{a_x}{2}\alpha_2 + \frac{a_x}{2}\alpha_3\right)\hat{x} + \left(\frac{a_y}{2}\alpha_1 + \frac{a_y}{2}\alpha_3\right)\hat{y} + \left(\frac{a_z}{2}\alpha_1 + \frac{a_z}{2}\alpha_2\right)\hat{z}. \qquad \text{(E32)}$$

The coefficients of these two bases are related by the following matrix,

$$\begin{pmatrix}\alpha_1'\\ \alpha_2'\\ \alpha_3'\end{pmatrix} = \begin{pmatrix} 0 & \frac{1}{2} & \frac{1}{2}\\ \frac{1}{2} & 0 & \frac{1}{2}\\ \frac{1}{2} & \frac{1}{2} & 0\end{pmatrix}\begin{pmatrix}\alpha_1\\ \alpha_2\\ \alpha_3\end{pmatrix}. \qquad \text{(E33)}$$

Inverting the matrix in Eq. (E33) we obtain the following mapping,

$$M_{\alpha\leftarrow\alpha'} = \begin{pmatrix} -1 & 1 & 1\\ 1 & -1 & 1\\ 1 & 1 & -1\end{pmatrix}. \qquad \text{(E34)}$$

In order to find the relationship between the $\vec{k}$ system, in reciprocal space, and the $\vec{x}$ system in real space we consider the product $\vec{k}\cdot\vec{x}$:

$$\vec{k}\cdot\vec{x} = k_x x + k_y y + k_z z = \frac{2\pi}{a_x}\left(-\beta_1 + \beta_2 + \beta_3\right)\left(\frac{a_x}{2}\alpha_2 + \frac{a_x}{2}\alpha_3\right)$$

$$+\frac{2\pi}{a_y}\left(\beta_1 - \beta_2 + \beta_3\right)\left(\frac{a_y}{2}\alpha_1 + \frac{a_y}{2}\alpha_3\right)$$

$$+\frac{2\pi}{a_z}\left(\beta_1 + \beta_2 - \beta_3\right)\left(\frac{a_z}{2}\alpha_1 + \frac{a_z}{2}\alpha_2\right). \qquad \text{(E35)}$$

$$\vec{k}\cdot\vec{x} = 2\pi\left(\beta_1\alpha_1 + \beta_2\alpha_2 + \beta_3\alpha_3\right). \qquad \text{(E36)}$$

$$\vec{k}\cdot\vec{x} = 2\pi\left(\vec{\beta}\cdot\vec{\alpha}\right) = 2\pi\left(\vec{\beta}'\cdot\vec{\alpha}'\right) = 2\pi\left(M_{\beta\leftarrow k}\cdot\vec{k}\right)^T\cdot\left(M_{\alpha\leftarrow x}\cdot\vec{x}\right)$$

$$= 2\pi\vec{k} \cdot M^{T}_{\beta\leftarrow k} \cdot \left(M_{\alpha\leftarrow x} \cdot \vec{x}\right) \tag{E37}$$

$$1 = 2\pi M^{T}_{\beta\leftarrow k} \cdot M_{\alpha\leftarrow x} \tag{E38}$$

$$M_{\alpha\leftarrow x} = \frac{1}{2\pi}\left(M^{T}_{\beta\leftarrow k}\right)^{-1} \tag{E39}$$

or equivalently

$$M_{x\leftarrow\alpha} = 2\pi \cdot M^{T}_{\beta\leftarrow k}\,. \tag{E40}$$

By the same reasoning we obtain

$$M_{x\leftarrow\alpha'} = 2\pi \cdot M^{T}_{\beta'\leftarrow k}\,. \tag{E41}$$

Let's find the relationship between $M_{\alpha\leftarrow\alpha'}$ and $M_{\beta\leftarrow\beta'}$

$$\vec{k}_{\vec{b}} = M_{\beta\leftarrow\beta'} \cdot \vec{k}_{\vec{b}'} = M_{\beta\leftarrow k} M_{k\leftarrow\beta'} \cdot \vec{k}_{\vec{b}'}\,. \tag{E42}$$

$$\vec{x}_{\vec{a}} = M_{\alpha\leftarrow\alpha'} \cdot \vec{x}_{\vec{a}'} = M_{\alpha\leftarrow x} M_{x\leftarrow\alpha'} \cdot \vec{x}_{\vec{a}'}\,. \tag{E43}$$

We also have that

$$\vec{k}_{\vec{b}} \cdot \vec{x}_{\vec{a}} = \vec{k}_{\vec{b}'} \cdot \vec{x}_{\vec{a}'} = \left(M_{\beta\leftarrow\beta'} \cdot \vec{k}_{\vec{b}'}\right)^{T} \left(M_{\alpha\leftarrow\alpha'} \cdot \vec{x}_{\vec{a}'}\right)$$

$$= \vec{k}_{\vec{b}'} \cdot M^{T}_{\beta\leftarrow\beta'} \left(M_{\alpha\leftarrow\alpha'} \cdot \vec{x}_{\vec{a}'}\right) \tag{E44}$$

$$M_{\alpha\leftarrow\alpha'} = \left(M^{T}_{\beta\leftarrow\beta'}\right)^{-1} \tag{E45}$$

or

$$M^{T}_{\beta\leftarrow\beta'} = M_{\alpha'\leftarrow\alpha}\,. \tag{E46}$$

All the matrices presented so far can be obtained from the WIEN package. Some of them directly from the output of the program and others by applying the relations we have

developed. For example, by reading the file structure from the *case.struc* file one can obtain from the knowledge of $M_{k\leftarrow\beta}$ and $M_{k\leftarrow\beta'}$ most of the previous matrices. The matrices $M_{k\leftarrow\beta'}$ and $M_{k\leftarrow\beta}$ are respectively the first and second matrices written in this file. The inverse symmetry matrices for the beta system are found on the file *case.symmatk* . The symmetry matrices in the $\vec{a}$ basis are calculated based on the file *case.symmatr* which contains the matrices in the $\vec{a}'$ basis, the relationship between these two matrices is the following: $S_\alpha = M_{\alpha\leftarrow\alpha'} S_{\alpha'} M_{\alpha'\leftarrow\alpha}$. The translational vector in the $\vec{a}$ basis is also obtained from this file by considering the translational vector in the $\vec{a}'$ basis and the relation $\vec{\tau}_\alpha = M_{\alpha\leftarrow\alpha'}\vec{\tau}_{\alpha'}$.

E.3.2. BCC Structure

The BCC primitive lattice vectors are

$$\vec{a}_1 = -\frac{a_x}{2}\hat{x} + \frac{a_y}{2}\hat{y} + \frac{a_z}{2}\hat{z}, \tag{E47}$$

$$\vec{a}_2 = \frac{a_x}{2}\hat{x} - \frac{a_y}{2}\hat{y} + \frac{a_z}{2}\hat{z}, \tag{E48}$$

$$\vec{a}_3 = \frac{a_x}{2}\hat{x} + \frac{a_y}{2}\hat{y} - \frac{a_z}{2}\hat{z}, \tag{E49}$$

$a_x, a_y,$ and a_z correspond to the vectors that span the unit cell (see Fig. E.10).

The reciprocal lattice vectors are

$$\vec{b}_1 = 2\pi\frac{\vec{a}_2\times\vec{a}_3}{\vec{a}_1\left(\vec{a}_2\times\vec{a}_3\right)} = 2\pi\left[\frac{1}{a_y}\hat{y} + \frac{1}{a_z}\hat{z}\right], \tag{E50}$$

$$\vec{b}_2 = 2\pi\frac{\vec{a}_3\times\vec{a}_1}{\vec{a}_1\left(\vec{a}_2\times\vec{a}_3\right)} = 2\pi\left[\frac{1}{a_x}\hat{x} + \frac{1}{a_z}\hat{z}\right], \tag{E51}$$

$$\vec{b}_3 = 2\pi\frac{\vec{a}_1\times\vec{a}_2}{\vec{a}_1\left(\vec{a}_2\times\vec{a}_3\right)} = 2\pi\left[\frac{1}{a_x}\hat{x} + \frac{1}{a_y}\hat{y}\right]. \tag{E52}$$

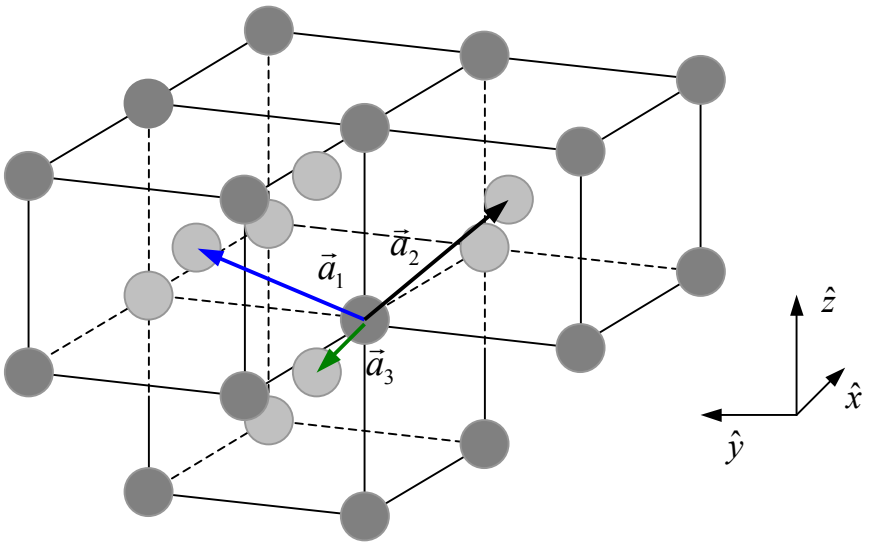

Fig. E.10. BCC crystal structure.

We can perform a mapping between the $\vec{b}$ basis and the unit vector basis by considering the following matrix:

$$\begin{pmatrix} \vec{b}_1 \\ \vec{b}_2 \\ \vec{b}_3 \end{pmatrix} = \begin{pmatrix} 0 & \frac{2\pi}{a_y} & \frac{2\pi}{a_z} \\ \frac{2\pi}{a_x} & 0 & \frac{2\pi}{a_z} \\ \frac{2\pi}{a_x} & \frac{2\pi}{a_y} & 0 \end{pmatrix} \begin{pmatrix} \hat{x} \\ \hat{y} \\ \hat{z} \end{pmatrix}. \tag{E53}$$

Now, a vector in reciprocal space can be written as

$$\vec{k} = \beta_1 \vec{b}_1 + \beta_2 \vec{b}_2 + \beta_3 \vec{b}_3 . \tag{E54}$$

Replacing Eq. (E53) into Eq. (E54) we have that

$$\vec{k} = \frac{2\pi}{a_x}(\beta_2 + \beta_3)\hat{x} + \frac{2\pi}{a_y}(\beta_1 + \beta_3)\hat{y} + \frac{2\pi}{a_z}(\beta_1 + \beta_2)\hat{z} . \tag{E55}$$

$$\vec{k} = k_x \hat{x} + k_y \hat{y} + k_z \hat{z} . \tag{E56}$$

The coefficients of Eqs. (E55) and (E56) are related by the following equation:

$$\begin{pmatrix} k_x \\ k_y \\ k_z \end{pmatrix} = \begin{pmatrix} 0 & \frac{2\pi}{a_x} & \frac{2\pi}{a_x} \\ \frac{2\pi}{a_y} & 0 & \frac{2\pi}{a_y} \\ \frac{2\pi}{a_z} & \frac{2\pi}{a_z} & 0 \end{pmatrix} \begin{pmatrix} \beta_1 \\ \beta_2 \\ \beta_3 \end{pmatrix}. \tag{E57}$$

For a BCC structure we have $a_x = a_y = a_z = a$

$$\begin{pmatrix} k_x \\ k_y \\ k_z \end{pmatrix} = \frac{2\pi}{a} \begin{pmatrix} 0 & 1 & 1 \\ 1 & 0 & 1 \\ 1 & 1 & 0 \end{pmatrix} \begin{pmatrix} \beta_1 \\ \beta_2 \\ \beta_3 \end{pmatrix}. \tag{E58}$$

Let's now consider the primitive unit cell in real space for an bcc structure described by the vectors $\vec{a}_x \perp \vec{a}_y \perp \vec{a}_z$.

Definition: $\vec{a}_1' = a_x\hat{x}$, $\vec{a}_2' = a_y\hat{y}$, and $\vec{a}_3' = a_z\hat{z}$. These are our new rescaled vectors in real space. We find now the reciprocal lattice vectors:

$$\vec{b}_1' = \frac{2\pi}{a_x}\hat{x}, \tag{E59}$$

$$\vec{b}_2' = \frac{2\pi}{a_y}\hat{y}, \tag{E60}$$

$$\vec{b}_3' = \frac{2\pi}{a_z}\hat{z}. \tag{E61}$$

The transformation between the coefficients of the b' basis and the unitary basis is given by the following equation:

$$\begin{pmatrix} k_x \\ k_y \\ k_z \end{pmatrix} = \begin{pmatrix} \frac{2\pi}{a_x} & 0 & 0 \\ 0 & \frac{2\pi}{a_y} & 0 \\ 0 & 0 & \frac{2\pi}{a_z} \end{pmatrix} \begin{pmatrix} \beta_1' \\ \beta_2' \\ \beta_3' \end{pmatrix}. \tag{E62}$$

Using Eq. (E58) we can write

$$2\pi \begin{pmatrix} 0 & \frac{1}{a_x} & \frac{1}{a_x} \\ \frac{1}{a_y} & 0 & \frac{1}{a_y} \\ \frac{1}{a_z} & \frac{1}{a_z} & 0 \end{pmatrix} \begin{pmatrix} \beta_1 \\ \beta_2 \\ \beta_3 \end{pmatrix} = \begin{pmatrix} \frac{2\pi}{a_x} & 0 & 0 \\ 0 & \frac{2\pi}{a_y} & 0 \\ 0 & 0 & \frac{2\pi}{a_z} \end{pmatrix} \begin{pmatrix} \beta_1' \\ \beta_2' \\ \beta_3' \end{pmatrix}. \tag{E63}$$

Solving for β_1, β_2, and β_3 we have that

$$\begin{pmatrix}\beta_1\\ \beta_2\\ \beta_3\end{pmatrix}=\begin{pmatrix}-\frac{1}{2} & \frac{1}{2} & \frac{1}{2}\\ \frac{1}{2} & -\frac{1}{2} & \frac{1}{2}\\ \frac{1}{2} & \frac{1}{2} & -\frac{1}{2}\end{pmatrix}\begin{pmatrix}\beta'_1\\ \beta'_2\\ \beta'_3\end{pmatrix}. \tag{E64}$$

Inverting this matrix we are lead to the following result:

$$\begin{pmatrix}\beta'_1\\ \beta'_2\\ \beta'_3\end{pmatrix}=\begin{pmatrix}0 & 1 & 1\\ 1 & 0 & 1\\ 1 & 1 & 0\end{pmatrix}\begin{pmatrix}\beta_1\\ \beta_2\\ \beta_3\end{pmatrix}. \tag{E65}$$

In summary, for the BCC structure we have $a_x = a_y = a_z = a$ and the matrices for change of bases become

$$M_{k\leftarrow\beta}=\frac{2\pi}{a}\begin{pmatrix}0 & 1 & 1\\ 1 & 0 & 1\\ 1 & 1 & 0\end{pmatrix}, \tag{E66}$$

$$M_{k\leftarrow\beta'}=\frac{2\pi}{a}\begin{pmatrix}1 & 0 & 0\\ 0 & 1 & 0\\ 0 & 0 & 1\end{pmatrix}, \tag{E67}$$

$$M_{\beta'\leftarrow\beta}=\begin{pmatrix}0 & 1 & 1\\ 1 & 0 & 1\\ 1 & 1 & 0\end{pmatrix}, \tag{E68}$$

$$M_{\beta\leftarrow\beta'}=\begin{pmatrix}-\frac{1}{2} & \frac{1}{2} & \frac{1}{2}\\ \frac{1}{2} & -\frac{1}{2} & \frac{1}{2}\\ \frac{1}{2} & \frac{1}{2} & -\frac{1}{2}\end{pmatrix}. \tag{E69}$$

Let's now consider the vector $\vec{x}$ in real space

$$\vec{x}=x\hat{x}+y\hat{y}+z\hat{z}=\alpha_1\vec{a}_1+\alpha_2\vec{a}_2+\alpha_3\vec{a}_3$$

$$= \alpha_1\left(-\frac{a_x}{2}\hat{x}+\frac{a_y}{2}\hat{y}+\frac{a_z}{2}\hat{z}\right)+\alpha_2\left(\frac{a_x}{2}\hat{x}-\frac{a_y}{2}\hat{y}+\frac{a_z}{2}\hat{z}\right)+\alpha_3\left(\frac{a_x}{2}\hat{x}+\frac{a_y}{2}\hat{y}-\frac{a_z}{2}\hat{z}\right)$$

$$\begin{aligned}&=\left(-\frac{a_x}{2}\alpha_1+\frac{a_x}{2}\alpha_2+\frac{a_x}{2}\alpha_3\right)\hat{x}+\left(\frac{a_y}{2}\alpha_1-\frac{a_y}{2}\alpha_2+\frac{a_y}{2}\alpha_3\right)\hat{y}\\&+\left(\frac{a_z}{2}\alpha_1+\frac{a_z}{2}\alpha_2-\frac{a_z}{2}\alpha_3\right)\hat{z}\end{aligned} \tag{E70}$$

The coefficients in these two bases are related by the following equation

$$\begin{pmatrix}x\\y\\z\end{pmatrix}=\begin{pmatrix}-\frac{a_x}{2} & \frac{a_x}{2} & \frac{a_x}{2}\\ \frac{a_y}{2} & -\frac{a_y}{2} & \frac{a_y}{2}\\ \frac{a_z}{2} & \frac{a_z}{2} & -\frac{a_z}{2}\end{pmatrix}\begin{pmatrix}\alpha_1\\\alpha_2\\\alpha_3\end{pmatrix}. \tag{E71}$$

This last matrix represents $M_{x\leftarrow\alpha}$. Inverting this mapping we obtain

$$M_{\alpha\leftarrow x}=\begin{pmatrix}0 & \frac{1}{a_y} & \frac{1}{a_z}\\ \frac{1}{a_x} & 0 & \frac{1}{a_z}\\ \frac{1}{a_x} & \frac{1}{a_y} & 0\end{pmatrix}. \tag{E72}$$

The vector $\vec{x}$ can also be expanded in the $\vec{a}'$ basis

$$\vec{x}=\alpha_1'\vec{a}_1'+\alpha_2'\vec{a}_2'+\alpha_3'\vec{a}_3'=\alpha_1'a_x\hat{x}+\alpha_2'a_y\hat{y}+\alpha_3'a_z\hat{z}$$

$$\begin{aligned}&=\left(-\frac{a_x}{2}\alpha_1+\frac{a_x}{2}\alpha_2+\frac{a_x}{2}\alpha_3\right)\hat{x}+\left(\frac{a_y}{2}\alpha_1-\frac{a_y}{2}\alpha_2+\frac{a_y}{2}\alpha_3\right)\hat{y}\\&+\left(\frac{a_z}{2}\alpha_1+\frac{a_z}{2}\alpha_2-\frac{a_z}{2}\alpha_3\right)\hat{z}\end{aligned} \tag{E73}$$

The coefficients in these two bases are related by the following equation

$$\begin{pmatrix} \alpha_1' \\ \alpha_2' \\ \alpha_3' \end{pmatrix} = \begin{pmatrix} -\frac{1}{2} & \frac{1}{2} & \frac{1}{2} \\ \frac{1}{2} & -\frac{1}{2} & \frac{1}{2} \\ \frac{1}{2} & \frac{1}{2} & -\frac{1}{2} \end{pmatrix} \begin{pmatrix} \alpha_1 \\ \alpha_2 \\ \alpha_3 \end{pmatrix}. \tag{E74}$$

Inverting the matrix en Eq. (E74) we obtain the inverse mapping,

$$M_{\alpha \leftarrow \alpha'} = \begin{pmatrix} 0 & 1 & 1 \\ 1 & 0 & 1 \\ 1 & 1 & 0 \end{pmatrix}. \tag{E75}$$

E.3.3 HCP Structure

The HCP primitive lattice vectors are

$$\vec{a}_1 = \frac{\sqrt{3}}{2} a_x \hat{x} - \frac{a_y}{2} \hat{y}, \tag{E76}$$

$$\vec{a}_2 = a_y \hat{y}, \tag{E77}$$

$$\vec{a}_3 = c\hat{z}, \tag{E78}$$

$a_x, a_y,$ and a_z correspond to the vectors that span the unit cell (see Fig. E.11).

The reciprocal lattice vectors are

$$\vec{b}_1 = \frac{4\pi}{\sqrt{3} a_x} \hat{x}, \tag{E79}$$

$$\vec{b}_2 = 2\pi \left[\frac{1}{\sqrt{3} a_x} \hat{x} + \frac{1}{a_y} \hat{y} \right], \tag{E80}$$

$$\vec{b}_3 = \frac{2\pi}{c} \hat{z}. \tag{E81}$$

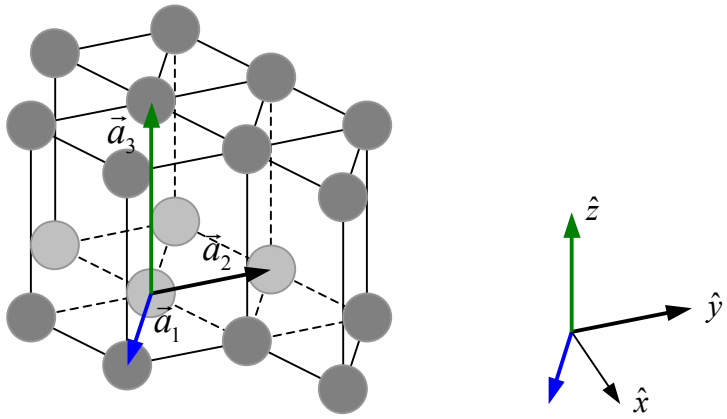

Fig. E.11. HCP crystal structure.

We can perform a mapping between the $\vec{b}$ vectors and the unit vectors by considering the following matrix:

$$\begin{pmatrix} \vec{b}_1 \\ \vec{b}_2 \\ \vec{b}_3 \end{pmatrix} = \begin{pmatrix} \frac{4\pi}{\sqrt{3}a_x} & 0 & 0 \\ \frac{2\pi}{\sqrt{3}a_x} & \frac{2\pi}{a_y} & 0 \\ 0 & 0 & \frac{2\pi}{c} \end{pmatrix} \begin{pmatrix} \hat{x} \\ \hat{y} \\ \hat{z} \end{pmatrix}. \tag{E82}$$

Now, a vector in reciprocal space can be written as

$$\vec{k} = \beta_1 \vec{b}_1 + \beta_2 \vec{b}_2 + \beta_3 \vec{b}_3 . \tag{E83}$$

Replacing Eq. (E82) into Eq. (E83) we have that

$$\vec{k} = \frac{2\pi}{a_x}\left(\frac{2}{\sqrt{3}}\beta_1 + \frac{\beta_2}{\sqrt{3}} \right)\hat{x} + \frac{2\pi}{a_y}(\beta_2)\,\hat{y} + \frac{2\pi}{c}(\beta_3)\,\hat{z} . \tag{E84}$$

$$\vec{k} = k_x \hat{x} + k_y \hat{y} + k_z \hat{z} . \tag{E85}$$

The coefficients of Eqs. (E84) and (E85) are related by the following equation:

$$\begin{pmatrix} k_x \\ k_y \\ k_z \end{pmatrix} = \begin{pmatrix} \frac{4\pi}{\sqrt{3}a_x} & \frac{2\pi}{\sqrt{3}a_x} & 0 \\ 0 & \frac{2\pi}{a_y} & 0 \\ 0 & 0 & \frac{2\pi}{c} \end{pmatrix} \begin{pmatrix} \beta_1 \\ \beta_2 \\ \beta_3 \end{pmatrix}. \tag{E86}$$

For the hcp structure we define:

$$\vec{a}_1' = \frac{\sqrt{3}}{2} a_x \hat{x} - \frac{a_y}{2} \hat{y} , \tag{E87}$$

$$\vec{a}_2' = a_y \hat{y} , \tag{E88}$$

$$\vec{a}_3' = c\hat{z} \,. \tag{E89}$$

So we will have the same matrix as before:

$$\begin{pmatrix} k_x \\ k_y \\ k_z \end{pmatrix} = \begin{pmatrix} \frac{4\pi}{\sqrt{3}a_x} & \frac{2\pi}{\sqrt{3}a_x} & 0 \\ 0 & \frac{2\pi}{a_y} & 0 \\ 0 & 0 & \frac{2\pi}{c} \end{pmatrix} \begin{pmatrix} \beta_1' \\ \beta_2' \\ \beta_3' \end{pmatrix}. \tag{E90}$$

In summary we have the following relationships:

$$M_{k\leftarrow\beta} = \begin{pmatrix} \frac{4\pi}{\sqrt{3}a_x} & \frac{2\pi}{\sqrt{3}a_x} & 0 \\ 0 & \frac{2\pi}{a_y} & 0 \\ 0 & 0 & \frac{2\pi}{c} \end{pmatrix}. \tag{E91}$$

$$M_{k\leftarrow\beta'} = \begin{pmatrix} \frac{4\pi}{\sqrt{3}a_x} & \frac{2\pi}{\sqrt{3}a_x} & 0 \\ 0 & \frac{2\pi}{a_y} & 0 \\ 0 & 0 & \frac{2\pi}{c} \end{pmatrix}. \tag{E92}$$

$$M_{\beta'\leftarrow\beta} = \begin{pmatrix} 1 & 0 & 0 \\ 0 & 1 & 0 \\ 0 & 0 & 1 \end{pmatrix}. \tag{E93}$$

$$M_{\beta\leftarrow\beta'} = \begin{pmatrix} 1 & 0 & 0 \\ 0 & 1 & 0 \\ 0 & 0 & 1 \end{pmatrix}. \tag{E94}$$

Let's now consider the vector $\vec{x}$ in real space

$$\vec{x} = x\hat{x} + y\hat{y} + z\hat{z} = \alpha_1\vec{a}_1 + \alpha_2\vec{a}_2 + \alpha_3\vec{a}_3$$

$$= \alpha_1\left(\frac{\sqrt{3}}{2}a_x\hat{x} - \frac{a_y}{2}\hat{y}\right) + \alpha_2\left(a_y\hat{y}\right) + \alpha_3\left(c\hat{z}\right)$$

$$= \left(\frac{\sqrt{3}}{2}a_x\alpha_1\right)\hat{x} + \left(-\frac{a_y}{2}\alpha_1 + a_y\alpha_2\right)\hat{y} + \left(c\alpha_3\right)\hat{z}\,. \qquad \text{(E95)}$$

The relationship between the coefficients of these two bases is given by

$$\begin{pmatrix} x \\ y \\ z \end{pmatrix} = \begin{pmatrix} \frac{\sqrt{3}}{2}a_x & 0 & 0 \\ -\frac{a_y}{2} & a_y & 0 \\ 0 & 0 & c \end{pmatrix}\begin{pmatrix} \alpha_1 \\ \alpha_2 \\ \alpha_3 \end{pmatrix}. \qquad \text{(E96)}$$

This last matrix represents $M_{x\leftarrow\alpha}$, Inverting this matrix we obtain

$$M_{\alpha\leftarrow x} = \begin{pmatrix} \frac{2}{\sqrt{3}a_x} & 0 & 0 \\ \frac{1}{\sqrt{3}a_x} & \frac{1}{a_y} & 0 \\ 0 & 0 & \frac{1}{c} \end{pmatrix}. \qquad \text{(E97)}$$

The vector $\vec{x}$ can also be expanded in the $\vec{a}'$ basis

$$\vec{x} = \alpha_1'\vec{a}_1' + \alpha_2'\vec{a}_2' + \alpha_3'\vec{a}_3' = \alpha_1'\left(\frac{\sqrt{3}}{2}a_x\hat{x} - \frac{a_y}{2}\hat{y}\right) + \alpha_2'\left(a_y\hat{y}\right) + \alpha_3'\left(c\hat{z}\right)$$

$$= \left(\frac{\sqrt{3}}{2}a_x\alpha_1'\right)\hat{x} + \left(-\frac{a_y}{2}\alpha_1' + a_y\alpha_2'\right)\hat{y} + \left(c\alpha_3'\right)\hat{z}$$

$$= \left(\frac{\sqrt{3}}{2}a_x\alpha_1\right)\hat{x} + \left(-\frac{a_y}{2}\alpha_1 + a_y\alpha_2\right)\hat{y} + \left(c\alpha_3\right)\hat{z}\,. \qquad \text{(E98)}$$

The coefficients for these two bases are related by the following equation,

$$\begin{pmatrix} \alpha'_1 \\ \alpha'_2 \\ \alpha'_3 \end{pmatrix} = \begin{pmatrix} 1 & 0 & 0 \\ 0 & 1 & 0 \\ 0 & 0 & 1 \end{pmatrix} \begin{pmatrix} \alpha_1 \\ \alpha_2 \\ \alpha_3 \end{pmatrix}. \tag{E99}$$

Inverting the matrix of Eq. (E99) we also obtain

$$M_{\alpha \leftarrow \alpha'} = \begin{pmatrix} 1 & 0 & 0 \\ 0 & 1 & 0 \\ 0 & 0 & 1 \end{pmatrix}. \tag{E100}$$

Appendix F Electron Density

F.1 Definition

The electron density in the Kohn-Sham formalism is defined in the following way:

$$\rho(\vec{x}) = \sum_{\vec{k}}^{BZ} \sum_{j} f_{\vec{k},j} \left| \Psi_{\vec{k},j}(\vec{x}) \right|^2 \tag{F1}$$

where $\vec{k}$ belongs to the first Brillouin zone, j is a band index, $f_{\vec{k},j}$ are the occupation numbers corresponding to the Bloch state $\Psi_{\vec{k},j}(\vec{x})$.

In most cases, in particular when we use the WIEN code to generate the ground state of a material, we will have only the information for the Bloch States that correspond to $\vec{k}$ vectors that are in the Irreducible Brillouin Zone (IBZ). It is then desirable to rewrite Eq. (F1) in a more suitable way for performing an actual calculation of the density. Defining $\rho_{\vec{k},j}(\vec{x}) \equiv \left| \Psi_{\vec{k},j}(\vec{x}) \right|^2$ we have that

$$\rho(\vec{x}) = \sum_{\vec{k}}^{BZ} \sum_{j} f_{\vec{k},j} \rho_{\vec{k},j}(\vec{x})$$

$$= \sum_{\underset{\sim}{\vec{k}}}^{IBZ} \sum_{\{R_{\underset{\sim}{k}}\}}^{star} \sum_{j} f_{R_{\underset{\sim}{k}}\vec{k},j} \rho_{R_{\underset{\sim}{k}}\underset{\sim}{\vec{k}},j}(\vec{x}), \tag{F2}$$

where $\underset{\sim}{\vec{k}}$ belongs to the IBZ. The star of $\underset{\sim}{\vec{k}}$ is composed of the distinct $\vec{k}$ points produced by applying all the symmetry operations of the Bravais lattice point group to $\underset{\sim}{\vec{k}}$. To every $\vec{k}$ point in the star of $\underset{\sim}{\vec{k}}$ we assign the symmetry operation that has been used to produce it. The set of these symmetry operations is denoted as $\left\{ R_{\underset{\sim}{\vec{k}}} \right\}$.

We can use the transformation properties of the Bloch states under rotation,

$$\Psi_{R_{\underset{\sim}{k}}\vec{k},j}(\vec{x}) = e^{iR_{\underset{\sim}{k}}\vec{k}\cdot\vec{\tau}\left(R_{\underset{\sim}{k}}\right)}\Psi_{\vec{k},j}\left(R_{\underset{\sim}{k}}^{-1}\left(\vec{x}-\vec{\tau}\left(R_{\underset{\sim}{k}}\right)\right)\right), \tag{F3}$$

where $\vec{\tau}$ is a space group partial lattice translation, along with the fact that the density has the space group symmetry of the crystal,

$$\rho\left(R\vec{x}+\vec{\tau}\right) = \rho\left(\vec{x}\right), \tag{F4}$$

for any symmetry operation of the space group, to write the sum over the stars in the following way:

$$\begin{aligned}\rho(\vec{x}) = \rho\left(R\vec{x}+\vec{\tau}\right) &= \sum_{\vec{k}}^{IBZ}\sum_{\left\{R_{\underset{\sim}{k}}\right\}}^{star}\sum_{j} f_{\vec{k},j}\rho_{R_{\underset{\sim}{k}}\vec{k},j}\left(R\vec{x}+\vec{\tau}\right) \\ &= \sum_{\vec{k}}^{IBZ}\sum_{\left\{R_{\underset{\sim}{k}}\right\}}^{star}\sum_{j} f_{\vec{k},j}\rho_{R_{\underset{\sim}{k}}\vec{k},j}\left(R\vec{x}+\vec{\tau}\right) = \sum_{\vec{k}}^{IBZ}\sum_{\left\{R_{\underset{\sim}{k}}\right\}}^{star}\sum_{j} f_{\vec{k},j}\left|\Psi_{R_{\underset{\sim}{k}}\vec{k},j}\left(R\vec{x}+\vec{\tau}\right)\right|^2 \\ &= \sum_{\vec{k}}^{IBZ}\sum_{\left\{R_{\underset{\sim}{k}}\right\}}^{star}\sum_{j} f_{\vec{k},j}\left|\Psi_{\vec{k},j}\left(R_{\underset{\sim}{k}}^{-1}\left(R\vec{x}+\vec{\tau}-\vec{\tau}\left(R_{\underset{\sim}{k}}\right)\right)\right)\right|^2,\end{aligned} \tag{F5}$$

where we have use the transformations properties of the occupation numbers under rotation $f_{R_{\underset{\sim}{k}}\vec{k},j} = f_{\vec{k},j}$.

We can choose $\left\{R,\vec{\tau}\right\}$ to satisfy

$$R_{\underset{\sim}{k}}^{-1}\left(R\vec{x}+\vec{\tau}-\vec{\tau}\left(R_{\underset{\sim}{k}}\right)\right) = \vec{x}, \tag{F6}$$

for every symmetry operation that has been assigned to each member of the star.

The expression for the density becomes

$$\rho(\vec{x}) = \sum_{\vec{k}}^{IBZ}\sum_{\left\{R_{\underset{\sim}{k}}\right\}}^{star}\sum_{j}^{occ} f_{\vec{k},j}\left|\Psi_{\vec{k},j}(\vec{x})\right|^2 = \sum_{\vec{k}}^{IBZ}\sum_{\left\{R_{\underset{\sim}{k}}\right\}}^{star}\sum_{j}^{occ} f_{\vec{k},j}\rho_{\vec{k},j}(\vec{x}). \tag{F7}$$

Notice that Eq. (F7) differs from Eq. (F2) in that $f_{\vec{k},j}$ and $\rho_{\vec{k},j}(\vec{x})$ do not depend in the sum over the star of $\vec{k}$ (they do not depend on $R_{\vec{k}}$), so we can perform the summation over the stars independently and we obtain:

$$\rho(\vec{x}) = \sum_{\vec{k}}^{IBZ} W_{\vec{k}} \sum_{j}^{occ} f_{\vec{k},j} \rho_{\vec{k},j}(\vec{x}), \tag{F8}$$

where $W_{\vec{k}}$ is the number of elements in the star of $\vec{k}$.

F.2 Charge Density Representation in the LAPW Method

In practice, the density will not satisfy Eq. (F4). The wave functions for $\vec{k}$ points outside the IBZ, which are produced from the wave functions for $\vec{k}$ points inside the IBZ by applying symmetry operations, would not be exact due to the variational character of our problem (we are not working with an infinite Hilbert space).

To ensure an accurate evaluation of the charge density, where there is enough flexibility to describe the density variations inside the atomic sphere, the density is constructed by performing an expansion in lattice harmonics in the atomic sphere region and in plane waves in the interstitial.

$$\rho(\vec{r}) = \begin{cases} \sum_{LM} \rho_{LM}(|\vec{r}|) K_{LM}\left(\Omega_{R^I_{loc}\vec{r}}\right) & \vec{r} \in \text{ Atomic sphere} \\ \sum_{\vec{G}} \rho_{\vec{G}} e^{i\vec{G}\cdot\vec{r}} & \vec{r} \in \text{ Interstitial} \end{cases} \tag{F9}$$

This procedure is sometimes called “symmetrization” of the density. This nomenclature comes from the fact that, by construction, the lattice harmonics are generated using the site symmetry (operations that leave the atomic position invariant), which guarantee that Eq. (F4) will remain valid. The use of these bases allows the use of symmetry to reduce the storage requirements in comparison, for example, to expansions using a spherical harmonics basis in the atomic sphere.

F.2.1 Electron Density in the Atomic Sphere

The density inside the I[th] atomic sphere is written as

$$\rho(\vec{r}) = \sum_{LM} \rho_{LM}(|\vec{r}|) K_{LM}\left(\Omega_{R^I_{loc}\,\vec{r}}\right), \tag{F10}$$

where R^I_{loc} is the local rotation matrix corresponding to the I[th] atomic sphere.

The Lattice Harmonics are defined as

$$K_{LM}\left(\Omega_{R^I_{lo}\vec{r}}\right) = \sum_{M'=-L}^{L} C^{M'}_{LM} Y_{LM'}\left(\Omega_{R^I_{lo}\vec{r}}\right), \tag{F11}$$

where $\vec{r} = \vec{x} - \vec{x}_I$, $\vec{x}_I$ is the position of the I[th] atom in the primitive unit cell, the $Y_{LM'}\left(\Omega_{R^I_{lo}\vec{r}}\right)$ are spherical harmonics evaluated at the angles θ and φ (defined by the unit vector $R^I_{lo}\vec{r}$) and the $C^{M'}_{LM}$ are the expansion coefficients chosen so that the $K_{LM}\left(\Omega_{R^I_{lo}\vec{r}}\right)$ are real.

In the WIEN2k package, for the total density inside the atomic sphere we can find in the file *case.clmsum* the product $r^2\rho_{LM}(|\vec{r}|)$ for all the combinations of (L,M), except for $(L,M)=(0,0)$ where we have $4\pi r^2\rho_{LM}(|\vec{r}|)$. The formula for the total density becomes:

$$\rho(\vec{r}) = \sum_{L\neq 0 M} \rho_{LM}(|\vec{r}|) K_{LM}\left(\Omega_{R^I_{lo}\vec{r}}\right) + \rho_{00}(|\vec{r}|) K_{00}\left(\Omega_{R^I_{lo}\vec{r}}\right) \Big/ \sqrt{4\pi}\,. \tag{F12}$$

For the valence density inside the atomic sphere we can find in the file *case.clmval* the product $r^2\rho_{LM}(|\vec{r}|)$ for all the combinations of (L,M). In this case there is no need to separate the term $(L,M)=(0,0)$ from the others as in Eq. (F12) and we can use Eq. (F10) to calculate the valence density. The format used to read the ρ_{LM} coefficients from the file *case.clmval(sum)* is '3X,4E19.12'.

F.2.2 Electron Density in the Interstitial Region

Recalling the expression for the fourier transform of $\rho_{\vec{G}}$, we have that

$$\rho_{R\vec{G}} = \frac{1}{\sqrt{\Omega}}\int d\vec{r} e^{-iR\vec{G}\cdot\vec{r}}\rho(\vec{r}) = \frac{1}{\sqrt{\Omega}}\int d\vec{r} e^{-i\vec{G}\cdot(R\vec{r}+\vec{\tau})}\rho(R\vec{r}+\vec{\tau})e^{-i\vec{G}\cdot\vec{\tau}}$$

$$= e^{-i\vec{G}\cdot\vec{\tau}}\rho_{\vec{G}}, \tag{F13}$$

where we have used Eq. (F4).

The expression for the density in the interstitial region becomes

$$\rho(\vec{r}) = \sum_{\vec{G}} \rho_{\vec{G}} e^{i\vec{G}\cdot\vec{r}}$$

$$= \sum_{\tilde{\vec{G}}}^{IW} \rho_{\tilde{\vec{G}}} W_{\tilde{\vec{G}}} \frac{1}{W_{\tilde{\vec{G}}}} \sum_{\left\{R_{\tilde{\vec{G}}}, \vec{\tau}_{R_{\tilde{\vec{G}}}}\right\}}^{star} e^{iR_{\tilde{\vec{G}}}\tilde{\vec{G}}\cdot\vec{r}} e^{i\vec{G}\cdot\vec{\tau}_{R_{\tilde{\vec{G}}}}}$$

$$= \sum_{\tilde{\vec{G}}}^{IW} \tilde{\rho}_{\tilde{\vec{G}}} \frac{1}{W_{\tilde{\vec{G}}}} \sum_{\left\{R_{\tilde{\vec{G}}}, \vec{\tau}_{R_{\tilde{\vec{G}}}}\right\}}^{star} e^{iR_{\tilde{\vec{G}}}\tilde{\vec{G}}\cdot\vec{r}} e^{i\vec{G}\cdot\vec{\tau}_{R_{\tilde{\vec{G}}}}}, \tag{F14}$$

where we have defined $\tilde{\rho}_{\tilde{\vec{G}}} = \rho_{\tilde{\vec{G}}} W_{\tilde{\vec{G}}}$ and $W_{\tilde{\vec{G}}}$ is the number of $\vec{G}$ vectors in the star of $\tilde{\vec{G}}$. The $\tilde{\rho}_{\tilde{\vec{G}}}$ coefficients, as well as the $\tilde{\vec{G}}$ vectors, to construct the total (valence) density are found at the end of the *case.clmsum(val)* file, the format used to read them is '3X,3I5,2E19.12'.

Vita

Oscar Dario Restrepo was born in Cali, Colombia, on June 23, 1976. After graduating from High School from the Licee Francais “Paul Valery” in 1994, he pursued a Bachelor’s Degree in Physics from the Universidad de Los Andes in Bogota, Colombia. He joined The University of Tennessee in the Fall of 1999 to pursue the Doctor of Philosophy Degree in Physics and graduated in August 2006.